Skoltech

Skolkovo Institute of Science and Technology

Skolkovo Institute of Science and Technology

Curtin University

Curtin University

INVESTIGATION OF ALKYL ETHER CARBOXYLATE SURFACTANTS
PERFORMANCE IN CARBONATE RESERVOIRS

Doctoral Thesis

by

ALEXANDRA SCERBACOVA

DOCTORAL PROGRAM IN PETROLEUM ENGINEERING JOINTLY WITH
SKOLKOVO INSTITUTE OF SCIENCE AND TECHNOLOGY AND CURTIN
UNIVERSITY

Supervisors:
Professor Alexey Cheremisin
Associate Professor Ahmed Barifcani
Co-supervisor: Associate Professor Chi Phan

Moscow – 2023

I hereby declare that the work presented in this thesis was carried out by myself at Skolkovo Institute of Science and Technology, Moscow, and Curtin University, Perth, except where due acknowledgement is made, and has not been submitted for any other degree.

Candidate:

Alexandra Scerbacova

Supervisors:

Professor Alexey Cheremisin

Associate Professor Ahmed Barifcani

Co-supervisor:

Associate Professor Chi Phan

Abstract

Low effectiveness of primary and secondary recovery techniques caused an intensive investigation and implementation of enhanced oil recovery (EOR) methods. The present study is focused on chemical EOR in carbonate reservoirs that is usually challenging. It is known that more than a half of hydrocarbon deposits in the world are concentrated in carbonates that are mainly located in Northern Africa, Kazakhstan, Russia, and the Middle East.

Chemical EOR implies the injection of polymers, surfactants, alkalis, and their mixtures. Surfactant-based flooding employment may be challenging in carbonate reservoirs mainly due to high surfactant adsorption loss and harsh reservoir conditions (high temperatures and brine salinities lead to stability and activity reduction of surfactant molecules). As the majority of anionic surfactants lose their stability under high salinity (up to 200 g/L) and high reservoir temperature (from 70°C to 120°C), anionic-nonionic surfactants attract the attention of researchers. They contain two hydrophilic groups in the structure, namely an ethylene oxide chain and a functional group (sulfate, sulfonate, or carboxylate). Ethoxylated alcohols with a carboxylic group are called alkyl ether carboxylates (AECs). Due to their two hydrophilic groups ($-CH_2COO-$ and $-CH_2CH_2O-$), they exhibit both anionic and nonionic properties, demonstrating salt tolerance and temperature stability. The common abbreviation for AEC surfactants is C_xE_yA (alternatively, C_nE_mA, C_xE_yC, C_xEO_yC, or A_xEC_y-Na), where y denotes the number of ethylene oxide units, and x is the number of carbon atoms in the alkyl chain. However, the stability of AECs is dependent on the structure, particularly the length of ethylene oxide chain.

The main idea of using surfactant flooding in carbonates is decrease of residual oil saturation through a combination of mechanisms that can be achieved during surfactant flooding, namely interfacial tension decrease and wettability alteration towards water-wet. Thus, this study presents evaluation of alkyl ether carboxylate surfactants in carbonates. The main goal of the present work is to study the effect of molecular structure of AEC surfactants on their performance in fluid-fluid and rock-fluid interactions that directly

3

influence on surfactant flooding effectiveness. Interfacial performance, wetting ability, adsorption capacity and displacement efficiency were examined as the key properties that determine the chemical flooding efficiency and economic feasibility. Experimental studies were completed with molecular dynamics simulations to scale up the experimental data and analyze the interfacial properties of a larger amount of AECs, as well as correlate it with their structures (alkyl chain and ethoxy fragment lengths). This thesis is concluded with an optimization of a commercial AEC-based surfactant blend by screening and evaluation of adsorption inhibitors that are stable under high temperature and high salinity conditions.

This work combines traditional and up-to-date approaches such as coreflooding with in-situ saturation control and molecular dynamics simulations. Application of both experimental and numerical methods allows the acquisition of a comprehensive dataset on AEC's behavior, filling a scientific gap that exists in the area of ethoxylated surfactants use in EOR. The findings described in this study show that AEC surfactants are promising agents for carbonate reservoirs.

The main findings of the present study demonstrate that the performance of AEC surfactants is highly influenced by their molecular structure, and mainly by the length of ethylene oxide chain. It was found that the EO segment length increase leads to compressibility reduction of surfactant molecules on the phase boundary and decrease of molecular packing density. Salinity has a strong impact of interfacial behavior of AECs in contact with both oil and rock. In the presence of electrolytes the interfacial tension decreases, and wetting ability improves. Surfactant composition with $C_{12}E_7A$ demonstrated the contact angle decrease from 115° until 20° in the system rock-water-air; oil recovery achieved by this surfactant was 72.5%. Static adsorption of AEC surfactants onto carbonate rock is high (reaches ~9 mg/g-rock), so consequently some agents decreasing adsorption loss should be applied. Adsorption inhibitors alternative to commonly used alkalis were successfully tested and described in this work.

Publications

1. **Scerbacova, A.**, Kopanichuk, I., & Cheremisin, A. (2023). Effect of temperature and salinity on interfacial behavior of alkyl ether carboxylate surfactants. *Petroleum Science and Technology*, 1-20. (Q3)
https://doi.org/10.1080/10916466.2022.2064872

2. Kopanichuk, I., **Scerbacova, A.**, Ivanova, A., Cheremisin, A., & Vishnyakov, A. (2022). The effect of the molecular structure of alkyl ether carboxylate surfactants on the oil-water interfacial tension. *Journal of Molecular Liquids*, 119525. (Q1)
https://doi.org/10.1016/j.molliq.2022.119525

3. **Scerbacova, A.**, Ivanova, A., Grishin, P., Cheremisin, A., Tokareva, E., Tkachev, I., Sansiev, G., Fedorchenko, G. & Afanasiev, I. (2022). Application of alkalis, polyelectrolytes, and nanoparticles for reducing adsorption loss of novel anionic surfactant in carbonate rocks at high salinity and temperature conditions. *Colloids and Surfaces A: Physicochemical and Engineering Aspects*, 653, 129996. (Q1)
https://doi.org/10.1016/j.colsurfa.2022.129996

4. **Scerbacova, A.**, Kozlova, E., Barifcani, A., Phan, C. M., Karamov, T., & Cheremisin, A. (2023). Rock–Fluid Interactions of Alkyl Ether Carboxylate Surfactants with Carbonates: Wettability Alteration, ζ-Potential, and Adsorption. *Energy & Fuels*. (Q1)
https://doi.org/10.1021/acs.energyfuels.2c04099

Non-thesis publications, relevant to the field:

1. **Scerbacova, A.,** Mukhina, E., Bakulin, D., Burukhin, A., Ivanova, A., Cheremisin, A., Spivakova, M., Ushakova, A. & Cheremisin, A. (2023). Water-and Surfactant-Based Huff-n-Puff Injection into Unconventional Liquid Hydrocarbon Reservoirs: Experimental and Modeling Study. *Energy & Fuels.* (Q1)
https://doi.org/10.1021/acs.energyfuels.3c01344

2. Pereponov, D., **Scerbacova, A.**, Kazaku, V., Hajiyev, M., Tarkhov, M. A., Shilov, E., & Cheremisin, A. (2023). Application of microfluidics to optimize oil and gas

field development technologies. *Kazakhstan journal for oil & gas industry*, 5(1), 57-73 (in Russian).

https://doi.org/10.54859/kjogi108639

Conferences and conference proceedings

1. **Scerbacova, A.** (2023, October). Investigation of Alkyl Ether Carboxylate Surfactants Performance in Carbonate Reservoirs. In SPE student paper contest featured at 99th *SPE Annual Technical Conference and Exhibition*.

2. **Scerbacova, A**., Pereponov, D., Tarkhov, M., Kazaku, V., Rykov, A., Filippov, I., Cheremisin, A. & Shilov, E. (2023, June). Visualization of Surfactant Flooding in Tight Reservoir Using Microfluidics. In *SPE EuropEC-Europe Energy Conference featured at the 84th EAGE Annual Conference & Exhibition.* OnePetro.

https://doi.org/10.2118/214419-MS

3. **Scerbacova, A**., Barifcani, A., Phan, C., & Cheremisin, A. (2023, March). Investigation of Anionic-Nonionic Surfactants for EOR in Carbonate Reservoirs. In *Gas & Oil Technology Showcase and Conference*. OnePetro.

https://doi.org/10.2118/214104-MS

4. **Scerbacova, A**., Ivanova, A., Mukhina, E., Ushakova, A., Bondar, M., & Cheremisin, A. (2021, October). Screening of surfactants for Huff-N-Puff injection into unconventional reservoirs. In *SPE Russian Petroleum Technology Conference*. OnePetro.

https://doi.org/10.2118/206431-MS

5. Ushakova, A., Mukhina, E., **Scerbacova, A**., Turakhanov, A., Bakulin, D., Cheremisin, A., & Kasyanenko, A. (2021, October). A comprehensive project of thermal, gas and chemical EOR method application for bazhenov shale formation. In *SPE Russian Petroleum Technology Conference*. OnePetro.

https://doi.org/10.2118/206424-MS

6. **Scerbacova, A.** (2021, September). Selection of Anionic Surfactant Adsorption Inhibitors onto Carbonate Rock in High Temperature and High Salinity Conditions.

In SPE student paper contest featured at *97th SPE Annual Technical Conference and Exhibition*.

7. Afanasev, P., **Scerbacova, A**., Tsyshkova, A., Mukhina, E., Grishin, P., Grishaev, V., Cheremisin, A., Koltsov, I., Dvoretskaya, E., Kasyanenko, A., Demo, V., Prochukhan, K., & Cheremisin, A. (2019, October). Compositions of Anionic and Non-Ionic Surfactants within a Hybrid EOR Technology for Unconventional Hydrocarbon Reservoirs. In *SPE Russian Petroleum Technology Conference*. OnePetro. https://doi.org/10.2118/196759-MS

Table of Contents

List of Symbols and Abbreviations

AEC – alkyl ether carboxylate

AFM – atomic force microscopy

APG – alkyl polyglucoside

ASP – alkali-surfactant-polymer flooding

CA – contact angle

CMC – critical micelle concentration

CTAB – cetrimonium bromide

C_xE_yA / C_nE_mA – abbreviation of alkyl ether carboxylate

DI – deionized water

EO – ethylene oxide

EOR – enhanced oil recovery

FTIR – Fourier-transform infrared spectroscopy

HLB – hydrophilic-lipophilic balance

HTHS – high temperature and high salinity conditions

IFT – interfacial tension

ISSM – in situ saturation monitoring

MD – molecular dynamics

NLS – nonlinear regression model

NPT – isothermal-isobaric ensemble, where amount of substance (N), pressure (P) and temperature (T) are conserved

NVT – canonical ensemble, where amount of substance (N), volume (V) and temperature (T) are conserved

PBC – periodic boundary conditions

PME – particle-mesh Ewald method

PSS – polystyrene sulfonate

PTFE – polytetrafluoroethylene

RE pyrolysis – Rock-Eval pyrolysis

      S0 – gaseous components of oil (according to RE pyrolysis)

S1 – light components of oil (according to RE pyrolysis)

S2 – heavy components of oil such as resins and asphaltenes (according to RE pyrolysis)

Salts:

C – calcium chloride $CaCl_2$

M – magnesium chloride $MgCl_2$

MB – sodium metaborate tetrahydrate $NaBO_2 \cdot 4H_2O$

MS – magnesium sulfate $MgSO_4$

S – sodium chloride $NaCl$

SBC – sodium bicarbonate $NaHCO_3$

SS – sodium sulfate Na_2SO_4

SDS – sodium dodecyl sulfate

SEM – scanning electron microscope

SWCTT – single well chemical tracer test

TGA – thermogravimetric analysis

VMD – visual molecular dynamics

WA – wettability alteration

WAG – water-alternating-gas injection

XRD – X-ray diffraction

ZPC – zero potential charge

List of Figures

18

List of Tables

Thesis organization

This work presents a detailed study of alkyl ether carboxylates as agents for surfactant flooding in carbonates and covers all areas of their performance such as stability, fluid-fluid interactions, rock-fluid interactions, fluid flow in porous medium and optimization of a commercial composition. The thesis is organized into chapters, and the short summary of each chapter is listed below:

Chapter 1 is a literature review that summarizes the challenges of oil recovery in carbonates and main challenges related to surfactant flooding in carbonate layers. Also, it describes the principle of surfactant flooding and possible technological solutions that can help overcoming the related difficulties and introduces the anionic-nonionic surfactants.

Chapter 2 correlates the stability issues with molecular structure of AECs and discusses their interfacial behavior and temperature and salinity effects on the IFT. The possible mechanisms are proposed and illustrated.

Chapter 3 presents the results of molecular dynamics simulations of AECs on the boundary water-decane at 25°C. This chapter discusses the molecular structure effect on orientation of surfactant molecules at the interphase.

Chapter 4 presents a comprehensive evaluation of rock-fluid interactions of AEC-based surfactant compositions with carbonate rock: wetting ability, zeta potential and adsorption capacity. The mechanisms of action are analyzed and supported with novel techniques.

Chapter 5 describes a coreflooding test with X-ray saturation control. Two methods of recovery factor determination are discussed – through material balance and saturation analysis.

Chapter 6 discusses application of chemicals (alkalis and polyelectrolytes) for reducing adsorption loss of a novel commercial AEC-based surfactant blend in harsh reservoir conditions.

Chapter 7 concludes the results obtained in the present work, namely application of anionic-nonionic surfactants in EOR and various approaches for their laboratory testing and presents recommendations for future research.

Chapter 1. Introduction

1.1. Carbonate oil reservoirs characterization and development challenges

According to literature data [1–4] and market analysis conducted by commercial companies [5,6], more than 60% of oil reserves in the world are located in carbonate layers. The general view of geographical distribution of carbonate, siliciclastic and other petroleum basins worldwide is shown in Figure 1.
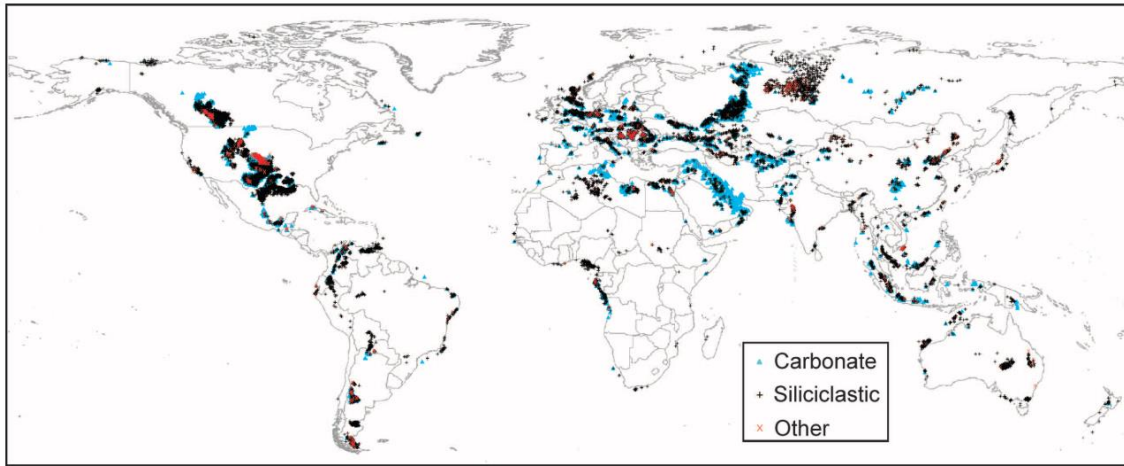
Figure 1. Geographical distribution of petroleum basins in terms of reservoir lithology [7]

Carbonate oil reserves refer to oil deposits that are found in carbonate rock formations, which are made up of sedimentary rocks such as limestone, dolomite, and marble that are composed primarily of calcium carbonate ($CaCO_3$) and dolomite $CaMg(CO_3)_2$. These rocks are formed in the result of marine animals' remains aggregation, such as coral and algae skeletons and shells. Carbonate oil reservoirs are found in different geological settings, including shallow marine environments, reefs, and deepwater basins. They are typically formed in warm, tropical environments where the conditions are favorable for the growth of marine organisms [6,8–10]. The largest hydrocarbon reserves have been found and are currently being developed in Northern Africa, Kazakhstan, Russia, and the Middle East [10].

Oil and gas in carbonate reservoirs are located in the pore spaces of the rock. Porosity and permeability are two important properties of layers that are directly connected with the productivity and recovery of oil and gas. Porosity refers to the amount of pore

space within the rock, which is the space between the grains or crystals that make up the rock. In carbonates, porosity is typically created by the dissolution of the calcium carbonate minerals that make up the rock by acidic fluids, such as groundwater or hydrocarbons (secondary porosity). The porosity of carbonate rocks can range from less than 1% to more than 30%, depending on the depositional environment and the degree of diagenesis (the process by which sediment is compacted and cemented into rock) [10,11].

Permeability refers to the ability of fluids to flow through the rock, and is determined by the size, shape, and connectivity of the pore spaces. In carbonate reservoirs, permeability is often controlled by the presence of low-permeability matrix and natural fractures, which can enhance the connectivity of the pore spaces and increase the flow of fluids through the rock. In such system the waterflooding channels move through high-permeability streak (Darcy range) and leave the low-permeability matrix (mDarcy range) unswept. Besides that, the presence of fractures can also make the reservoir more complex and difficult to model and predict [10,11]. Carbonate reservoirs are characterized with multi-scale heterogeneity that results in a complex porosity-permeability (poro-perm) relationship and poor pore connectivity. Figure 2 demonstrates typical correlation between porosity and permeability in sandstones and carbonates, and it can be observed that there is no linear relationship for carbonates contrary to sandstones [10,11].
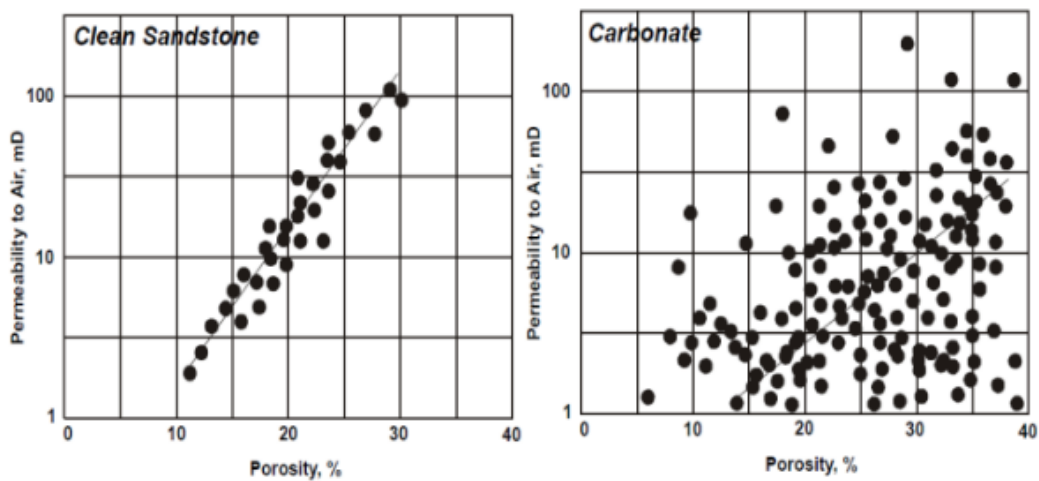
Figure 2. Typical porosity-permeability relationship for (a) sandstone rock and (b) carbonate [11]

Second challenge of oil recovery in carbonates is rock surface hydrophobicity [12]. It was reported that the oil-wetness of carbonates mainly occurs due to (1) adsorption of polar oil components onto the rock surface such as resins and asphaltenes, and (2) adsorption of carboxylic acids (palmitic, stearic, benzoic) [13–16]. The wettability in the reservoir determines the spreading of fluids and their relative permeability values. In a water-wet reservoir, the non-wetting fluid tends to occupy the larger pores, creating binding routes, while the wetting fluid is spread among small pores [12,13]. In an oil-wet reservoir, water resides in the larger pores while oil fills the smaller ones [17]. Therefore, spontaneous water imbibition in the pore network is weak and has a low recovery rate. In these wetting conditions, a significant volume of oil remains trapped in smaller pores after waterflooding, and the residual oil saturation prevails to be high [18,19]. To achieve effective fluid imbibition and successful oil displacement, the imbibing fluid has to overcome the capillary forces in microchannels [2], and this may be possible if the wettability of the rock surface tends to be water-wet [4,18,20,21].

Hence, two main issues contribute to the low efficiency of oil production in carbonates. First, complex heterogeneous structure and pore network [22,23]. Second, the complex wettability due to adsorbed polar components of oil [4,13,24]. Also, implementation of some EOR techniques such as chemical flooding is complicated by high reservoir temperatures and brine salinities (especially hardness ions Ca^{2+} and Mg^{2+}) that is a common issue in the reservoirs located in the Middle East [25].

Consequently, the development of carbonates is associated with many difficulties that result in low average oil recovery factor value that does not exceed 35% after primary and secondary recovery methods implementation [22,26]. Thus, about 60% of liquid hydrocarbons (HC) remain unswept [3]. To analyze the recovery techniques suitable for complex carbonate layers, it is necessary to characterize the fluid flow behavior in the porous medium.

1.2. Fluid flow characteristics in carbonate reservoirs

The complex texture and pore network of carbonates usually result from their depositional history and later diagenesis [22]. At all levels of carbonate rocks, including pores, grains, and textures, there may be differences, known as heterogeneity. There are three main types of porosity in carbonate rocks: intergranular, vuggy, and fracture porosity, each with its unique properties affecting fluid flow.

Intergranular porosity is the porosity found between the grains of the rock matrix. It is the most common type of porosity in carbonate rocks and is connected, meaning that fluids can flow freely through the pores. Vuggy porosity is unconnected and created by the dissolution of minerals such as calcite by water during diagenesis. Vugs are irregularly shaped and vary in size, from tiny to very large. Fracture porosity is caused by stresses during deposition, which can cause the rock to fracture and create open pathways for fluids to flow through. The interplay of these three types of porosities makes fluid pathways complex and directly influences well productivity [22,26,27]. In fractured reservoirs, fluids may infiltrate into the fractures from the rock matrix via self-absorption mechanism, resulting in oil migration from the matrix to the fracture network [2]. The schematic fluid migration in vuggy carbonate reservoirs is demonstarted in Figure 3 [2].
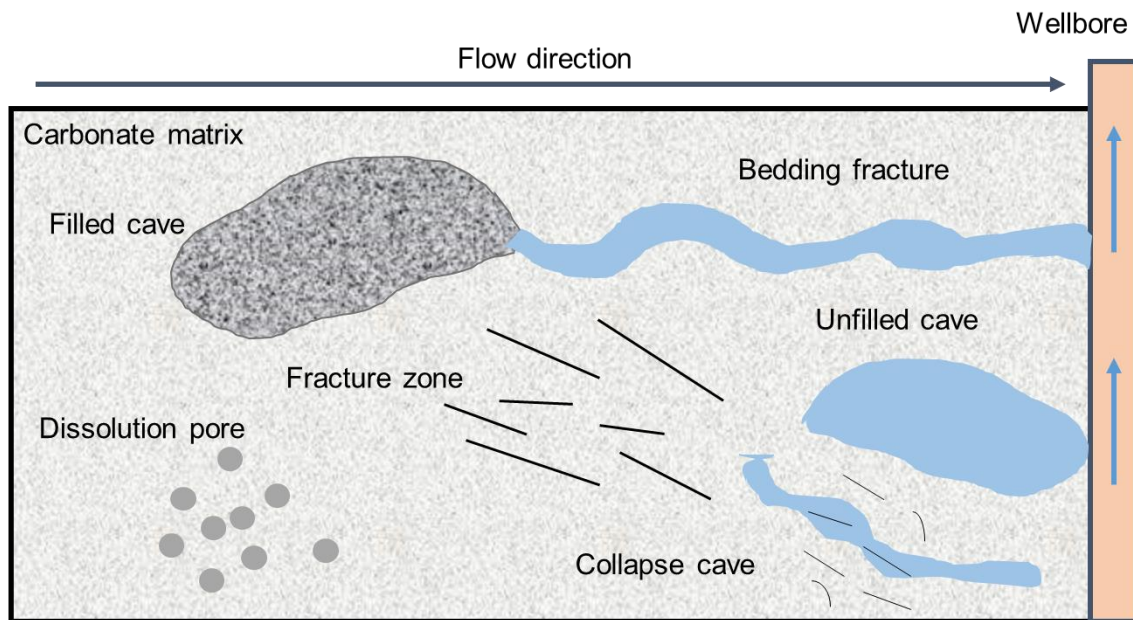
Figure 3. Flow media in the fractured vuggy reservoir. Modified from [2]

Wettability of the rock surface determines the spreading of fluids in the porous medium and is the key factor of fluid propagation during the flooding process. Figure 4 demonstrates the pore cross section where the wetting phase is located near the rock grains, and the non-wetting fluid occupies the large pores and can be easily displaced. Thus, the oil reservoir is preferred to be water-wet [12].
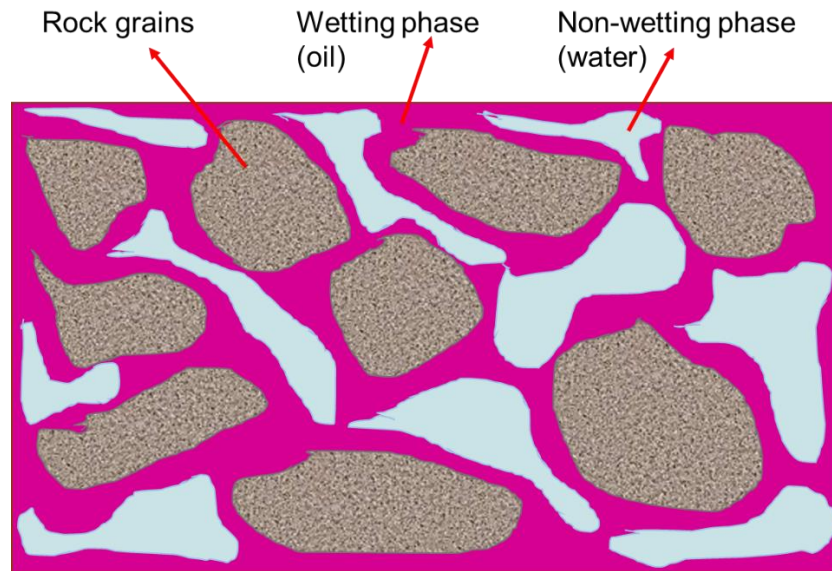
Figure 4. Pore cross section with distribution of wetting and non-wetting phase. Modified from [12]

The indicator of wettability is contact angle (CA) that is defined as the angle between the solid surface and the tangent to the droplet of the liquid at the point of contact, Figure 5. Contact angle can be measured in system "rock – water – oil" (Figure 5a, [28]) or "rock – water – air" (Figure 5b, [29]). The CA is always measured through the more dense phase and labeled as θ [30]. When the liquid wets the surface completely, the contact angle is zero, when the liquid does not wet the surface at all, the contact angle is 180°. The intermediate values indicate the degree of wetting of the surface by the liquid. The main classification is given in Table 1. However, the contact angle chosen as the cutoff varies in the literature [31,32].

It should be noted that surface roughness (Figure 5c) has a significant effect on the contact line behavior and therefore the CA values may vary on macro-scale (mm) and

26

micro-scale (μm) [15,24]. In addition, the wettability of carbonate rocks can be mixed-wet, i.e. having different preferences depending on saturation history [12] that complicates the development [28]. In rocks with mixed wettability micro-pores are water-wet while larger pores are oil-wet, or vice versa. It was reported in past literature that among 50 evaluated reservoirs, 84% of carbonates were oil-wet, 8% – intermediate-wet and only 8% were water-wet [33].
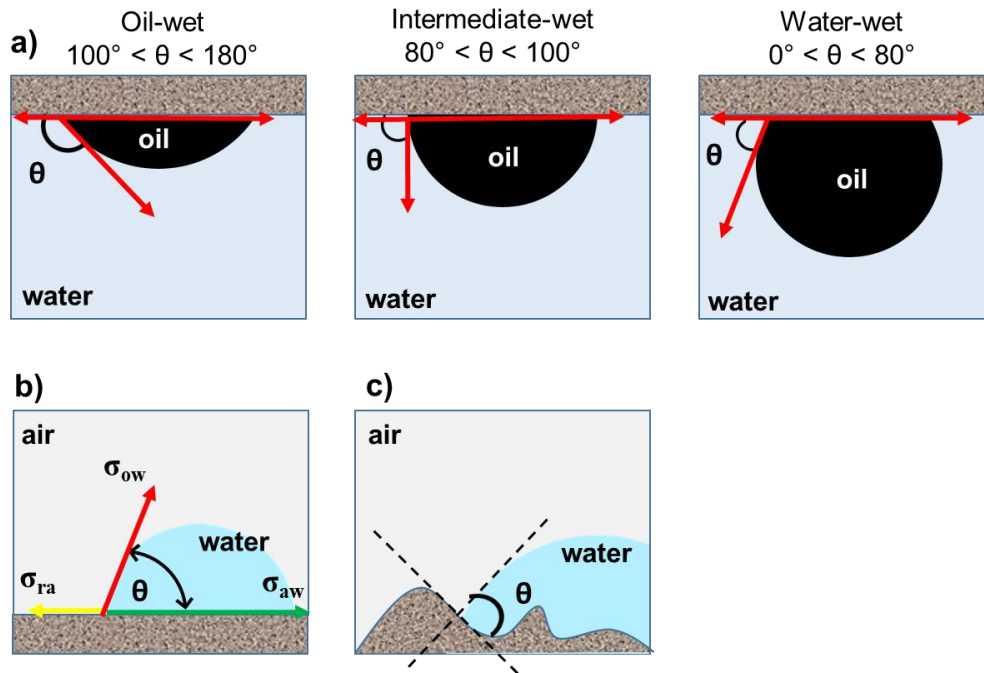
Figure 5. Wettability of reservoir rock based on contact angle measurements: (a) rock-water-oil contact; (b) rock-water-air contact; (c) contact line on a rough surface. Modified after [28,29,31,34]

Table 1. Rock wettability classification [32]

Type	Contact angle θ (°)
Water-wet	0 – 80
Intermediate-wet	80 – 100
Oil-wet	100 – 160
Strongly oil-wet	160 – 180

During the water flooding, driving pressure, gravity, and capillary forces all work together. The water displaces oil by flowing through the connected and vuggy porosity of the rock matrix, and the driving force is the pressure difference between the injection well and the production well. Capillary pressure arises due to the interaction of fluids with the rock surface and can cause the flow of fluids to be restricted [2,35].

Capillary pressure (P_c) is the pressure difference across the curved interface between two immiscible fluid phases that interact in a narrow capillary tube and can be expressed as follows according to Young-Laplace equation [30,36]:

$$P_c = P_{nw} - P_w = \frac{2\sigma cos\theta}{r_{pore}},\qquad(1)$$

Where σ is oil-water IFT, θ is the contact angle and r_{pore} is the pore-throat radius; P_{nw} is the pressure in a non-wetting phase, and P_w is pressure in a wetting phase. The capillary pressure can be positive or negative depending on θ value as $cos\theta \geq 0$ for the range of $0 > \theta > 90$ and $cos\theta < 0$ for $90 > \theta > 180$.

To achieve the effective production, the displacing fluid should overcome the capillary forces. When the $P_c > 0$, the capillary forces provide a driving force for spontaneous imbibition and effective fluid propagation. Negative capillary pressure, on the other hand, implies that more water pressure is required to release more oil in the case of imbibition. In water-wet systems, the capillary pressure is positive throughout the majority of the saturation range. The capillary pressure can be positive or negative as the wettability shifts toward oil-wetness, meaning that some of the surface will adsorb oil and some will absorb water [30,37]. The illustration of capillary pressure in narrow tubes is given in Figure 6. The hydrophilicity of carbonates can be increased using several methods: (1) changing brine ionic composition, (2) adding surfactants, (3) adding nanoparticles or (4) heating the reservoir through steam or hot water injection [4].
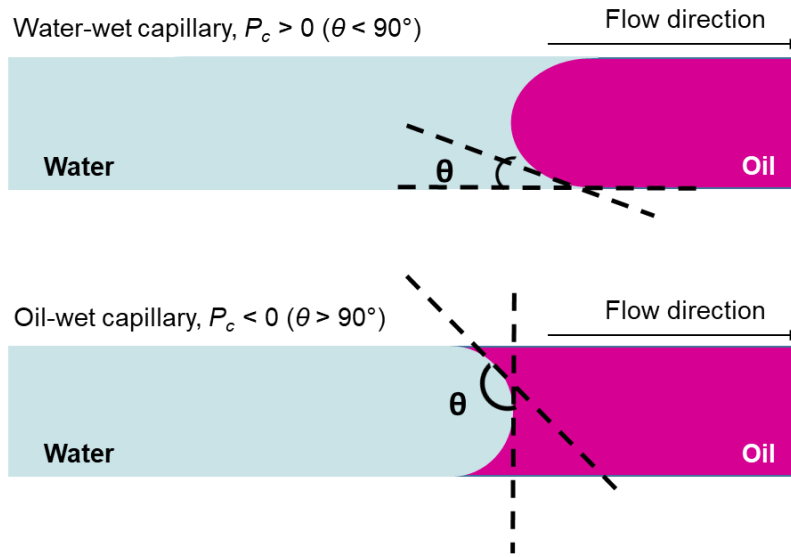
Figure 6. A simplified demonstration of water displacing oil in hydrophilic and hydrophobic channels. Modified after [37]

Overall, carbonate oil reservoirs are an important source of oil and gas, and their development requires a combination of geological, engineering, and technological expertise. Various enhanced oil recovery (EOR) techniques are implemented in oil reservoirs that are selected based on field lithological characteristics and water cut, oil properties, thermobaric conditions, economic feasibility, logistics and other important factors. The EOR methods applied for carbonate oil reservoirs are reviewed in the next section.

1.3. Enhanced oil recovery methods for carbonates

As it was discussed before, the two main challenges of carbonate reservoirs effective development are (1) complex structure and high heterogeneity and (2) rock surface oil-wetness. Figure 7 demonstrates the application of EOR methods by lithology. It can be seen that the number of implemented projects in sandstone reservoirs (78%) is significantly higher than in carbonates (18%) due to the complexity of their development [38]. These statistics indicate the potential for the advancement of carbonate reservoir development methods.

29
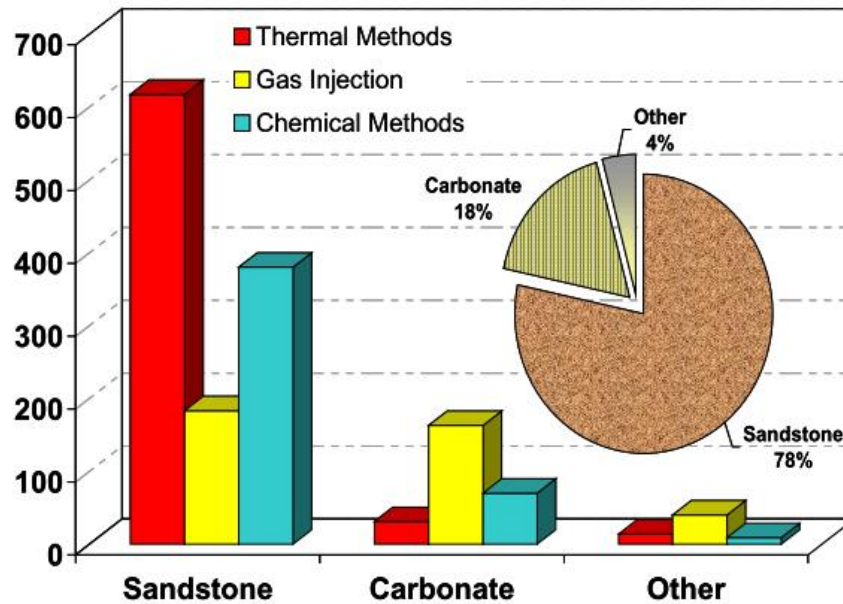
Figure 7. Statistics of EOR methods implementation by lithology (based on 1507 projects) [38]

Despite demonstrating the technical feasibility of different EOR methods in carbonate reservoirs, gas injection (either continuously or in WAG mode) remains the most widely used EOR technique in this type of rock formation. However, gas injection implementation is limited to oil gravity and reservoir pressure values. Thermal EOR methods have made a relatively minor contribution to global oil production from carbonate reservoirs. As for chemical EOR, polymer flooding is the main method proven to be effective in carbonate formations [2,38]. Implementation of chemical flooding allows avoiding the breakthrough of injected gas and thus result in improved sweep efficiency [2]. Polymer flooding is used for displacing fluid viscosity increase and sweep efficiency improvement due to reduction of mobility ratio value [39,40]. Although the polymer injection can lead to more effective oil displacement, an essential amount of trapped and adsorbed oil remains in carbonate layers. To produce this oil, surfactants should be injected [41,42].

1.4. Surfactant flooding in carbonates

For many years, significant efforts have been made to recover trapped oil from conventional mature reservoirs using surfactant injection as a post-waterflood procedure [42]. Surfactants are commonly used to improve microscopic sweep efficiency on the pore level through residual oil saturation reduction. Their main capabilities are rock wettability alteration towards more water-wet and oil-water interfacial tension reduction that lead to capillary number *(N_c)* value increase [35,43]. Capillary number is a dimensionless ratio of capillary and viscous forces [35,41,44,45]:

$$N_C = \frac{F_v}{F_c} = \frac{v\mu}{\sigma\cos(\theta)} , \qquad (2)$$

Where v is the velocity of the displacing fluid, μ is the viscosity of the displacing fluid, σ is the oil-water interfacial tension, θ is the contact angle. Typical waterflooding projects correspond to a capillary number in the range from 10^{-7} to 10^{-6}. In order to produce additional oil from the waterflood, the capillary number needs to be increase until $\sim 10^{-5}$ that can be achieved by capillary forces reduction, namely σ and θ decrease [28,46]. To remove oil from pores, the differential pressure must be combined with other forces to overcome the high capillary pressure [43].

The interfacial tension is attributed to the energy that keeps the stabilized interface between non-miscible phases. When IFT decreases, it becomes easier to destroy the two-phase contact and thus reduce capillary forces and improve interface elasticity [47,48]. As it was discussed above, wettability defines the spreading of water and hydrocarbon phases in porous medium, as well as the affinity of immiscible fluids for a specific solid [36]. Wettability alteration (WA) towards water-wetness leads to capillary forces decrease and thus recovery improvement. Although it has been discussed in great detail, there is still disagreement over the respective contributions of IFT reduction and wettability modification. Deng et al. [32] found that IFT reduction alone leads to improved residual oil recovery in all wettability cases. On contrary, the wettability alteration effect varies because of initial wetting conditions. The main types of surfactants applied in EOR should be discussed.

All surfactants can be divided into two main groups based on the type of hydrophilic part – ionic and nonionic. Ionic surfactant, it their turn, can be classified into anionic, cationic and zwitterionic [49,50]. They are schematically shown in Figure 8.
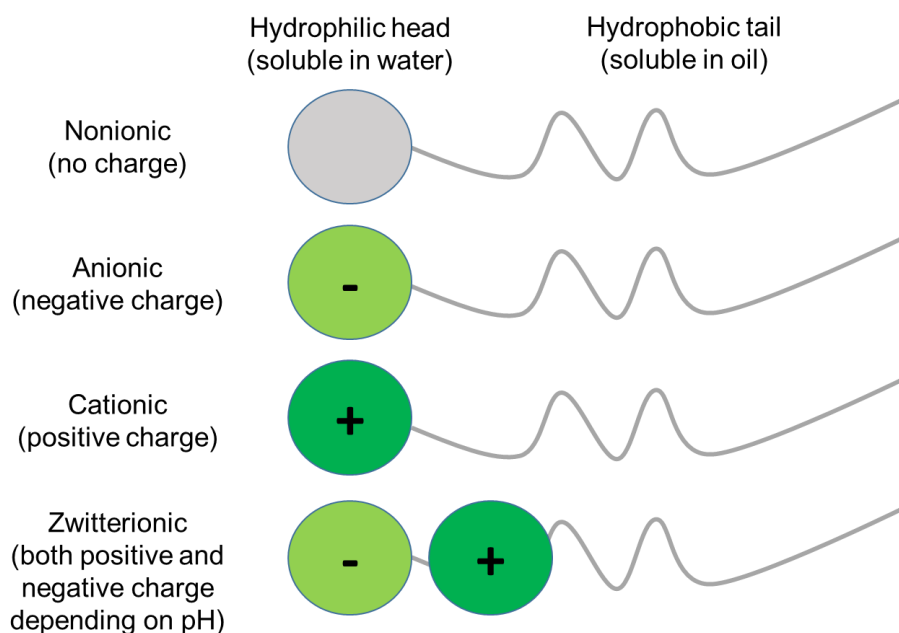
Figure 8. Main types of surfactants based on headgroup charge

Molecules of nonionic surfactants are neutral and have no charge in water. Their hydrophilic parts do not dissociate in water and thus the main force that governs the dissolution is hydrogen bonding between oxygen atoms in surfactant headgroups and water molecules [42,43,51]. The main types used in EOR are alkoxylated alcohols (fatty alcohol ethoxylates, fatty alcohol propoxylates, alkylphenol ethoxylates) and sugar-based surfactants (alkylpolyglucosides). Nonionic surfactants are mainly used as co-solvents during chemical flooding. Their main limitation is cloud point – stability loss at specific temperatures in the presence of salts [44].

Anionic surfactants dissociate into metal cation and a big anion that is negatively charged. The main examples of anionic surfactants are alkyl sulfates, alpha olefin sulfonates, methyl ester sulfonates, alkylbenzene sulfonates, sulfosuccinates. Besides that, anionic surfactants with two hydrophilic groups are known such as ethoxylated sulfates,

sulfonates and carboxylates [43,50,52]. They demonstrate a better salinity resistance. Anionic surfactants are mainly employed in EOR because of their strong ability to reduce oil-water IFT [43] but they have not demonstrated good wettability alteration properties [53,54]. The main limitations of anionic surfactants use are (1) poor temperature and salinity tolerance and (2) tendency to high adsorption in carbonates so some additional chemicals should be added to decrease the adsorption loss [55,56].

Cationic surfactants carry a positive charge when dissociated in water. The main classes are quaternary ammonium salts, amine oxides and ethoxylated amines [50]. They are not able to achieve ultralow interfacial tension values like anionic ones, but have demonstrated a good wetting ability in carbonate rocks due to removal of adsorbed oil components [57].

Amphoteric (zwitterionic) surfactants carry both positive and negative charge after dissociation in water depending on pH value. Despite their promising properties (stability in harsh reservoir conditions, IFT reduction, etc.) there are no known field projects with zwitterionic surfactants because of their high cost.

The main restrictions of surfactant flooding implementation in carbonates are the following: (1) high temperature, (2) high salinity and hardness ions content and (3) significant adsorption of anionic surfactants onto carbonate rock [58]. Harsh reservoir conditions (HTHS – high temperature and high salinity) cause the stability loss of surfactant compositions. Bourdarot and Ghedan in 2011 [58] reported the stability limitations of surfactants and polymers available in commercial scale that are shown in Figure 9. It can be seen that surfactant flooding can be conducted only under low and moderate temperatures and salinities. Surfactant compositions with high salinity tolerance degrade at high temperatures and vice versa. However, over the past 10 years, new products have been released to the market able to maintain more severe conditions [59,60].
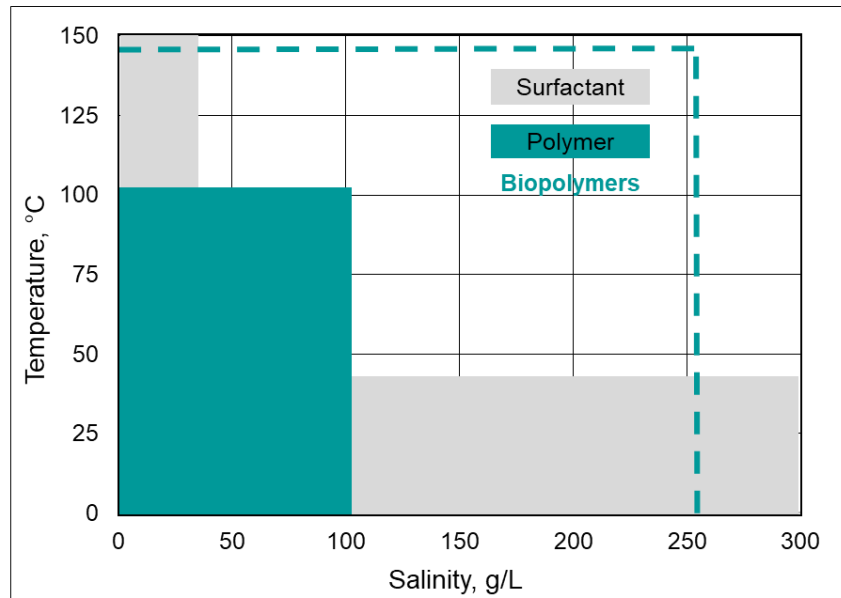
Figure 9. Salinity-temperature cross plot to compare conditions of offshore fields to market available surfactants and polymers. Redrawn from [58]

Hence, not all classes of surfactants are suitable for application in carbonates, especially in reservoirs with harsh conditions. The effectiveness of surfactant flooding is mainly influenced by IFT reduction, wettability alteration and surfactant retention on the rock surface [61,62]. Thus, all these three aspects will be discussed in next paragraphs.

1.4.1. Interfacial tension reduction

The interfacial tension is highly influenced by such factors as salinity, temperature, alkane carbon number (ACN) of oil and surfactant molecular structure [35,51]. The optimum surfactant concentration is usually selected on the base of laboratory screening taking into account the CMC value of a particular surfactant and target conditions.

The quantity of surfactant molecules per unit surface area determines the interfacial tension of surfactant solutions. The decreased IFT is caused by a given surfactant's higher surface concentration of surfactant molecules [63]. However, the interfacial concentration of surfactants is a necessary condition but not sufficient one. The key factor in IFT reduction is surfactant's molecular size, which is reflected in the cross-sectional area of the molecules that are adsorbed [64].

34

Electrolytes have a stronger impact on anionic surfactants that are negatively charged in the aqueous phase, and salinity effect refers to two factors. First is surfactant solubility in water decrease. Consequently, surfactant partitioning in oil phase improves due to the salting-out effect. Second, counterions reduce the electrostatic repulsion between similarly charged heads of surfactant molecules, thus making it easier for the molecules to achieve the interface. The ability of bivalent cations Ca^{2+} and Mg^{2+} to binding with surfactant molecules is higher than that of Na^+ ions [64–66]. The effect of counterions type on molecular packing is shown in Figure 10.
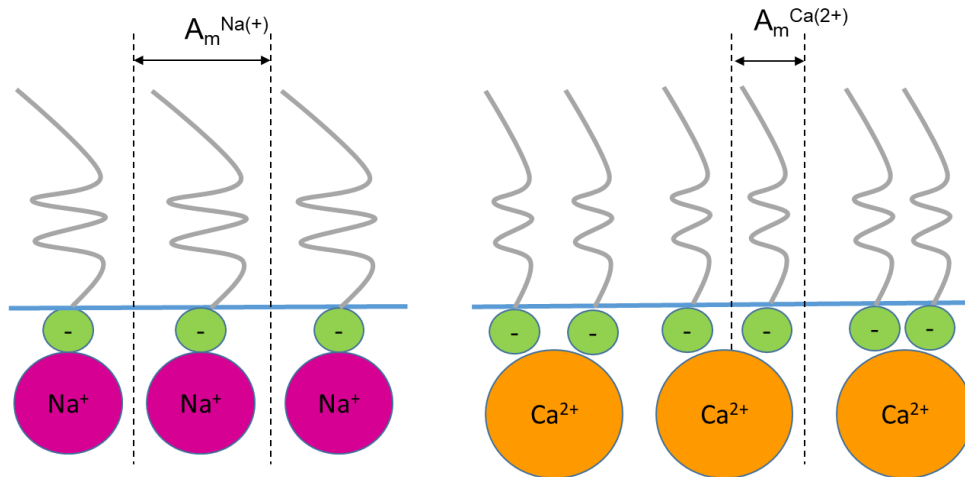
Figure 10. Schematic illustration of counterion effect on molecular packing of anionic surfactants. Modified from [66]

Temperature also plays a significant role in interfacial behavior of surfactants, especially of nonionic ones as they lose stability when the temperature increases due to destruction of hydrogen bonds between surfactant and water molecules [35,64]. Besides that, temperature growth accelerates the adsorption rate of surfactant molecules at the interface that leads to IFT drop. Another explanation is attributed to oil viscosity reduction that also inputs in surfactant migration rate [51].

Oil properties, namely alkane carbon number and content of active components (resins and asphaltenes) also play a significant role in surfactant molecules arrangement on the oil-water interface. Oil active components may affect the characteristics of mixed

adsorption layer on the boundary with water. This mechanism of oil polar components effect on IFT was proposed by S.S.Sheng [67] and is illustrated in Figure 11. The authors suggest that resins and asphaltenes influence on molecular packing density of surfactants through interactions with hydrocarbon tails of surfactant molecules.
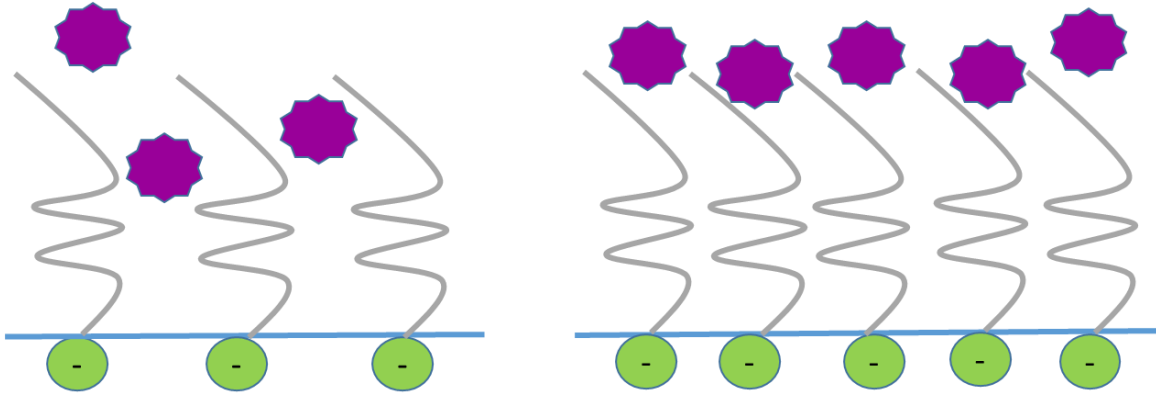
Figure 11. Schematic mixed adsorption layer of surfactants and resins/asphaltenes at oil-water interface

The significance of all these factors (temperature, salinity and hardness ions content, oil alkane carbon number) explain why the surfactant compositions are selected individually for each chemical flooding project.

1.4.2. Wettability alteration by surfactants

Wettability plays an important role in chemical flooding, and a relative contribution of IFT reduction and wettability shift is still discussed [47,68]. As wettability modifiers for carbonates, almost all kinds of surfactants used in enhanced oil recovery (EOR) were investigated. Yao et al. [69] performed a statistical analysis of surfactants tested as wetting fluids for huff-n-puff injection in carbonate rocks based on data reported in scientific publications. The data shows that cationic surfactants dominate the distribution, with the remaining surfactants falling into the following categories: anionic (28%), nonionic (19%), zwitterionic (4%), gemini (1%), and combinations (12%). In addition, the type of surfactant affects the wettability shift process, and the mechanisms will be discussed below [70,71].

Standnes and Austad studied a list of surfactants with a focus made on cationic ones of the cetrimonium bromide C_nTAB family [54,72]. The authors found that cationic surfactants restored the hydrophilic surface character by irreversibly desorbing carboxylic oil components from the chalk. In addition, a spontaneous imbibition test that lasted 30 days at 70°C resulted in the displacement of 70% of the oil. The proposed mechanism of wettability alteration (WA) by the authors involved the formation of ion pairs between negatively charged adsorbed polar oil components and positively charged cationic surfactants, which was followed by the "washing" of these oil components [54,72]. The chemical structure has a strong impact on oil displacement efficiency and decreases in the following order: $C_{10}TAB \approx C_{12}TAB > C_{16}TAB > C_8TAB$ [54].

Zwitterionic or amphoteric surfactants are chemicals with both negatively and positively charged head groups in their structure [43], and the charge of the molecule depends on the pH value of the system. Qi et al. [73] tested the wetting ability of several betaines in carbonates through contact angle measurements and a spontaneous imbibition test in Amott cells at 95°C and salinity of 67 g/L. The contact angle values for two surfactant samples dropped from 95° to 24° and 27°. The additional oil recovery produced by these surfactants imbibition after water imbibition stage was 14% and 6%, respectively. Han et al. [74] reported that a betaine-type amphoteric surfactant reduced the contact angle of a carbonate rock sample from 160° to 132° and displaced 66% of oil at 75°C for 23 days. Another of that kind of surfactant recovered 50% of the oil and displayed a contact angle value of 67°. However, the application of amphoteric surfactants on an industrial scale is limited due to their expensive cost [44].

Anionic surfactants are less efficient in wettability alteration than cationic ones as they cannot permanently desorb the carboxylic components of oil [54]. However, numerous research groups have conducted in-depth studies on the wetting properties of anionic surfactants. The proposed mechanism of wettability alteration by anionic surfactants implies hydrophobic interactions of surfactant tails with adsorbed oil components followed by the formation of a double-layer structure [54,75]. Hydrophobic interactions are weaker and more easily broken than electrostatic interactions created by

cationic surfactants. As a result, the change in wettability toward the water-wet condition is reversible [54,75]. Chen and Mohanty evaluated Enordet A092 surfactant (a branched C16 alkoxyl sulfonate with 9 EO groups) dissolved in seawater as a wetting fluid for the dolomitic core. The authors reported that A092 shifted the wettability towards a water-wet state and displaced 53% [76] and 70% [77] of oil at 100°C in spontaneous imbibition tests with some additives to the surfactant composition. Jarrahian et al. compared the wetting ability of cationic C_{12}TAB, nonionic Triton X-100, and anionic SDS surfactants and described their mechanism through TGA (thermogravimetric analysis), AFM (atomic force microscopy), and FTIR (Fourier transform infrared spectroscopy) analysis. The wettability of the rock changed to neutral-wet (contact angle of 80°) as a result of sodium dodecyl sulfate (SDS) surfactant adsorption on the rock surface due to hydrophobic interactions mechanism. Nonionic and cationic surfactants demonstrated better effectiveness. As such, Triton X-100 decreased the CA until ~60° and C_{12}TAB until ~20° [75].

Nonionic surfactants have shown promising results in wettability alteration. Wu et al. [78] examined the wetting ability of several nonionic surfactants of Tegritol (ethoxylated C11-C15 secondary alcohol), Igepal (nonyl phenoxy poly(ethyleneoxy) ethanol), and Neodol (C12-C15 linear ethoxylated alcohol) series. Calcite crystals aged with various naphthenic acids dissolved in decane were used as rock samples, and the experiments were conducted in deionized water at 25°C. Igepal surfactant surpassed the other compounds in terms of effectiveness with a 51% oil recovery. Das et al. [70] evaluated two secondary alcohol ethoxylates (SAE-9 and SAE-15) as wettability modifiers. Contact angle measurements on calcite samples revealed that both SAE-9 and SAE-15 reduced CA values, and SAE-15 achieved 47% oil recovery at 50°C in the presence of NaCl and $CaCl_2$ salts and SO_4^{2-} ions. SAE surfactants can be used in mixtures with anionic sulfonates to increase the cloud point and expand the range of reservoir conditions where they can be used [79]. Souayeh et al. developed a cost-effective wettability alteration (WA) process based on a combination of polyethoxylated nonionic surfactant with low-salinity brine [80]. Contact angle measurements showed that the

38

wettability changed from oil-wet to water-wet state. TGA analysis results proved that nonionic surfactants partly removed carboxylic oil compounds [80].

1.4.3. Adsorption of surfactants onto carbonate rock

The leading cause of reduced surfactant flooding efficiency and economic performance is the loss of surfactants in the reservoir. Depending on the mechanism, it can be divided into precipitation, phase trapping, and adsorption. Numerous factors, including oil saturation, rock mineralogical composition (primarily clay content), reservoir temperature, brine salinity, the presence of divalent metal cations, and surfactant structure, all affect the adsorption of surfactants on rock [26,42,45,81,82].

Adsorption can be considered as the distribution of the adsorbate (the substance to be adsorbed) between the interface and the bulk solution. This process can take place if the interface is energetically more appealing to the surfactant molecules than the bulk. The adsorption process is driven by covalent bonding, electrostatic attraction, hydrogen bonding, formation of molecular associates, solvation, and desolvation. Total adsorption is usually the combined result of all or several of these forces [83]. Depending on the interactions involved, the adsorption can be practically divided into physical and chemical. Physical adsorption is caused by electrostatic interactions, hydrogen bonds, and interactions between hydrophobic sites/radicals. It is a weak and reversible process, characterized by a high velocity of a process and the formation of multilayers. Covalent bond formation results in irreversible chemical adsorption with substantial energy changes. The defining characteristics of chemisorption are low rate of the process and the formation of monolayers [84]. In a system where the ionic surfactants and the rock surface are charged, electrostatic interactions play a leading role in adsorption.

It is commonly known that the carbonate rocks are predominantly oil-wet or mix-wet because of adsorbed surface-active oil components such as resins, asphaltenes, or carboxylic acids [15,54,85]. The surface charge of calcite is related to the reservoir brine pH and zero point of charge (ZPC) that determines the excessive species on the surface [86]. The surface is negatively charged above ZPC, and positive below ZPC that varies in

the range between 8 and 9.5 for calcite [71]. As it was accepted that brine pH in carbonates is below ZPC, the calcite surface charge tends to be positive [32,71]. Thus, both hydrophilic and hydrophobic interactions can occur between the adsorbed polar oil components and the injected surfactants. In the case of hydrophilic interactions, ionic pairs form between surfactant "heads" and the polar oil components [87]. In hydrophobic interactions, intermolecular bonds are formed among the "tail" of the surfactant molecule and the adsorbed components of oil [54].

1.4.4. Application of surfactant adsorption inhibitors

The loss of anionic surfactant due to adsorption is a severe issue of chemical EOR processes in carbonate reservoirs. Thus, several strategies have been proposed to reduce surfactant adsorption on the rock. Application of cationic surfactants (they adsorb much less than anionic surfactants), salinity gradients during injection, and adding adsorption inhibitors to the composition [42]. So-called "sacrificial agents" are used as surfactant adsorption inhibitors, and they can be divided into three main groups: alkalis, polyelectrolytes and nanoparticles. The first group includes organic and inorganic alkalis, which can change the charge of the rock surface to negative. The second group comprises polyelectrolytes ready to be more actively adsorbed than the surfactant itself [88–90]. Finally, nanoparticles are solid ultrafine particles with the diameter ranging between 10 and 100 nm (sometimes up to 500 nm). They are arranged at the interface thus not allowing surfactant molecules to adsorb on the rock surface. The schematic mechanisms of alkalis, polyelectrolytes and nanoparticles action are shown in Figure 12.
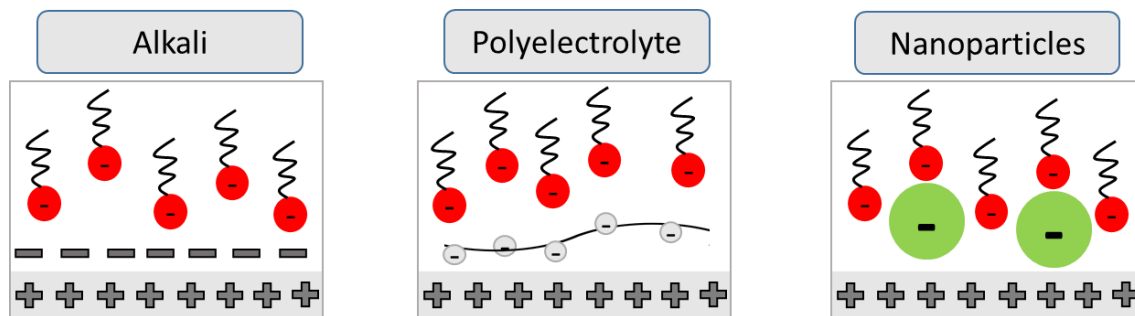
Figure 12. Mechanism of different adsorption inhibitors action

40

One of the most common inhibitors of surfactant adsorption is alkali. Most surfactants used in oil production are anionic, and the carbonate rock is typically charged positively. When a negative potential is created between reservoir brine and rock due to hydroxide ions OH$^-$, the surfactant molecules repel, resulting in reduced adsorption [8,9]. The recommended pH range is 9÷12. The most commonly used alkalis are sodium hydroxide NaOH and sodium carbonate Na_2CO_3 [52,93]. The main limitation of using them as adsorption inhibitors in hard water with high TDS content is the possibility of precipitation. As a result of salts' reaction in brine with alkali, insoluble or poorly soluble hydroxides can be formed [84]. In harsh reservoir conditions, alternative alkalis have been investigated [94–96].

Recently, *sodium metaborate NaBO$_2$* was suggested as an alternative to traditional alkalis [97,98]. It is a chelating agent and forms complexes with calcium and magnesium cations, increasing the surfactant compatibility threshold with divalent cations to 6000 ppm in solution [92]. At low temperatures (55°C) and water salinity of 147.5 g/L with a hardness of ~20k ppm, the compositions that contain an anionic surfactant, polymer, and 3.75% or 2.4% of sodium metaborate are stable. In the first case, the surfactant adsorption on the carbonate rock is 0.197 mg/g-rock; in the second case, it is 0.231 mg/g-rock. The oil recovery factor obtained from the core flooding experiments was 99% and 94%, respectively [95].

Sodium tetraborate Na$_2$B$_4$O$_7$ was proposed as a less expensive alternative to sodium metaborate. It can decrease the adsorption of alkylbenzene sulfonate onto kaolinite surface in the presence of 10 g/L NaCl at 30°C better than more common sodium carbonate and sodium metaborate despite the lower pH value [99]. The performance of sodium tetraborate was also evaluated by Azam et al. [100,101]. Its application as an additive to an alkyl sulfonate surfactant decreased adsorption value from 0.96 until 0.28 mg/g-rock at 25°C. Berea sandstone was used in this study, and the pH value reached 10.5.

Ammonium hydroxide NH$_4$OH has also been considered as a component of ASP or AS flood formulations [11,15,16]. Sharma et al. [95] developed an ASP composition that contained 3% NH$_4$OH alkali. Experiments showed that the surfactant adsorption on the

carbonate rock was 0.25 mg/g-rock, and the oil recovery factor was 87.5%. This result indicates that ammonium hydroxide was stable under reservoir conditions and has not led to precipitation and pore space blockage.

Sodium silicate Na_2SiO_3 was also used as an alternative to alkali in various surfactant flooding scenarios [104]. The surfactant adsorption on the rock was 0.15 mg/g-rock, and the oil recovery factor was 69.6%.

In addition to inorganic alkalis, the use of organic ones such as sodium polyaspartate (sodium salt of polyaspartic acid) is possible. Its salinity tolerance is higher than of inorganic alkalis sodium carbonate, hydroxide, and metaborate. Sodium polyaspartate can be used in brines comprising Ca^{2+}, Mg^{2+}, Fe^{2+}, Sr^{2+}, Ba^{2+} ions [105]. However, the sodium polyaspartate effectiveness as an adsorption inhibitor needs further investigation.

One more organic alkali is ethanolamine C_2H_7NO [19,20]. The introduction of ethanolamine to surfactant composition leads to a further reduction in interfacial tension at the boundary with oil and recovery factor increase. However, the ethanolamine performance as an adsorption inhibitor requires further research.

Polyelectrolytes are the second type of sacrificial agent used to decrease the adsorption loss of anionic surfactants. They should be of the same charge with surfactant molecules and exhibit the ability to adsorb more actively onto the rock surface than anionic surfactants. This mechanism is called "competitive adsorption". Electrostatic repulsion develops between the solid surface and surfactants when electrolytes are preferably adsorbed on rock and produce a negatively charged layer [88,89,108].

ShamsiJazeyi et al. [88,89,108] investigated a list of sodium polyacrylates with different molecular weights supplied by several manufacturers. The results showed that polyacrylates' molecular weight and concentration play crucial role in the competitive adsorption process. The increasing the polyacrylate mass leads to its efficiency improvement, but is limited with the mass value of 4500 Da. At this mass and above, the desorption of molecules from the rock surface is almost impossible. Thus, the recommended molecular weight of sodium polyacrylate is 4500 Da. It should be noted that

42

surfactant has no effect on the adsorption of polyacrylate, and the amount of surfactant adsorbed can be decreased by almost an order of magnitude in its presence.

Sodium polystyrene sulfonate (PSS) is another polyelectrolyte that decreases surfactant adsorption onto the rock surface. The effectiveness of PSS as a "sacrificial" agent has been studied under high salinity conditions over 300 g/L. It was found that the effectiveness depends on PSS molecular weight, and it must be above 20 kDa. Application of PSS can reduce adsorption by five times [109].

It is a challenge to select or develop surfactant compositions suitable for target reservoir, especially if it has harsh conditions. Application and main properties of anionic-nonionic surfactants with two hydrophilic groups is discussed in next section.

1.5. Alkyl ether carboxylate surfactants

As the majority of surfactants used in sandstones are not stable or not suitable for carbonates, the researchers from industry and academia are searching the new effective chemicals. A particular focus is currently made on nonionic-anionic surfactants. Alkyl ether sulfates show tolerance to brines with high hardness ions content, but their use is limited to 60°C. Alkyl ether sulfonates demonstrate excellent thermal stability, but the production cost is high [59]. Hence, alkyl ether carboxylate (AEC), or fatty alcohol polyoxyethylene ether carboxylate surfactants, attract scientists' attention [60,67,110–114].

Carboxylates, or soaps like sodium stearate ($C_{17}H_{35}COONa$), are perhaps the earliest known surfactants [115]. Their primary benefits include low cost and excellent biodegradability; nevertheless, in brines containing divalent cations Ca^{2+} and Mg^{2+}, they have a tendency to form sediments. To solve this problem, a number of oxyethylene (EO) units were introduced into the molecule, thus expanding its hydrophilic part. As a result, alkyl ether carboxylates with structure $RO(CH_2CH_2O)_nCH_2COONa$ or $R(CH_2OCH_2)_nCOONa$ were obtained [49,50,115]. They have two hydrophilic groups (-CH_2COO- and –CH_2CH_2O-) and hence exhibit both anionic and nonionic properties displaying temperature stability and salt tolerance. AEC surfactants are usually abbreviated

as C_xE_yA (else C_mE_nA, C_xE_yC, C_xEO_yC, A_xEC_y-Na), where x is the number of carbon atoms in the alkyl chain, and y is the number of ethylene oxide units [67,114,116]. The general structure is given in Figure 13.
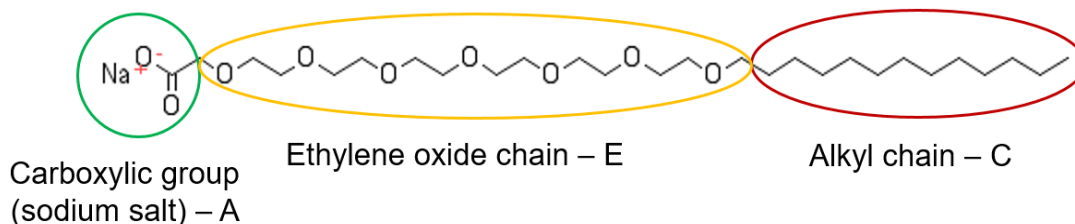
Figure 13. General structure and abbreviation of alkyl ether carboxylates by the example of sodium trideceth-7 carboxylate $C_{12}E_7A$

Interfacial behavior. Liu et al. [66] investigated the behavior of sodium laureth-4 $C_{12}EO_3C$ carboxylate synthesized in a home laboratory; $C_6 - C_{14}$ alkanes were used as hydrocarbon phase. The temperature and salinity effect on dynamic interfacial tension was investigated. The temperatures from 30 to 85°C were considered, and the salts used were NaCl, $CaCl_2$, $MgCl_2$. The authors found that the sodium chloride concentration has no significant impact on the IFT value. At the same time, the presence of divalent cations in the solution leads to the IFT decrease until an ultralow value of 10^{-4} mN/m at temperature 85°C. Moreover, magnesium ions have a more substantial influence on the IFT reduction than calcium ions. Adding a nonionic fatty alcohol polyoxyethylene $C_{12}E_3$ to nonionic-anionic $C_{12}EO_3C$ results in an ultralow IFT value of 10^{-5} mN/m in the presence of sodium and calcium chlorides in the system at temperature 85°C, using n-dodecane as the hydrocarbon phase [65].

S.S.Sheng [67] evaluated the interfacial performance of anionic-nonionic AEC series synthesized in their laboratory. The surfactant molecules contained various numbers of EO units, and the alkyl chain length also varied. N-alkanes, crude oil, and several oil models were used as hydrocarbon phases. By calculating the space taken up by AEC molecules at the interface, the authors came to the conclusion that the quantity of oxyethylene units and hydrophilic-lipophilic balance (HLB) are crucial factors in the IFT

reduction. The oxyethylene chain forms a spiral located on the border between two immiscible phases. At the contact, the AEC molecules with shorter EO chains produce a denser adsorption layer.

Zhang et al. [117] compared the surface properties of AEC with branched and linear hydrocarbon chains with 5 and 7 EO units abbreviated as $A_{13}EC_5$-Na and $A_{13}EC_7$-Na. The authors experimentally determined static and dynamic surface tension values and compared these surfactants' foaming and wetting properties. It was assumed that alkyl ether carboxylates with branched alkyl chains more effectively reduce surface tension than AEC with a linear one. The CMC value of a surfactant with 5 EO units is lower than that of an AEC with 7 EO groups. The authors propose that $A_{13}EC_5$-Na molecules adsorb onto the interface faster than $A_{13}EC_7$-Na.

Belhaj et al. [60] described a partitioning behavior of binary surfactant mixture consisting of commercially available alkyl ether carboxylate and alkyl polyglucoside (APG), which increases salt tolerance and thermal stability. The authors investigated long-term stability (90 days), and oil-water interfacial tension of surfactant compositions with different mixing ratios under reservoir conditions reproduced in the laboratory – temperatures 80 and 106°C and various brine salinities up to 32k ppm.

Wetting ability. Research groups from different universities tested AECs as wettability modifiers. Standnes and Austad evaluated the effectiveness of an AEC with 9 EO groups of Akypo series at 40°C and mineralization of ~45 g/L [54]. The authors found that Akypo surfactant solution decreased the advancing contact angle on the oil-wet calcite surface until the value of 48±3° compared with 70±3° of pure brine. Akypo surfactant can be imbibed into the porous media in significant amounts but showed low displacement efficiency and swept only traces of oil [54]. It should be noted that the highest activity of AECs is known to occur in the presence of salts and heating. For example, AECs reduce the interfacial tension between oil and water to extremely low levels (10^{-2} – 10^{-3} mN/m) when bivalent cations like Ca^{2+} and Mg^{2+} are present and when the temperature is high (70°C and above) [59,60,66,67,112,118–120]. Souayeh et al. [121] studied the performance of an AEC Soloterra 938 in artificial brine and a diluted brine (197 g/L and

1.97 g/L, respectively) under the temperature of 75°C. The results revealed that a 0.3 wt% surfactant solution in a low salinity brine reduced the contact angle of the oil-wet calcite sample from 160° to 130° but resulted in 61% recovery factor in a spontaneous imbibition test. The authors also discovered that adding a nonionic ethoxylated alcohol to an anionic AEC can increase its efficiency [121].

Adsorption capacity. The adsorption of AECs on the rock is also a subject of interest. Herawati et al. [122] recently studied the adsorption of an AEC with the linear structure on sandstone with Ca-montmorillonite and kaolinite clays. Then, the authors correlated the adsorption of surfactants with wetting ability. The study showed that the contact angle and adsorption have an inverse relationship: the higher the adsorption, the lower the contact angle (stronger wetness is attained). Belhaj et al. studied the adsorption of an AEC-based surfactant composition and alkyl polyglucoside (APG) under harsh reservoir conditions separately and in a mixture [114]. Sand rock (mainly quartz) was used as the adsorbent, the operation temperature was 106°C, and brine salinity was 32k ppm. The highest adsorption value was about 2 mg/g-rock at 1 wt. % of surfactant, but extensively increased in the presence of crude oil due to surfactant partitioning in the hydrocarbon phase [123,124]. An increased interest in anionic-nonionic surfactants during the last 10 years resulted in many publications that describe their performance under various conditions. A brief summary of published data is given in Table 2.

Table 2. Recent experimental studies of AECs rock-fluid interactions

Reference	Surfactant	Rock	Temperature, °C	Salinity, g/L	Experiments	Main outcomes
[114]	AEC-based commercial blend in mixture with APG	Quartz (model)	106	32	Static adsorption test and prediction	The adsorption capacity of AEC and APG was 2 mg/g and 5.6 mg/g at 1 wt.%
[59]	AEC-based commercial blend	Berea sand grains	100	30	Dynamic adsorption in a sandpack	Dynamic adsorption on the sand was 0.2 mg/g
[121]	Soloterra 938	Iceland Spar	75	196	Contact angle, zeta potential,	AEC decreased the contact angle from 160° to 130° and

					spontaneous imbibition test	recovered 61% OOIP
[125]	Commercial AECs with linear and branched structure	Iceland Spar	75	196	Contact angle measurements, TGA, static adsorption test	WA from a strong oil-wet to a strong water-wet state was achieved by an AEC with the shortest alkyl chain (most hydrophilic)
[122]	$C_{12}E_7A$	Quartz, quartz+montmorillonite, quartz+kaolinite	60	7.42	Static adsorption test, contact angle measurements	The higher the adsorption of surfactant, the smaller CA achieved.

1.6. Laboratory methods of surfactant flooding performance assessment

The aim of surfactant screening in laboratory is to find an effective and economically feasible formulation [51]. Technical screening criteria of surfactants includes several basic requirements: (1) stability under ambient and reservoir conditions and compatibility with alkalis or polymers present in the composition, (2) IFT value of 10^{-2} – 10^{-3} mN/m, (3) adsorption on rock lower than 1 mg/g-rock (typically 0.1 – 0.2 mg/g-rock), (4) commercial availability and economic feasibility and (5) incorporation in EOR [126].

The screening procedure includes a number of standard tests that can be divided in two groups: (1) conducted in bulk and (2) conducted in porous media. A workflow of a full screening procedure is schematically illustrated in Figure 14, but not all experiments are usually performed.
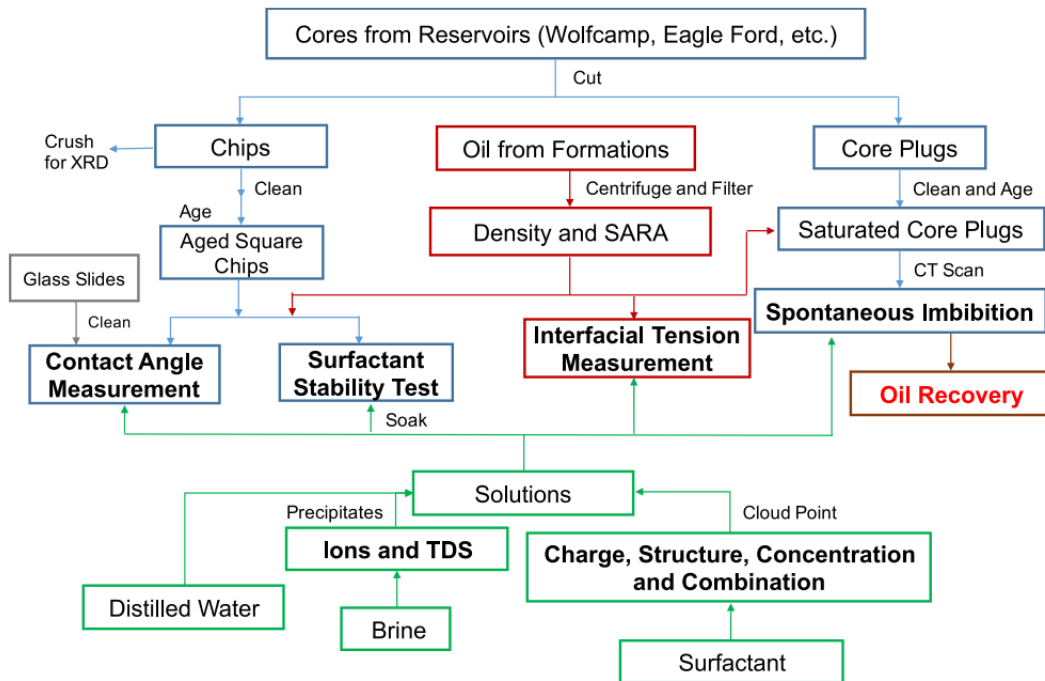
Figure 14. A comprehensive workflow of surfactant selection [36]

A typical screening starts with a compatibility (with brine) and stability tests (under reservoir conditions). Then, stable compositions are selected and used in oil-water interfacial tension measurements. Several techniques of IFT measurements are known, such as spinning drop for measurements in dynamic mode, and Du Noui ring method and Wilhelmy plate for static measurements. IFT measurements can be supplemented with a phase behavior test with oil, i.e. salinity scan. After that, wettability modification of core chips and adsorption capacity in static regime are evaluated [41,44,51].

After the first part of screening is finished, the most promising surfactant formulations are examined in the porous medium. A commonly used method of surfactant oil displacement ability assessment is core flooding test that allows to mimic fluid flow under reservoir conditions [28]. Coreflooding can be conducted in core cylindrical samples or sandpack models composed of crushed rock. Various techniques are applied for saturation control depending on practicability and technical capabilities such as computed tomography [127], X-ray scanning [128] or NMR [129].

48

There is an opinion in recent literature that the future of surfactant screening belongs to microfluidics [51]. Microfluidics studies the movement and distribution of liquids in nano-, micro- and macroscale. The experiments are conducted in transparent microfluidic chips that are typically produced from polymers or silica covered with glass. A characteristic advantage of using microfluidics for EOR is the ability to visualize single-phase or multi-phase fluid flow in the pore space. Thanks to this, it is possible to analyze both the flow at the microscale with the distribution of phases and hidden local effects [130–133].

According to Sheng [41], minimum three tests should be conducted: stability test, salinity scan and coreflooding. However, the program may be changed depending on target object properties. For example, in low-permeability unconventional layers the main focus should be made on wetting ability of surfactants, while in conventional reservoirs IFT still has the leading role. The behavior of surfactants on molecular scale can be studied with computational instruments such as molecular dynamics.

1.7. Computational methods for surfactant performance assessment

As the number of experiments that can be conducted is limited with time and availability of synthesized samples, computational methods can be applied to scale up the studies. Besides that, simulations of surfactants behavior can provide molecular insight of their aggregation, interactions, arrangements, etc. Molecular dynamics (MD) simulation is a powerful computational method for studying the behavior of surfactant molecules at the molecular level. The principle of MD simulation is to use a numerical approach to simulate the motion and interaction of atoms and molecules in a system, based on classical mechanics and statistical thermodynamics [134–138].

In the context of surfactants, MD simulations can be used to study the behavior of surfactant molecules at liquid-liquid or liquid-solid interfaces, as well as in bulk solutions. The simulations are based on a detailed description of the atomic-level interactions between the surfactant molecules and other components in the system, such as water molecules, oil molecules, and solid surfaces. The MD simulations are typically performed

by dividing the system into a large number of small "particles" (atoms or molecules) and numerically integrating the equations of motion for each particle over a period of time. The motion of each particle is determined by the forces acting on it, which are calculated based on the interactions with other particles in the system [139–141].

1.8. Summary and problem statement

Carbonate reservoirs are at the leading area of research currently. The main challenges of carbonates development are rock heterogeneity and oil-wetness that make production process more complex. To produce trapped oil left in hydrophobic reservoirs after waterflooding, surfactant injection should be applied, as surfactants are able to decrease the residual oil saturation on the pore level. However, the main challenges of surfactant flooding implementation in carbonates are (1) high temperature, (2) high brine salinity with hardness ions and (3) adsorption of anionic surfactants onto carbonate rock.

The industrial problem of effective surfactant flooding in carbonate reservoirs can be solved through scientific approach. Specialists are seeking for novel solutions, namely project designs and chemicals. There are three possible solutions for surfactant flooding technology improvement. (1) First, it is suggested to shift the focus from detailed evaluation of surfactants that decrease the IFT until ultralow values of $10^{-3} – 10^{-4}$ mN/m to the studies of compositions that effectively change the wettability from hydrophobic to hydrophilic. It is usually difficult or even not possible to combine both effects achieved. (2) Besides this, selection of surfactants should be done on molecular level for target conditions with application of computational techniques. (3) The screening of chemical compositions should be improved, mainly using visualization tools for saturation control such as microfluidics or X-ray scanning.

To solve these problems, a systematic methodology work should be done. Thus, concerning the effective wettability shift, the current focus is made on anionic-nonionic surfactants with two hydrophilic groups that demonstrate promising salinity and temperature tolerance, as well as interfacial performance. Their behavior is highly

influenced by molecular structure and should be discussed on micro- and macroscale applying computational and experimental approaches.

As it was already discussed, the effectiveness of surfactant flooding is highly influenced by interfacial tension, wettability alteration and adsorption values, as well as fluid flow characteristics. All these features are usually evaluated in laboratory according to a standard screening procedure that is customized for each project depending on reservoir properties. Typically, two series of tests are conducted: in bulk and in porous medium. A commonly known method for oil displacing ability assessment is coreflooding experiment that requires complex sample preparation and effective saturation monitoring techniques. However, a technology that is rapidly evolving and aiming to take a regular place in surfactant screening is microfluidics that enables visual assessment of fluid flow. This technique is promising, but still needs improvement and adaptation for sustainable implementation in petroleum industry. Detailed analysis of surfactant properties requires a molecular level approach. One of the examples is molecular dynamics simulations that give insights on interfacial behavior of surfactants mainly on fluid-fluid interface.

Overall, as modern EOR need new effective formulations and up-to-date evaluation techniques both on micro- and macroscale, a detailed study of ethoxylated surfactants and the role of ethoxy chains in surfactants is important. The thesis combines experimental and computational approaches that allow to obtain a full picture of molecule structure and linear EO chain effect on main properties of AEC surfactants.

1.9. Research goal and research objectives

The *main goal* of the present work is to study the effect of molecular structure of alkyl ether carboxylate surfactants on their performance in fluid-fluid and rock-fluid interactions that directly influence on surfactant flooding effectiveness Further, it was a target to link theoretical knowledge and practical application through an optimization of a complex commercial AEC-based surfactant composition designed for the use in a real carbonate field.

This work combines classic and advanced approaches of surfactant flooding evaluation, including molecular dynamics simulations and fluid flow evaluation with X-ray saturation monitoring. These paths allow obtaining a full picture of surfactant performance before SWCTT (single well chemical tracer test) or pilot test. The *research objectives* are the following:

- Correlation of molecular structure of AECs with thermal stability and salinity tolerance. Investigation of interfacial performance and analysis of obtained trends under various temperature and stability conditions (Chapter 2).

  The results were published in: **Scerbacova, A.**, Kopanichuk, I., & Cheremisin, A. (2023). Effect of temperature and salinity on interfacial behavior of alkyl ether carboxylate surfactants. *Petroleum Science and Technology*, 1-20.

- Scaling up the experimental data using molecular dynamics simulations and analyzing the interfacial behavior of AECs with various molecular structures, namely alkyl chain and ethoxy fragment lengths (Chapter 3).

  The results were published in: Kopanichuk, I., **Scerbacova, A.**, Ivanova, A., Cheremisin, A., & Vishnyakov, A. (2022). The effect of the molecular structure of alkyl ether carboxylate surfactants on the oil-water interfacial tension. *Journal of Molecular Liquids*, 119525.

- Evaluation of rock-fluid interactions of AECs with carbonate rock. Study of wetting ability of AECs as a key property of surfactants during chemical flooding. Comparison with published data and analysis of mechanism. Determination of adsorption capacity and analysis of governing forces (Chapter 4).

  The results were published in: **Scerbacova, A.**, Kozlova, E., Barifcani, A., Phan, C. M., Karamov, T., & Cheremisin, A. (2023). Rock–Fluid Interactions of Alkyl Ether Carboxylate Surfactants with Carbonates: Wettability Alteration, ζ-Potential, and Adsorption. *Energy & Fuels*.

- Improvement of a coreflooding test design through including a shut-in stage that is typically applied for low-permeability (shale and tight) reservoirs (Chapter 5).

- Optimization of a commercial AEC-based surfactant blend by screening and evaluation of adsorption inhibitors that are stable under high temperature – 70°C, and high salinity conditions – 201 g/L (Chapter 6).

The results were published in: **Scerbacova, A.**, Ivanova, A., Grishin, P., Cheremisin, A., Tokareva, E., Tkachev, I., Sansiev, G., Fedorchenko, G. & Afanasiev, I. (2022). Application of alkalis, polyelectrolytes, and nanoparticles for reducing adsorption loss of novel anionic surfactant in carbonate rocks at high salinity and temperature conditions. *Colloids and Surfaces A: Physicochemical and Engineering Aspects*, 653, 129996.

Chapter 2. Effect of temperature and salinity on stability and interfacial performance of alkyl ether carboxylate surfactants

2.1. Motivation

As it was concluded from the literature review, an average recovery factor after waterflooding in carbonates is about 35%, and consequently various EOR techniques should be applied to improve oil production. To reduce residual oil saturation in porous media and mobilize trapped oil, surfactant flooding should be applied. However, a successful field project should be designed properly starting from surfactant composition selection using a laboratory screening. Surfactants of the same class can behave differently depending on their molecular structure, and optimal chemicals may be selected for particular field conditions when the main trends in their behavior are known.

Stability and interfacial performance on the boundary with oil determine the applicability of surfactants in EOR. In this chapter, we investigate the basic properties and behavior of alkyl ether carboxylate surfactants as agents for chemical EOR. Four linear AECs, i.e. $C_{11}E_5A$, $C_{11}E_{11}A$, $C_{12}E_4A$, and $C_{12}E_7A$ were examined. The thermal stability and salinity tolerance were correlated with the molecular structure of AECs. The temperatures considered were moderate: 25°C, 40°C, 50°C, 60°C and 70°C. Salinity was moderate and varied from 0 to 100000 ppm, and the effect main cations present in reservoir brines Na^+, Ca^{2+}, Mg^{2+}, and anions Cl^-, SO_4^-, HCO_3^- was studied separately and in mixtures. IFT on the boundary with n-decane and crude oil was evaluated with the spinning drop tensiometry method. The main mechanisms of AEC molecules orientation were discussed.

2.2. Materials and Methods

2.2.1. Materials

Surfactants. This research used four commercially available alkyl ether carboxylate surfactants with a different number of EO units. AECs with linear structures were selected for the study to enable assessment of EO chain and hydrocarbon fragment

lengths on their performance. The main properties of surfactants are specified in Table 3, and chemical structures are shown in Figure 15.

Table 3. Main properties of surfactants used in this study

Characteristic	Sodium laureth-5 carboxylate	Sodium laureth-11 carboxylate	Sodium trideceth-4 carboxylate	Sodium trideceth-7 carboxylate
Abbreviation	$C_{11}E_5A$	$C_{11}E_{11}A$	$C_{12}E_4A$	$C_{12}E_7A$
Number of EO units	5	11	4	7
Molecular weight, g/mol	442	706	412	544
Manufacturer	Kao Chemicals Europe	Kao Chemicals Europe	Nikko Chemicals	Nikko Chemicals
Appearance	Clear, viscous liquid	Clear, viscous liquid	Light yellow, viscous liquid	Light yellow, viscous liquid
Surfactant content, wt%	60	70	100	100
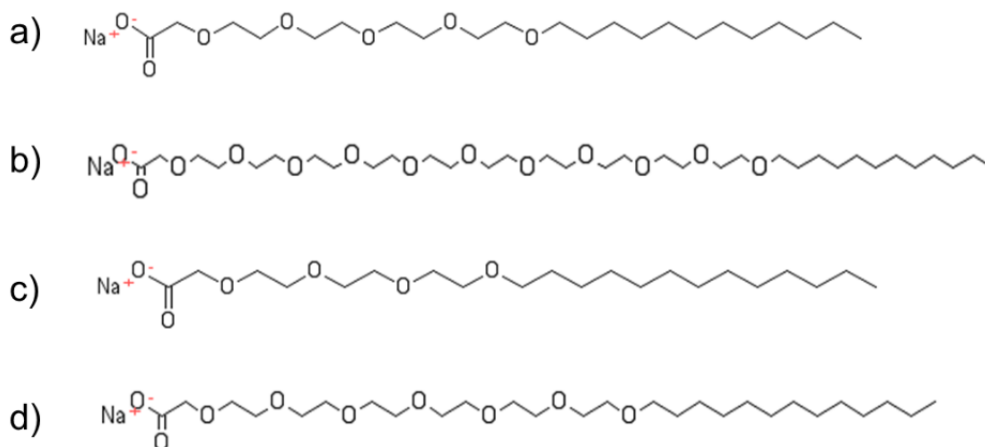
Figure 15. The structures of the surfactants used: a) Sodium laureth-5 carboxylate; b) Sodium laureth-11 carboxylate; c) Sodium trideceth-4 carboxylate; d) Sodium trideceth-7 carboxylate

Salts. Artificial brines with different salinities were prepared on the base of deionized water. Inorganic salts sodium chloride NaCl, calcium chloride dehydrate $CaCl_2 \cdot 2H_2O$, magnesium chloride hexahydrate $MgCl_2 \cdot 6H_2O$, sodium bicarbonate

NaHCO$_3$, sodium sulfate Na$_2$SO$_4$, magnesium sulfate heptahydrate MgSO$_4$·7H$_2$O were of chemical grade. All chemicals were used as received.

Hydrocarbon phase. Normal-decane with purity ≥99% from Sigma Aldrich was used as a model hydrocarbon phase. Crude oil was obtained from a carbonate field with a reservoir temperature of 70°C and was dehydrated before work until water content was less than 0.3 wt.%. Oil density was measured with Mettler Toledo D4 Excellence, and the viscosity measurements were performed with a rheometer Anton Paar MCR 302. The composition was determined through chromatographic analysis with Agilent 7890B SimDis. The oil composition is shown in Figure 16 and main properties are summarized in Table 4.

Table 4. Oil properties at ambient pressure

Properties	Values
Density at 25°C, g/mL	0.88
Density at 70°C, g/mL	0.85
Dynamic viscosity at 25°C, cP	22.38
Dynamic viscosity at 70°C, cP	8.03
Saturates (wt%)	28.98
Aromatics (wt%)	24.60
Resins (wt%)	9.15
Asphaltenes (wt%)	10.89
Light fractions (wt%)	26.38
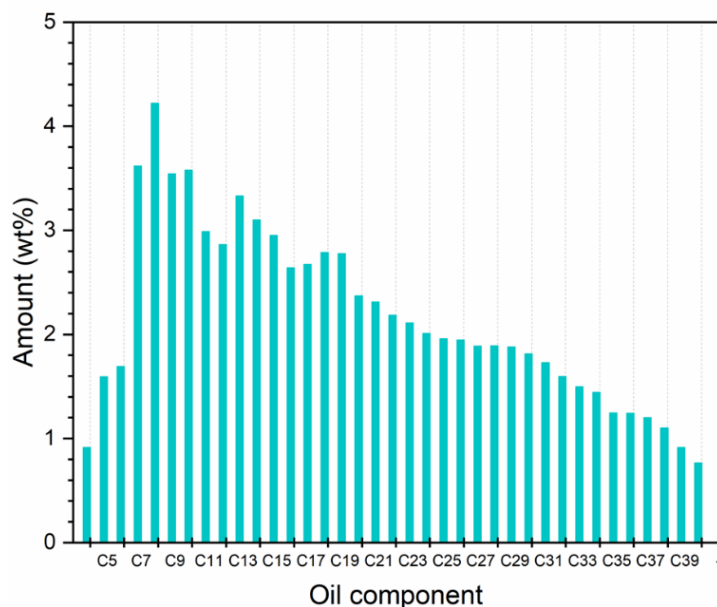
Figure 16. Chromatographic analysis of oil sample

2.2.2. Methods

Surfactant solutions preparation. Synthetic brines were prepared by dissolving the specified amount of salts in deionized water. The list of brines is shown in Table 5. Surfactant solutions were obtained by diluting a required amount of surfactant in brine and mixing with a magnetic stirrer for 1 hour. Then the solutions were left to equilibrate for at least 8 hours (typically overnight). All brines and surfactant compositions were prepared at ambient temperature.

Thermal stability and salinity tolerance test. The stability test included two stages: pre-screening and main experiment. To perform the pre-screening, surfactant solutions with an active matter concentration of 1 wt% were prepared in artificial brines with various NaCl content, the pH was not adjusted with acid or alkali. As AECs may oxidize in the presence of oxygen at elevated temperatures, the oxygen was removed from each solution. Vials were "washed" with nitrogen, and each artificial brine was purged with N_2 for ~10 minutes to remove the dissolved oxygen. Further, each solution was also treated with N_2 for several minutes and nitrogen "cap" was created [60,142]. The stability of AECs was assessed at room temperature (23 – 25°C), 40°C, 50°C, 60°C, and 70°C. Only NaCl was used in this experiment with the range of concentrations from 0 to 10 wt% with a step of

57

1 wt%. NaCl concentrations of 15 wt% and 20 wt% also were tested, but all AECs lost their stability in such conditions. As such, the experiments were conducted in moderate salinities up to 10 wt%. The compositions were inspected visually for 14 days and all changes were noted such as opalescence, turbidity, precipitation, and stratification.

In the main experiment, the effect of various anions and cations was evaluated individually and in mixture at two temperatures (room and 70°C). The list of brines used in the study is given in Table 5. One batch of the solutions was left at ambient temperature, and another was placed into the oven preheated until 70°C. The compositions were also evaluated visually during 14 days.

Table 5. List of brines used in this study

Brine	NaCl, wt%	CaCl$_2$, wt%	MgCl$_2$, wt%	MgSO$_4$, wt%	Na$_2$SO$_4$, wt%	NaHCO$_3$, wt%	Total salinity, wt%	Total salinity, mol/L	Ionic Strength, M	pH
DI	0	0	0	0	0	0	0	0	0	5.65
S1	2	0	0	0	0	0	2	0.342	0.342	6.17
S2	5	0	0	0	0	0	5	0.856	0.856	6.52
S3	10	0	0	0	0	0	10	1.711	1.711	6.49
C1	0	0.1	0	0	0	0	0.1	0.009	0.027	6.65
C2	0	0.5	0	0	0	0	0.5	0.045	0.135	6.14
C3	0	1	0	0	0	0	1	0.090	0.27	6.73
M1	0	0	0.1	0	0	0	0.1	0.011	0.033	5.95
M2	0	0	0.5	0	0	0	0.5	0.053	0.159	6.91
M3	0	0	1	0	0	0	1	0.105	0.315	6.95
MS1	0	0	0	0.1	0	0	0.1	0.008	0.032	8.46
MS2	0	0	0	0.5	0	0	0.5	0.042	0.168	7.21
MS3	0	0	0	1	0	0	1	0.083	0.332	6.71
SS1	0	0	0	0	0.1	0	0.1	0.007	0.021	9.23
SS2	0	0	0	0	0.5	0	0.5	0.035	0.105	6.52
SS3	0	0	0	0	1	0	1	0.070	0.210	7.11
SBC1	0	0	0	0	0	0.1	0.1	0.012	0.012	9.03
SBC2	0	0	0	0	0	0.5	0.5	0.060	0.060	9.23
SBC3	0	0	0	0	0	1	1	0.119	0.119	9.47
H1	5	0.1	0.1	0	0	0	5.2	0.875	0.916	6.59
H2	5	0.5	0.5	0	0	0	6	0.953	1.15	5.77
H3	5	1	1	0	0	0	7	1.051	1.441	6.00
H4	5	0.1	0.1	0	0.1	0	5.3	0.882	0.937	6.63
H5	5	0.5	0.5	0	0.5	0	6.5	0.998	1.255	6.19

Conductivity and pH measurements. Electrical conductivity was measured for critical micelle concentration (CMC) determination. pH and conductivity measurements were performed with the Mettler Toledo SevenCompact pH/Cond S213 unit at room temperature. The unit was calibrated before work with the standards supported by the manufacturer. Each measurement was repeated three times to calculate the arithmetic mean.

Interfacial tension measurements. IFT was determined for (1) temperature effect evaluation in pre-screening, (2) critical micelle concentration determination, and (3) interfacial behavior analysis of AECs.

The dynamic interfacial tension between n-decane and surfactant solutions was measured with a spinning drop method using a tensiometer Kruss SDT. The procedure is based on image analysis of n-decane/oil's spinning drop shape (light hydrocarbon phase) surrounded by an aqueous solution (heavy phase). A glass capillary tube was filled with a water-based solution, and a PTFE plug was filled with a hydrocarbon phase. Then, the capillary was closed with that plug and inserted into the tensiometer. After the rotation was started, the drop of the hydrocarbon phase formed [143,144]. When the target temperature was achieved, the measurement started. The ambient temperature of 25°C and an elevated one of 70°C, a temperature in one carbonate reservoir, were selected for measurements. The temperature deviation was ±0.5°C. Densities of n-decane, oil, and aqueous solutions were measured under appropriate temperatures with density meter Mettler Toledo D4 Excellence. All measurements were conducted until the interfacial tension meanings appeared stable (deviation ±2%) for 30 min [65,66,145].

2.3. Results and discussion

2.3.1. Preliminary screening of selected AECs

The solubility, thermal stability and salinity tolerance of four AECs was assessed in this test. NaCl content was gradually increased from 0 to 10 wt% with a step of 1 wt%, namely 0, 1, 2, 3, 4, 5, 6, 7, 8, 9 and 10 wt%. The temperature range was set from 23°C to 70°C, i.e. 23°C, 40°C, 50°C, 60°C, and 70°C. The concentration of surfactants was 1 wt%.

The results are presented in Table 6: clear solutions are marked with green, opalescent – with orange, turbid or stratified – with red.

Table 6. Summary of stability test results after 14 days

23°C

Surfactant	NaCl content, wt%											pH
	0	1	2	3	4	5	6	7	8	9	10	
$C_{11}E_5A$	green	green	green	green	green	green	green	green	green	green	green	7.13
$C_{11}E_{11}A$	green	green	green	green	green	green	green	green	green	green	green	7.96
$C_{12}E_4A$	green	green	green	red	red	red	red	red	red	red	red	7.85
$C_{12}E_7A$	green	green	green	green	green	green	green	green	green	green	green	7.62

40°C

Surfactant	NaCl content, wt%											-
	0	1	2	3	4	5	6	7	8	9	10	
$C_{11}E_5A$	green	green	green	green	green	green	green	green	green	green	green	-
$C_{11}E_{11}A$	green	green	green	green	green	green	green	green	green	green	green	-
$C_{12}E_4A$	green	green	green	red	red	red	red	red	red	red	red	-
$C_{12}E_7A$	green	green	green	green	green	green	green	green	green	green	green	-

50°C

Surfactant	NaCl content, wt%											-
	0	1	2	3	4	5	6	7	8	9	10	
$C_{11}E_5A$	green	green	green	green	green	green	green	green	green	green	green	-
$C_{11}E_{11}A$	green	green	green	green	green	green	green	green	green	green	green	-
$C_{12}E_4A$	green	green	green	red	red	red	red	red	red	red	red	-
$C_{12}E_7A$	green	green	green	green	green	green	green	green	green	green	green	-

60°C

Surfactant	NaCl content, wt%											-
	0	1	2	3	4	5	6	7	8	9	10	
$C_{11}E_5A$	green	green	orange	orange	orange	orange	orange	orange	orange	orange	red	-
$C_{11}E_{11}A$	green	green	green	green	green	green	green	green	green	green	green	-
$C_{12}E_4A$	red	red	red	red	red	red	red	red	red	red	red	-
$C_{12}E_7A$	green	green	green	green	green	green	orange	orange	orange	orange	orange	-

70°C

Surfactant	NaCl content, wt%											-
	0	1	2	3	4	5	6	7	8	9	10	
$C_{11}E_5A$	green	green	green	orange	orange	orange	orange	orange	orange	orange	red	-
$C_{11}E_{11}A$	green	green	green	green	green	green	green	green	green	green	green	-
$C_{12}E_4A$	red	red	red	red	red	red	red	red	red	red	red	-
$C_{12}E_7A$	green	green	green	green	green	green	orange	orange	orange	orange	orange	-

As one can see, $C_{11}E_{11}A$ with 11 ethylene oxide units in the structure was stable in the full range of conditions considered in the experiment. On contrary, $C_{12}E_4A$ with the shortest EO chain lost stability at room temperature when 3 wt% of NaCl was added. When the temperature was higher than 50°C, AECs $C_{11}E_5A$ and $C_{12}E_7A$ became opalescent in the presence of NaCl. Thus, it can be concluded that the increased EO chain length leads to a higher salinity tolerance because of the formation of hydrogen bonds with water molecules [125]. Considering the stability test results, the most stable $C_{11}E_{11}A$ and $C_{12}E_7A$ were selected for further investigation.

As the temperature has a significant effect on the stability of AECs, it was decided to evaluate the impact of temperature on the interfacial performance. N-decane was used as a hydrocarbon phase to obtain more uniform results. The IFT between decane and aqueous solutions of $C_{11}E_{11}A$ and $C_{12}E_7A$ in deionized water and in the presence of 2 wt% NaCl was measured at 25°C, 40°C, 50°C, 60°C, and 70°C. The concentration of surfactant in each composition was 1 wt%. The results are shown in Figure 17. It was found that the IFT gradually decreased with the temperature growth. However, the effect was not significant and the IFT values remained within the same order of magnitude. Thus, it was decided to continue the experiments at two temperatures to demonstrate the trends – 25°C and 70°C using two surfactants $C_{11}E_{11}A$ and $C_{12}E_7A$.
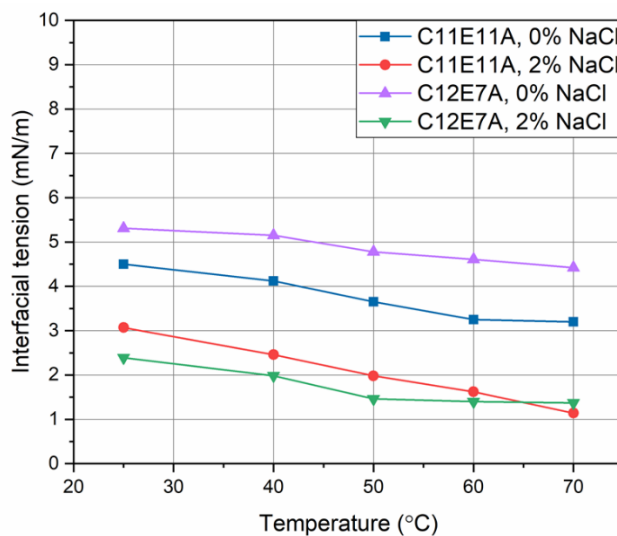
Figure 17. Interfacial tension of $C_{11}E_{11}A$ and $C_{12}E_7A$ on the boundary with n-decane as a function of temperature (the concentration of surfactant in each solution is 1 wt%)

2.3.2. Critical micelle concentration of AECs

Surfactant molecules adsorb on the oil-water boundary, thus building more contact between two immiscible phases and reducing the interfacial tension. When surfactants concentrate on the interface, the hydrophilic part of the molecule interacts with the water molecules, and the hydrophobic part interacts with the hydrocarbons [66,145]. CMC is a key parameter that describes surfactant behavior and indicates the concentration region where the surface activity is optimum. The critical micelle concentration of $C_{11}E_{11}A$ and $C_{12}E_7A$ was determined using two methods – electrical conductivity measurements and interfacial tension determination.

The CMC value corresponds to the breakpoint of the conductivity curve slope plotted versus surfactant concentration. The sharp shift of the slope can be explained by the binding of counterions with micelles and the following formation of agglomerates that are less mobile than surfactant monomers [146,147]. The conductivity measurement results are shown in Figure 18. The CMC of $C_{11}E_{11}A$ surfactant was found to be 0.025 wt%, and the CMC value of $C_{12}E_7A$ was 0.05 wt%.
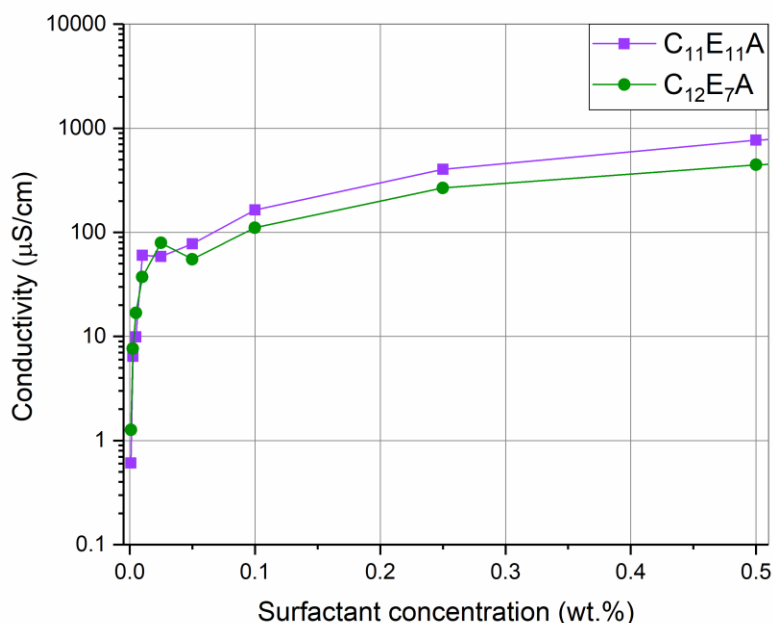
Figure 18. Conductivity versus surfactant concentration at room temperature

Figure 19 shows the IFT as a function of surfactant concentration under 25 and 70°C for $C_{11}E_{11}A$ (a) and $C_{12}E_7A$ (b). Solutions were prepared based on deionized water, and the surfactant concentrations varied from 0.001 to 1 wt%. Typical characteristic IFT profiles were obtained.
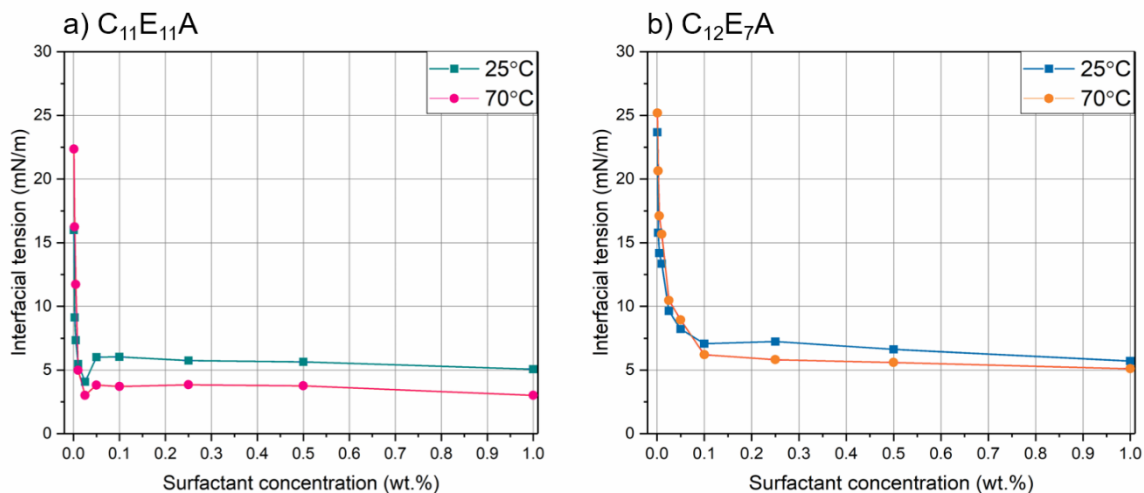
Figure 19. IFT profiles of (a) $C_{11}E_{11}A$ and (b) $C_{12}E_7A$ in DI water at 25 and 70°C

One can see that the IFT of $C_{12}E_7A$ decreases sharply with increasing surfactant concentration in the region before CMC and then goes into a plateau starting from 0.1 wt% where the IFT is 7.08 and 6.21 mN/m at 25 and 70°C, respectively. This behavior is explained by more surfactant molecules being adsorbed at the interface and replacing the solvent molecules as the concentration increases [65,66]. The CMC experimental value of $C_{12}E_7A$ was determined as 0.05 wt%. The IFT at this point is 8.22 mN/m (25°C) and 8.94 mN/m (70°C).

The IFT pattern for $C_{11}E_{11}A$ is slightly different from $C_{12}E_7A$, and its values are lower. The IFT decreases with increasing concentration in the pre-CMC region, passes through a minimum, rises slightly, and forms a constant trend starting from 0.05 wt%. The IFT values at this point are 6.02 and 3.82 mN/m at 25 and 70°C, respectively. Analogous surface behavior was described by Zhang et al. [117]: the surface tension profile for an AEC surfactant with 5 EO units is similar to that described in this paper $C_{12}E_7A$, and for an AEC with 7 EO groups is identical to $C_{11}E_{11}A$.

The critical micelle concentration of $C_{11}E_{11}A$ was determined to be 0.025 wt% with IFT values 4.08 and 3.03 mN/m at 25 and 70°C, respectively. It is worth noting that the CMC value for an AEC with a larger oxyethylene chain is lower than for an AEC with fewer EO units, which is different from nonionic surfactants with analogous structures. This outcome agrees with the results published by Yue et al. [119].

According to Rosen [49], the CMC of ionic surfactants in water decreases with increased carbon atoms number. The CMC is twice as low when a methylene group is added to a straight saturated alkyl chain. In the case of $C_{11}E_{11}A$ and $C_{12}E_7A$, the CMC value of the second one is greater by approximately two times. Consequently, the hydrophilic part of the molecule contributes more significantly in this case. According to S.S.Sheng [67], oxyethylene units play a key role in IFT reduction, and only an optimal number of them will lead to lower IFT values. The authors hypothesize that the EO chain is twisted in a spiral shape at the oil-water interface, and the increase of the chain length can result in two factors simultaneously. These factors are an expansion in distance between adsorbed molecules at the interface due to the steric effect with a decrease in packing density (C16-C18) and an increase in the area occupied by surfactant molecules (C6-C10). The alkyl chains of the surfactants studied in this work are C12 and C13, roughly in the middle of this distribution. Thus, the higher number of EO units and the surface area occupied by the surfactant molecules has a more significant effect on the IFT than dense molecular packing (the density of molecular packing is determined by the area occupied by one molecule at the interface [148]). Wang et al. [149] suggested a similar model of AECs orientation, it is schematically illustrated in Figure 20. This explanation refers to the orientation of the molecules in deionized water in the absence of electrolytes. Presumably, increasing the EO chain length reduces the repulsive forces between the carboxylic groups, simplifying the formation of micelles and making the process easier [119]. This phenomenon makes the AEC surfactants different from nonionic ethoxylated alcohols as an inverse relationship was observed for nonionic surfactants with similar structure: the longer the EO chain is, the higher the CMC value in both experiment and simulation [150].

The assumption that the EO chain plays a more significant role in IFT reduction is supported by the CMC values obtained through static surface tension measurements described by Song et al. [151]. Among three AECs with identical heads and different hydrocarbon chain lengths (C12, C14, C16), the CMC of the surfactant with the longer chain C16 was the smallest.
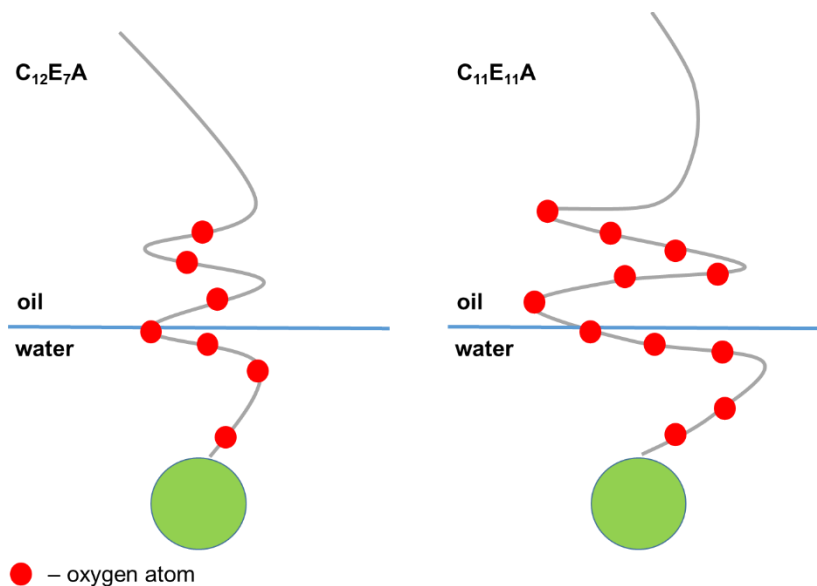
Figure 20. Schematic orientation of $C_{12}E_7A$ and $C_{11}E_{11}A$ on oil-water interface

The IFT values for both surfactants at 70°C are higher in the pre-CCM region than at 25°C, and once the CMC is reached, the trend reverses, and IFT decreases more actively at high temperature. Similar results were reported by Belhaj et al. [60] for alkylpolyglucoside and alkyl ether carboxylate surfactants and their mixtures. This is caused by the higher mobility of the surfactant molecules at elevated temperatures and the better solubility of the hydrophobic part of the surfactant molecules in water. Consequently, the adsorption of the surfactant at the interface is more active [35,144,152].

The temperature increase significantly affects $C_{11}E_{11}A$ surfactant behavior in pre-CMC and post-CMC regions (Figure 19). The IFT decreases noticeably at 70°C compared to 25°C after the critical micelle concentration is reached. In contrast, the temperature rise has no significant effect on $C_{12}E_7A$ behavior. In both cases, the temperature increase has

almost no impact on the CMC value. The experimental data obtained were analyzed using the adsorption isotherm. The CMC values were determined more accurately.

2.3.3. Adsorption isotherm fitting

The Langmuir equation simply describes the adsorption isotherm of surfactants on any oil-water interface as follows [153]:

$$\frac{\Gamma}{\Gamma_0} = \frac{KC}{1+KC},$$ (3)

where Γ is the interfacial excess of a surfactant in mol/m², K is Langmuir constant, Γ_0 is the adsorption limit, and C is the equilibrium concentration of a surfactant in the bulk phase. This work aims to find the direct dependence between the interfacial tension and the bulk surfactant concentration. Gibbs isotherm was used to do this:

$$d\gamma = -2RT\ \Gamma d\ln C,$$ (4)

where γ is the interfacial tension and T is the temperature. Applying equation (3) to (4), we can obtain $\gamma(C)$ dependence by integration [154]:

$$\gamma - \gamma_0 = -2RT\Gamma_0 \ln(1 + KC),$$ (5)

where γ_0 is the oil-water IFT in the absence of a surfactant at temperature T. Equation (5) shows a decrease in the IFT with an increase in the concentration of a surfactant. The equation (5) is used to fit the experimental IFT values of the surfactant-decane-water systems with $C_{11}E_{11}A$ and $C_{12}E_7A$ surfactants by a nonlinear regression model (NLS). Equation (5) is relevant only if $C \leq$ CMC. The IFT value γ_{cmc} was calculated as the mean of all $\gamma(C >$ CMC). Thus, the preliminary location of CMC as the concentration was chosen, where the decrease in the IFT value stops. Then the exact location of CMC as the intersection point of the curve (4) and the horizontal line $\gamma = \gamma_{cmc}$ (see Figure 21) were found. All discussed parameters are listed in Table 7.

66

Table 7. Adsorption parameters in systems without salt

Surfactant	T, °C	γ_{cmc}, mN/m	CMC, wt%	CMC, mmol/kg	K, kg/mol	Γ_0, µmol/m²
$C_{11}E_{11}A$	25	5.4	0.0099	0.14	3.5e10	0.53
	70	3.7	0.013	0.18	6.7e5	1.4
$C_{12}E_7A$	25	6.5	0.082	1.5	2.1e9	0.53
	70	5.5	0.082	1.5	2.6e6	0.74
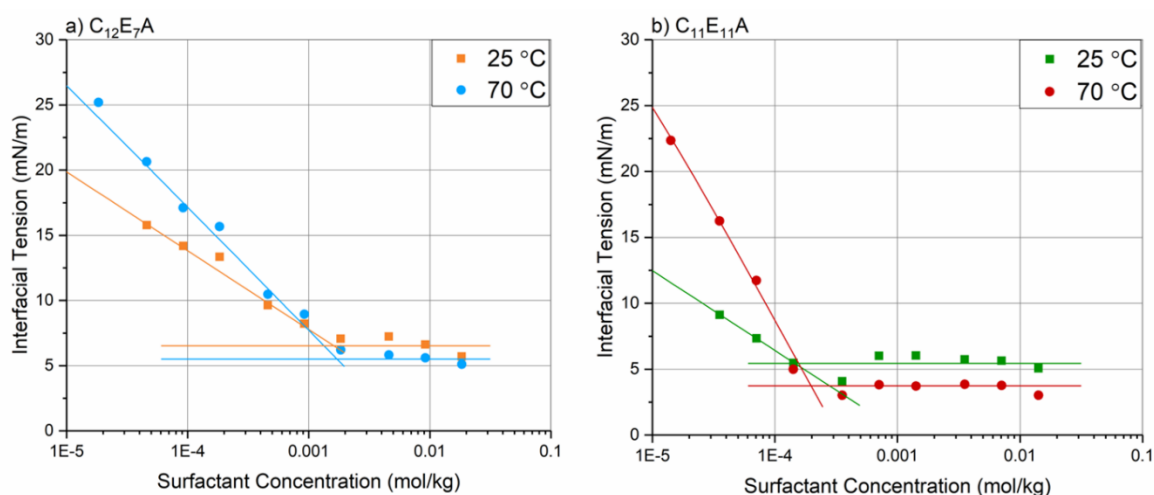
Figure 21. The adsorption isotherm for $C_{12}E_7A$ (a) and $C_{11}E_{11}A$ (b) at 25 and 70°C. Points are experimental values; lines are regressions estimated by the equation (3)

2.3.4. Effect of temperature and electrolytes stability of AEC surfactants

In this test, sodium laureth-11 carboxylate and sodium trideceth-7 carboxylate were examined for salinity tolerance and temperature resistance at 25 and 70°C. The concentration of $C_{11}E_{11}A$ was 0.25 wt%, and of $C_{12}E_7A$ was 0.5 wt% in each solution. Such concentrations were chosen as ones suitable for potential field applications. The compositions of all brines are given in Table 5, and the results of 14-days observations are shown in Table 8. Thus, $C_{11}E_{11}A$ was stable under all range of considered conditions due to a longer EO chain. $C_{12}E_7A$ was significantly influenced by divalent cations Ca^{2+} and Mg^{2+} and HCO_3^- anion. In the presence of calcium ions, $C_{12}E_7A$ solutions became

67

opalescent at room temperature. Mg^{2+} and HCO_3^- ions lead to stability limitations at high temperatures only.

Table 8. Summary of stability test results after 14 days

Brine ID	$C_{12}E_7A$		$C_{11}E_{11}A$	
	25°C	70°C	25°C	70°C
DI	clear	clear	clear	clear
S1	clear	clear	clear	clear
S2	clear	clear	clear	clear
S3	clear	clear	clear	clear
C1	opalescent	opalescent	clear	clear
C2	opalescent	opalescent	clear	clear
C3	opalescent	opalescent	clear	clear
M1	clear	opalescent	clear	clear
M2	clear	opalescent	clear	clear
M3	clear	opalescent	clear	clear
MS1	clear	opalescent	clear	clear
MS2	clear	opalescent	clear	clear
MS3	clear	opalescent	clear	clear
SS1	clear	clear	clear	clear
SS2	clear	clear	clear	clear
SS3	clear	clear	clear	clear
SBC1	clear	opalescent	clear	clear
SBC2	clear	opalescent	clear	clear
SBC3	clear	opalescent	clear	clear
H1	clear	opalescent	clear	clear
H2	opalescent	opalescent	clear	clear
H3	opalescent	turbid	clear	clear
H4	clear	opalescent	clear	clear
H5	opalescent	turbid	clear	clear

2.3.5. Effect of temperature and electrolytes on interfacial behavior of AEC surfactants

Brine salinity can dramatically influence the interfacial behavior of surfactants and even decrease the IFT by several orders of magnitude. This work investigates the effect of salts in different reservoir brines NaCl, CaCl$_2$, MgCl$_2$, Na$_2$SO$_4$, MgSO$_4$, NaHCO$_3$ [44] on interfacial tension. The list of brines used in this study is shown in Table 5. The temperature impact was also assessed. Surfactant concentrations of 10 times the experimental CMC values were chosen for further research: 0.5 wt% for C$_{12}$E$_7$A and 0.25 wt% for C$_{11}$E$_{11}$A.

Monovalent cations concentration effect on IFT of AECs. Sodium chloride NaCl is the most common component of reservoir brines, and its content can exceed 10 wt% in some cases. Four NaCl concentrations of 0, 2, 5, and 10 wt% were introduced to solutions with fixed surfactant concentrations. Figure 22 shows the IFT trend at the n-decane boundary with increasing sodium chloride content in the water phase.
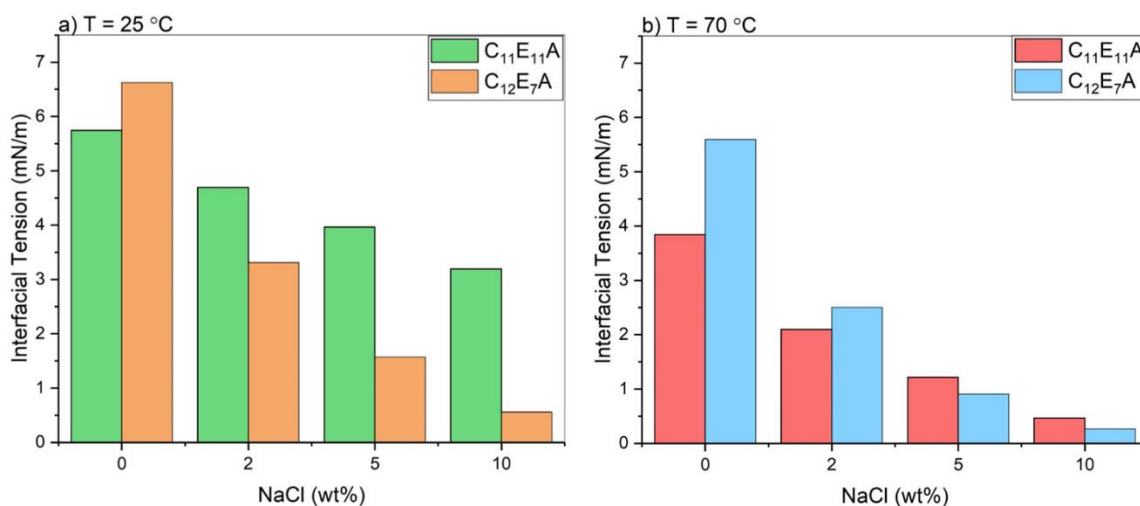
Figure 22. The interfacial tension as a function of NaCl concentration for C$_{12}$E$_7$A and C$_{11}$E$_{11}$A at 25 (a) and 70°C (b)

It can be seen from Figure 22 that the addition of salt leads to an IFT decrease, and its effect on the interfacial behavior of C$_{12}$E$_7$A is more significant and appears nonlinearly. When 10 wt% of NaCl is added, the IFT reduces by order of magnitude compared to IFT values in deionized water and is 0.56 and 0.26 mN/m at 25 and 70°C, respectively. The IFT of C$_{11}$E$_{11}$A decreases linearly with increased salt content and achieves the value of less

than 1 mN/m only when 10 wt% NaCl is added and the temperature is elevated to 70°C. It should be noted that this conclusion was made only for the considered range of salinity.

According to Liu et al. [66] and Cao et al. [64], the behavior of surfactants is influenced by the addition of electrolytes. First, the solubility of surfactant in the aqueous phase decreases, followed by further partitioning into the oil phase. Second, counterions reduce the electrostatic repulsion between surfactant headgroups, which are charged similarly, more surfactant molecules concentrate at the oil-water interface and facilitate IFT decline [49]. It was observed (Figure 22) that the NaCl concentration has little effect on the IFT of sodium laureth-11 carboxylate compared to sodium trideceth-7 carboxylate. As was discussed previously, the interfacial tension depends on the molecular packing and adsorption density of surfactant molecules on the phase boundary [155]. Hence, we can suggest that $C_{12}E_7A$ molecules with a shorter EO chain and a closer molecular packing are more affected by sodium ions. Accordingly, the second tendency driven by the presence of electrolytes contributes more to the IFT reduction, namely the weakened electrostatic repulsive force between the surfactants' heads.

The temperature elevation has a more significant effect on surfactants with a longer oxyethylene chain than on ones with fewer EO groups in both the absence and presence of salt. As the temperature increases, the molecular motion in the system speeds up. Hydrogen bonds existing between water molecules and oxygen atoms in ethyleneoxide chain of the AEC molecule break up with the temperature elevation and cause higher affinity of surfactant to oil phase [156]. This results in decreased IFT values, and the mechanism is similar to increasing the concentration of electrolytes [66].

Divalent cations concentration effect on IFT of AECs. The effects of calcium and magnesium chlorides were evaluated individually and in a mixture with sodium chloride (described below). Bivalent cations have a more powerful ability to decrease the electrostatic repulsion between hydrophilic parts of surfactant molecules [64] and lead to lower IFT values, but can also lead to precipitations in some cases. As the concentrations of $CaCl_2$ and $MgCl_2$ in reservoir brines are usually lower than of NaCl, model brines with smaller calcium and magnesium content than sodium were considered.

Figure 23 shows the impact of 0, 0.1, 0.5, 1 wt% $MgCl_2$ on the IFT of surfactants on the border with n-decane [155]. Similar to Na^+, the presence of the Mg^{2+} ions has a more substantial effect on sodium trideceth-7 carboxylate $C_{12}E_7A$. With the addition of 0.1 wt% $MgCl_2$, the IFT reduces by order of magnitude when heated to 70°C and is 0.21 mN/m. It can be noted that the temperature effect decreases with magnesium chloride concentration growth.
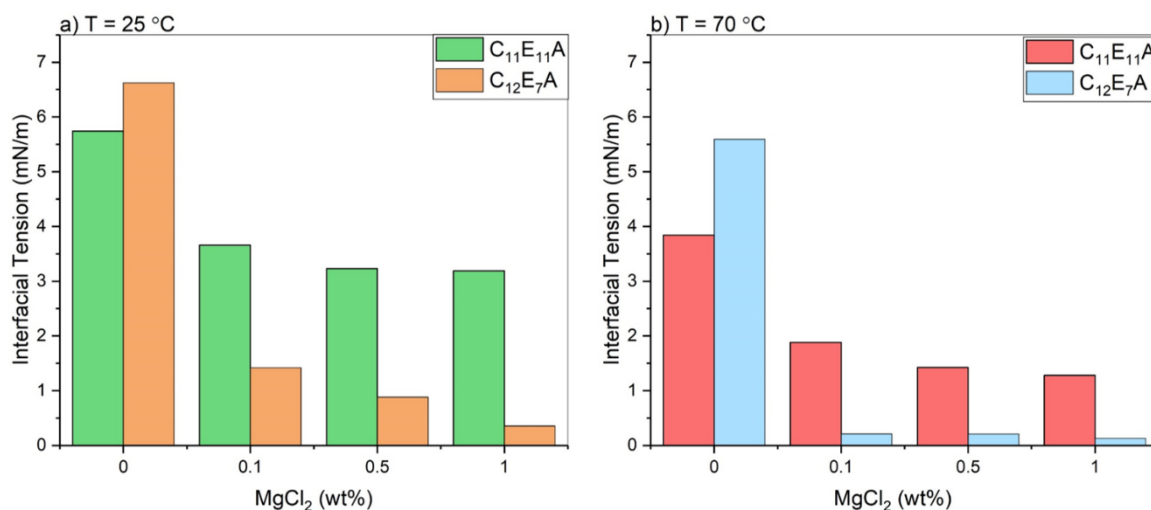
Figure 23. The interfacial tension as a function of $MgCl_2$ concentration for $C_{12}E_7A$ and $C_{11}E_{11}A$ at 25 (a) and 70°C (b)

The identical calcium chloride concentrations (0, 0.1, 0.5, and 1 wt%) were used to assess the effect of calcium ions on IFT. According to data in Figure 24, adding even a small amount of calcium chloride to $C_{12}E_7A$, such as 0.1 wt%, leads to IFT reduction by one order of magnitude at 25°C and two orders of magnitude when heated to 70°C (0.22 and 0.06 mN/m, respectively). The salt effect rapidly reaches saturation, and further introduction of salt does not lead to a decrease in interfacial tension. The temperature increase influence does not depend on the concentration of calcium chloride.

In the case of sodium laureth-11 carboxylate $C_{11}E_{11}A$ (Figure 24), the influence of calcium ions is not so significant and comparable to that of magnesium (Figure 23). We can say the experimental values are within the measurement error. The IFT remains in the

same order of magnitude at both 25°C and elevated temperatures of 70°C, not declining below 1 mN/m. The salt effect is not reaching saturation, and the IFT decreases linearly with the $MgCl_2$ or $CaCl_2$ concentration growth. The temperature rise leads to reduced interfacial tension by half compared to values obtained at 25°C regardless of the salt amount in the considered range. The temperature effect is similar to described previously in section 2.3.2.
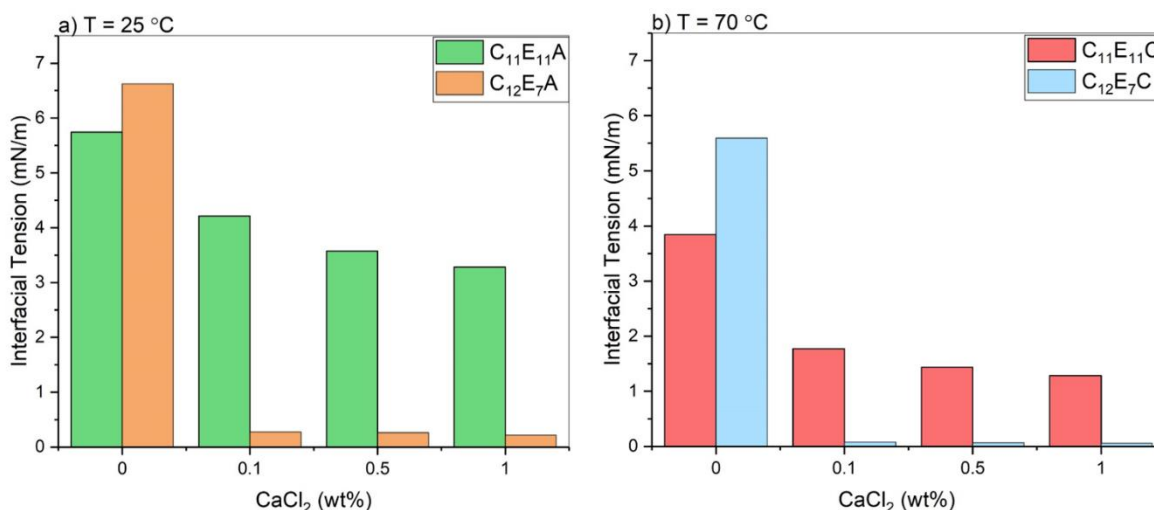
Figure 24. The interfacial tension as a function of $CaCl_2$ concentration for $C_{12}E_7A$ and $C_{11}E_{11}A$ at 25 (a) and 70°C (b)

Our results are different from those reported by Liu et al. [66]. The authors say that the effect of magnesium chloride on alkyl ether carboxylate $C_{12}EO_3C$ is more vital than that of calcium chloride. The degree of the counterion binding with the surfactant molecule decreases as its hydrated radius increases and can be arranged as follows in our case: $Na^+ < Mg^{2+} < Ca^{2+}$. This relationship can be seen in the $C_{12}E_7A$ case, where the surfactant molecules are more densely packed. Concerning the $C_{11}E_{11}A$, the influence of calcium and magnesium cations is identical, although they have different hydrated radii. It was schematically shown in Figure 10.

As mentioned above, the introduction of electrolytes leads to decreased solubility of surfactants in water. In the stability test result, we found that $C_{12}E_7A$ partly loses stability in the aqueous phase in the presence of calcium ions. At the same time, the lowest IFT at

the boundary with decane is achieved, and we can conclude that the oil-soluble nature of this surfactant is enhanced in the presence of Ca^{2+} ions as a result of the salting-out effect [157]. Furthermore, $C_{12}E_7A$ with a shorter EO chain and more dense molecular packing at the oil-water interface is influenced by calcium ions many times stronger than $C_{11}E_{11}A$ at both 25 and 70°C.

Effect of anions on IFT of AECs. Sulfate SO_4^{2-} and bicarbonate HCO_3^- ions are common anions in reservoir brines and can affect the oil-water interfacial tension. Thus, the behavior of AEC surfactants in the presence of Na_2SO_4, $MgSO_4$, and $NaHCO_3$ was evaluated at 25 and 70°C under ambient pressure. Similar to previous experiments, the concentrations of salts were 0, 0.1, 0.5, and 1 wt%. The concentration of $C_{11}E_{11}A$ is 0.25 wt%, and $C_{12}E_7A$ is 0.5 wt% in each solution (post-CMC region).

Figure 25 shows the influence of Na_2SO_4 concentration on the IFT of considered surfactants at 25 and 70°C. The behavior is not similar to that in the presence of bivalent cations Mg^{2+} and Ca^{2+}, as shown in Figure 23 and Figure 24. At 25°C, the IFT values of both $C_{11}E_{11}A$ and $C_{12}E_7A$ are almost equal but slightly lower for the first surfactant with a longer EO chain. In addition, the impact of Na_2SO_4 concentration is not noticeable, as the IFT does not change with salt content growth. Akhlaghi et al. [155] reported similar results: the IFT change of a nonionic surfactant Triton X-100 in the post-CMC region is negligible in the presence of sodium sulfate.

As it was discussed previously, the temperature has more impact on $C_{11}E_{11}A$ than $C_{12}E_7A$ with a shorter EO chain. The data from Figure 25 confirm this idea as IFT values of sodium laureth-11 carboxylate are reduced by half at 70°C and are about 2.5 mN/m compared to 4.2 mN/m at 25°C. This behavior is similar to the tendency noticed for the S2 (2 wt% NaCl) solution shown in Figure 22. On the contrary, sodium trideceth-7 carboxylate is not influenced by temperature growth or Na_2SO_4 salt concentration. This can be explained by the better ability of bivalent cations Ca^{2+} and Mg^{2+} to decrease the electrostatic repulsion between polar heads of anionic surfactant molecules.

Figure 26 shows the IFT plotted vs. magnesium sulfate concentration. The behavior of both surfactants repeats their performance in the presence of magnesium chloride

(Figure 23). We can conclude that magnesium cations have a stronger effect on surfactant behavior, while the contribution of sulfate ions is not substantial. Generally, anions have a less significant effect on anionic surfactants than cations.
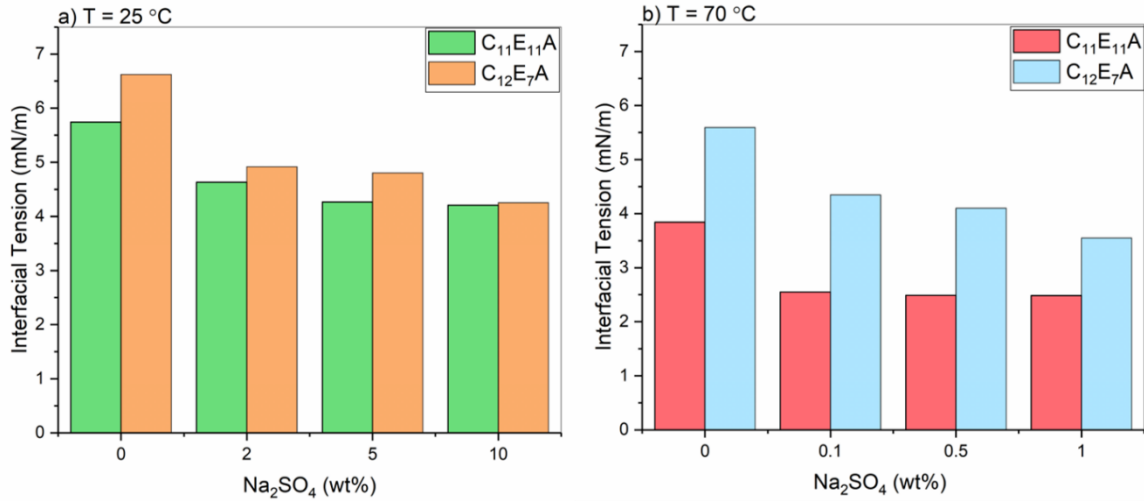
Figure 25. The interfacial tension as a function of Na_2SO_4 concentration for $C_{12}E_7A$ and $C_{11}E_{11}A$ at 25 (a) and 70°C (b)
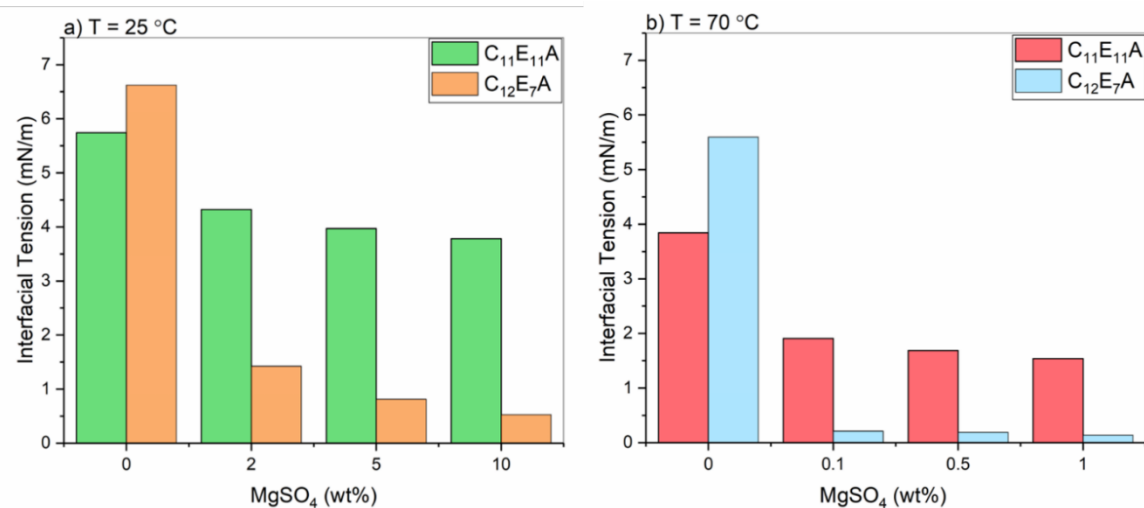
Figure 26. The interfacial tension as a function of $MgSO_4$ concentration for $C_{12}E_7A$ and $C_{11}E_{11}A$ at 25 (a) and 70°C (b)

Sodium bicarbonate $NaHCO_3$ can occur in the reservoir as a brine constituent and a component of chemical flooding formulations. As shown in Table 5, $NaHCO_3$ in a

solution can maintain a higher pH in the slightly alkaline range, namely 8.5-9. The IFT of $C_{11}E_{11}A$ and $C_{12}E_7A$ as a function of $NaHCO_3$ concentration is plotted in Figure 27. The behavior of surfactants is similar to their performance in Na_2SO_4 solutions: the IFT decrease is more significant in the case of $C_{11}E_{11}A$ with a longer EO chain, but the temperature rise has almost no effect on both surfactants. Despite the ability of alkalis to positively affect the oil-water IFT, wettability alteration, and emulsification in combination with surfactants [103], $NaHCO_3$ has no significant impact on AECs considered.
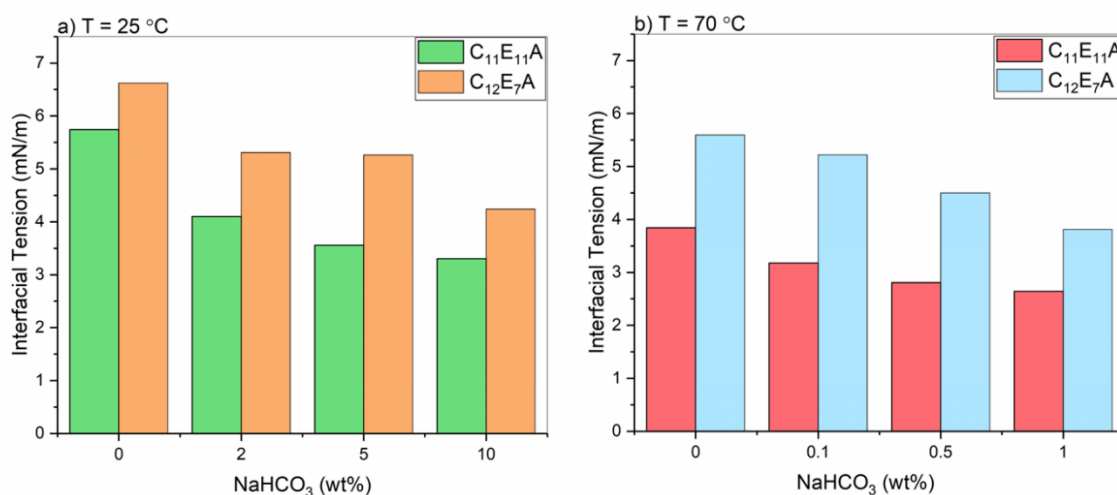
Figure 27. The interfacial tension as a function of $NaHCO_3$ concentration for $C_{12}E_7A$ and $C_{11}E_{11}A$ at 25 (a) and 70°C (b)

Hard brine effect on IFT of AECs. After considering the effects of Na^+, Mg^{2+}, Ca^{2+}, SO_4^{2-} and HCO_3^- ions individually, five artificial brines were composed with a constant sodium chloride concentration of 5 wt%: H1, H2, H3, H4, H5. All brines are characterized in Table 5. The interfacial tension values as functions of brine type are shown in Figure 28. The IFT of $C_{12}E_7A$ in H5 brine was not measured due to poor stability. Sodium laureth-11 carboxylate behavior in hard brines repeats its characteristics in magnesium chloride (Figure 23a) and calcium chloride (Figure 24a) solutions at 25°C. The temperature effect is more evident in this case, and the IFT of $C_{11}E_{11}A$ reaches values below 1 mN/m at 70°C. We can see that the difference between IFT values at 25 and 70°C increases with higher

salt concentration and is 5.75 for H3 brine. Noticeably, H3 brine has the highest salinity and ionic strength and thus has the strongest impact on IFT values of AECs.
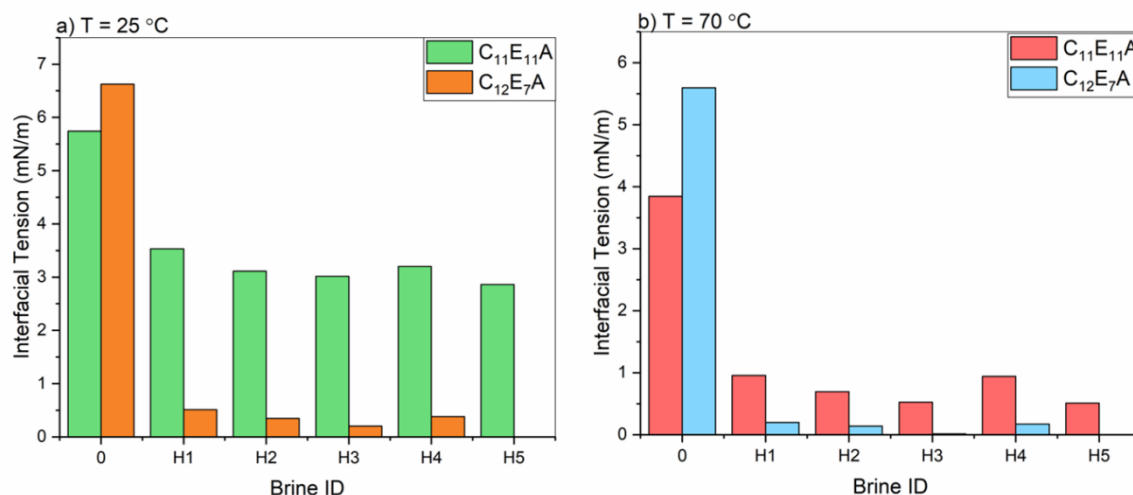
Figure 28. The interfacial tension as a function of hard brine type for $C_{12}E_7A$ and $C_{11}E_{11}A$ at 25 (a) and 70°C (b). All brines are characterized in Table 5

The interfacial tension of sodium trideceth-7 carboxylate in H1 and H2 hard brines is lower than in the presence of $MgCl_2$ only but higher than in solutions of $CaCl_2$. Thus, we can say that the calcium ions have the most significant impact on $C_{12}E_7A$ interfacial behavior. The temperature effect for H1 and H2 brines is almost equal, and the IFT values at 25°C are approximately 2.5 times higher than at 70°C. In the case of H3 brine, the interfacial tension decreases 13.5 times when heated compared to values at 25°C. The behavior of AECs in H4 brine is similar to that in H1; likewise, H5 almost repeats the H2 case. Thus, we can conclude that the influence of SO_4^{2-} ions is negligible for alkyl ether carboxylates. The results obtained are summarized in Table 9.

Table 9. The summary of the results obtained

| Brine | Interfacial tension on the boundary with n-decane, mN/m | | | |
| | $C_{12}E_7A$ | | $C_{11}E_{11}A$ | |
	25°C	70°C	25°C	70°C
DI	6.62	5.60	5.74	3.84
S1	3.31	2.50	4.70	2.10

S2	1.57	0.91	3.97	1.22
S3	0.56	0.26	3.20	0.47
C1	0.28	0.08	4.21	1.77
C2	0.26	0.07	3.58	1.44
C3	0.22	0.06	3.28	1.29
M1	1.42	0.21	3.66	1.88
M2	0.88	0.21	3.23	1.42
M3	0.35	0.13	3.19	1.28
MS1	1.42	0.21	4.32	1.91
MS2	0.81	0.18	3.97	1.69
MS3	0.53	0.14	3.78	1.54
SS1	4.92	3.12	4.63	2.55
SS2	4.80	4.10	4.27	2.49
SS3	4.25	3.55	4.21	2.48
SBC1	5.31	5.22	4.10	3.18
SBC2	5.27	4.50	3.56	2.81
SBC3	4.24	3.81	3.31	2.64
H1	0.51	0.20	3.53	0.96
H2	0.35	0.14	3.11	0.69
H3	0.20	0.02	3.01	0.52
H4	0.38	0.17	3.20	0.94
H5	-	-	2.86	0.51

Effect of hydrocarbon phase on IFT. Oil from a carbonate field with a reservoir temperature of 70°C was used as a natural hydrocarbon phase. The measurements were conducted with a more stable AEC $C_{11}E_{11}A$. The IFT values between 0.25 wt% $C_{11}E_{11}A$ solutions in hard brines (Table 5) on the boundary with n-decane and oil at 70°C are compared in Figure 29. The IFT values between surfactant solutions and oil are lower than between n-decane in the presence of salts. IFT values at the boundary with decane are lower only in deionized water, although the values are almost equal. As was discussed previously, electrolytes decrease the electrostatic repulsion between similarly charged surfactant heads and allow surfactant molecules to reach the oil-water interface, thus decreasing the IFT. Besides that, crude oil contains polar components, such as aromatics, resins, and asphaltenes, which can influence the original arrangement of surfactants at the interface [64]. S.S.Sheng et al. [67] proposed an adsorption model of AEC surfactants and aromatics/asphaltenes at the interface. According to this model, AECs with a more dense

77

packing are more affected by polar oil components and thus can produce lower IFT. The model is schematically illustrated in Figure 11. In the case of $C_{11}E_{11}A$ the IFT decrease is negligible, and we can conclude that its molecular packing does not allow the polar oil components to influence the arrangement on the interface.
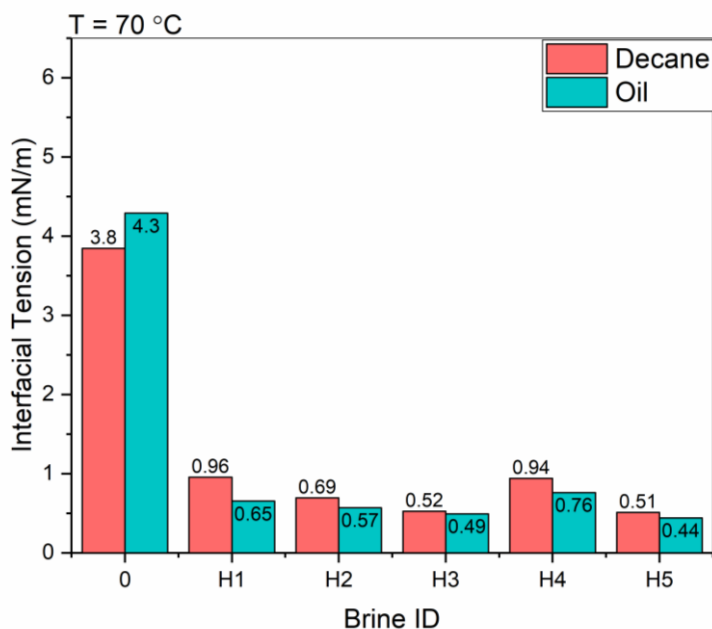
Figure 29. IFT of $C_{11}E_{11}A$ (0.25 wt%) on the boundary with oil and n-decane at 70°C as a function of hard brine type. All brines are characterized in Table 5

2.4. Conclusions

In this study, two AECs ($C_{11}E_{11}A$ and $C_{12}E_7A$) were selected for further investigation based on stability test results. The effect of temperature and salinity on their interfacial behavior was evaluated through dynamic interfacial tension measurements on the boundary with n-decane and oil. First, typical "L-shaped" IFT profiles were obtained at 25 and 70°C, and critical micelle concentrations in deionized water were determined. A model of surfactant adsorption at the liquid-liquid interface, which satisfactorily describes the experimental data, was used to refine the CMC values more accurately. It was found that the temperature increase has no significant impact on CMC values for both surfactants. The interfacial tension for $C_{11}E_{11}A$ and $C_{12}E_7A$ in the pre-CCM region is higher at 70°C

78

than at 25°C, and after the CMC is reached, the trend reverses, and IFT decreases more actively at high temperature. Noticeably, the difference between $C_{11}E_{11}A$ IFT values before and after heating is greater. Thus, we concluded that temperature rise has a stronger impact on surfactants with a larger head and a higher number of EO units than surfactants with fewer EO groups.

Unlike the temperature, salinity has a more substantial effect on $C_{12}E_7A$ interfacial behavior. With increasing salt concentration, the interfacial tension decreases linearly in $C_{11}E_{11}A$ solutions and nonlinearly in $C_{12}E_7A$ ones. In the case of $C_{12}E_7A$, the salt effect quickly reaches saturation regardless of the salt type. The influence of calcium and magnesium chlorides is almost identical for $C_{11}E_{11}A$ but different for $C_{12}E_7A$, with the impact of calcium ions being stronger. Anions have less substantial impact on the IFT of AECs compared to cations, especially hardness ions Ca^{2+}, Mg^{2+}. In the presence of salts mixtures (hard brine), the adsorption of the surfactant on the liquid-liquid interface reaches saturation in both cases. Finally, in the presence of salt, the temperature influence is more significant for $C_{11}E_{11}A$ than $C_{12}E_7A$. Polar components of the oil cannot affect the interfacial molecular arrangement of AECs when the adsorption density is insufficient. An example of $C_{11}E_{11}A$ demonstrated this.

Chapter 3. Investigation of molecular structure effect on interfacial behavior of AECs using molecular dynamics simulations

3.1. Motivation

According to the experimental results obtained in previous chapter, the molecular structure of AECs, and particularly the length of EO chain strongly influence on their interfacial performance. However, it is time-consuming to experimentally evaluate a long list of surfactant samples, and some computational techniques may be helpful for this purpose. Molecular dynamics is an effective technique that provides the information about arrangement of surfactant on the molecular level. The main idea of using the molecular dynamics simulation in this work is to evaluate a wider range of C_nE_mA (C_xE_yA) surfactants than it can be done experimentally. In this chapter, two primary tasks were resolved: (1) IFT values obtained through experimental and numerical methods were compared and (2) the structure-property relationship was established, i.e. how EO and alkyl chain length affects the adsorption of surfactant molecules on liquid-liquid phase boundary.

To do this, precise IFT profiles of $C_{11}E_{11}A$ and $C_{12}E_7A$ in deionized water on the boundary with n-decane were experimentally obtained as references. The data was interpreted with the Redlich-Peterson adsorption model that fitted the experiments well. Then, the excess surface density of the surfactant molecules at decane-water interface was calculated with Redlich-Peterson model and compared with the molecular dynamics simulations.

Simulations of surfactants with different lengths of the alkyl tail and ethylene oxide head segments revealed general tendencies related to the surfactants interactions in the layer.

3.2. Models and methods

Experimental data. Interfacial tension measurements were performed with $C_{11}E_{11}A$ and $C_{12}E_7A$ surfactants that were described in section 2.2. N-decane was used as

hydrocarbon phase. IFT measurement procedure at 25 and 70°C was also described in section 2.2.

Molecular dynamics simulations. The MD simulations were performed by the GROMACS software package (version 2020.2) [162,163] using a time step of 2 fs. Two different forcefields describing the molecular interactions were tried: TraPPE-UA, a united atom forcefield aimed at accurate predictions of phase equilibria and partition coefficients at a wide range of conditions [164–167], and OPLS-AA that prioritizes molecular structure description [164]. Both aspects are important for surfactant self-assembly [161].

Sodium was chosen as the counterion, and all carboxyls were assumed dissociated. Water was represented by the TIP4P/2005 model, a simple four-point forcefield [165]. TIP4P/2005 accurately reproduced the interfacial tension with water using TraPPE parameterizations of oil [161]. The Madrid 2019 scaled charges model represents sodium and chloride ions, which showed good compatibility with the TIP4P/2005 water model [166].

VMD package [167] was utilized for molecules representation and visualization. Coulombic (long-range electrostatic) interactions were computed with the particle-mesh Ewald (PME) method.

The simulation boxes were constructed by placing water molecules and surfactant layers around the hydrophobic (n-decane) phase. The size of each layer was calculated for each case according to the expected density of each liquid. The initial box size was 5x5x20 nm^3 in all simulations. The periodic boundary conditions (PBC) were applied in all directions, and thus two interfaces formed between water and hydrocarbon phases. Different numbers of surfactant molecules, 20 to 100, were placed at each side of the hydrocarbon layer corresponding to obtain surface concentration (Γ) values from 0.4 to 2.0 nm^{-2}. These concentrations accounted for the concentrations before the CMC, near the CMC and above the CMC of surfactants. All surfactant molecules stayed at the interface in the course of the entire simulation run. It means that in simulations Γ could be approximated as the surface concentrations, because the dissolution of the surfactant in water and decane was negligible.

After the box was constructed, energy minimization was performed with the steepest descent algorithm to avoid overlaps and ensure a smooth simulation start, and a short NVT equilibration was carried out to avoid high-pressure gradients. Then NPT simulation at 1 bar was carried out with the volume and potential energy monitored to ensure proper equilibration that is always reached in less than 1 ns. The interfacial tension was equilibrated with another 3 ns NVT run, and then the production run was performed for 10 ns in NVT ensemble with the velocity-rescale thermostat. The structural characteristics such as distribution functions and density profiles were calculated from recorded trajectories. The interfacial tension was determined from the difference between the normal and lateral components of the pressure tensor in a standard fashion. The error bars were obtained by mean square deviation. This technique only produces reasonable results with uniform films parallel to the *xy* plane. Strong inhomogeneity rough interfaces and micelles lead to unphysical (typically negative) interfacial tension at a high concentration of surfactant. All suspicious points were removed from consideration.

Adsorption isotherm model fitting. Experimental results of IFT were analysed and described with an adsorption model. According to the Gibbs adsorption equation:

$$-d\gamma = \sum \Gamma_i d\mu_i \approx \eta RT \, \Gamma \, d\ln(c), \tag{6}$$

in the dilute surfactant solution approximation coefficient η is related to the surfactant dissociation. We assume that $\eta = 2$ (that is, surfactant molecules are completely dissociated, and the charge of the counterion is 1). At higher c the adsorbed layer is dense, Γ depends on c only slightly, and therefore $-d\gamma/d\ln c \approx \eta RT \, \Gamma_{CMC}$ Above CMC, c stops growing as c_T increases (it, in fact, decreases as the surfactant is added to the system, and the dilute solution approximation is no longer valid) and γ becomes almost constant, $\gamma \approx \gamma_{CMC}$. The interfacial tension at CMC is typically around 5-10 mN/m and cannot be exactly measured in our experiments, but can (as the CMC itself) be reasonably estimated from the crossover from the linear decay to nearly constant γ.

Since $\gamma(c)$ is available in a relatively narrow concentration interval close to CMC (in our experiments just as in the majority of published papers), in order to build a

relationship between γ, c, and Γ, one needs to approximate the adsorption isotherm over the entire range. In our case, surfactant adsorption can be reasonably described by the Redlich-Peterson (RP) model, which covers a sufficient variety of isotherm shapes typical to surfactant adsorption at liquid—liquid interfaces and is thermodynamically consistent:

$$\Gamma = \frac{AC}{1+BC^\beta} ,$$
(7)

where A, B, and β are constants. $\beta = 1$ results in the Langmuir equation that describes the adsorption of hard spheres at the flat interface, and thus β characterizes the softness of the effective repulsion between surfactant molecules, which originates, first of all, from the electrostatic nature of the repulsion between the charged carboxylate ions, and next, from the entropic repulsion between the EO fragments. At high c, $1 \ll BC^\beta$ and thus:

$$c = \left(\frac{B}{A}\Gamma\right)^{\frac{1}{1-\beta}} \quad \Rightarrow \quad d\ln c = \frac{d\ln \Gamma}{(1-\beta)},$$
(8)

This can be applied to equation (7), which can now be integrated by $d\Gamma$, rather than by $d\ln c$, from any reference point Γ_R in the high concentration region:

$$\gamma - \gamma_R = -2RT \frac{1}{1-\beta} (\Gamma - \Gamma_R),$$
(9)

which makes $\gamma(\Gamma)$ a linear dependence. Equation 9 allows estimation of Γ_0, the hypothetical adsorption at which the interfacial tension approaches zero $\gamma(\Gamma_0) = 0$, which means the surface is no longer stable and corrugation becomes visible in MD configurations. One may note that the isotherm at high c depends only on β and A/B ratio. β is an important structural parameter that can be directly determined from either experimental or simulation results at high c. Individually, constants A and B can be estimated by fitting to γ_0 value:

$$\gamma_0 - \gamma(c) = \int_0^c 2RT d\ln C = 2RT \int_0^c \frac{AdC}{1+BC^\beta} ,$$
(10)

Simulation results $\gamma(\Gamma)$ are treated with the same RP equation. Unfortunately, the CMC is not known for the model surfactants (for molecular models, it is complicated to obtain reliably). Parameter β can be estimated from equation 9, and then A and B are fitted to the simulated isotherm, which enables a comparison of the c-Γ-γ relationship obtained in simulations to the experimental data.

3.3. Results and discussion

3.3.1. Thermodynamic analysis of the results

The interfacial tension of the decane-water interface in the absence of surfactant at a given temperature T is denoted as γ_0. The experimental data was taken from [168] and water-decane IFT at ambient conditions was set as 46 mN/m. The analysis of past literature showed that there is no agreement in the decane-water IFT value and it varies from ~40 mN/m until ~56 mN/m.

Figure 30 compares simulated and experimental temperature dependences of water-decane IFT obtained with TraPPE and OPLS forcefields. One can see that TraPPE-UA slightly overestimates and OPLS-AA significantly underestimates γ_0. Thus, OPLS-AA forcefield was not used in further calculations.
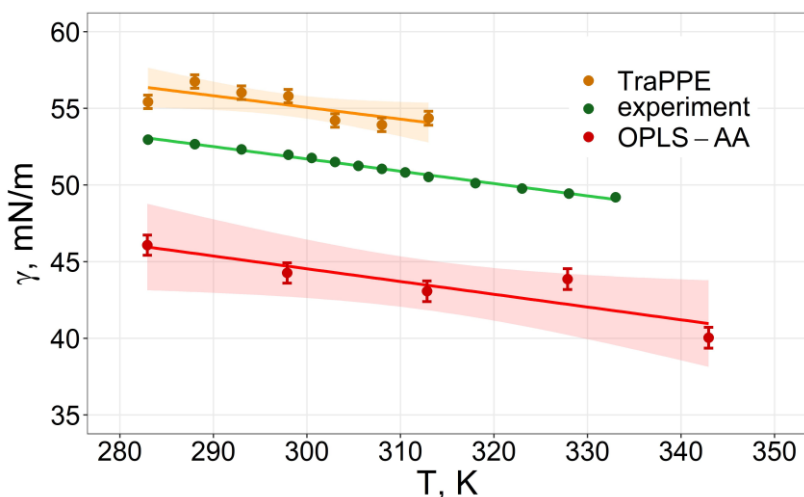
Figure 30. Validation of TraPPE-UA+TIP4P/2005 model and OPLS-AA+TIP3P water model by decane–water system, experimental data from

3.3.2. Experimental adsorption isotherm fitting

The decane-water IFT in the presence of AECs was measured more detailed than in section 2.3.2. where we obtained experimental CMC values and main trends in AECs' behavior. Knowing the CMC range, we analyzed more concentrations in this region to determine CMC more precise and describe the surfactant adsorption isotherms on liquid-liquid interface more properly. Figure 31 shows the experimental results for both surfactants ($C_{11}E_{11}A$ and $C_{12}E_7A$) at two temperatures: 25°C and 70°C. The interfacial tension is plotted as a function of the total surfactant content in the system c_T. The dependence of $\gamma(c)$ is typical for any surfactant-loaded interface at high c. Below CMC $c \approx c_T$, that is, the total concentration approximately equals the concentration in equilibrium bulk molecular solution c, since the surfactant amount at the interface is negligible.

The experimental data were fitted well with the RP model. IFT γ varies practically linearly with $\ln(c)$ according to Gibbs theory, and from the slope, we have determined the adsorbed monolayer density and surface area per surfactant molecule. Γ_{CMC} values are shown in Table 10. We have to note a relatively low parameter β, which effectively describes the interactions of the surfactant molecules in the monolayer. In AEC surfactants, the interactions of the nonionic EO head segment with decane are more or less favorable (analysis can be found in [169]). The charged carboxylate has a strong preference for water. As a result, the surfactant molecules enjoy the freedom of motion with respect to the phase boundary, which likely contributes to lower β values. We should note that β parameter differs within the error margin between the two surfactants and temperatures. The same is observed in the simulations.
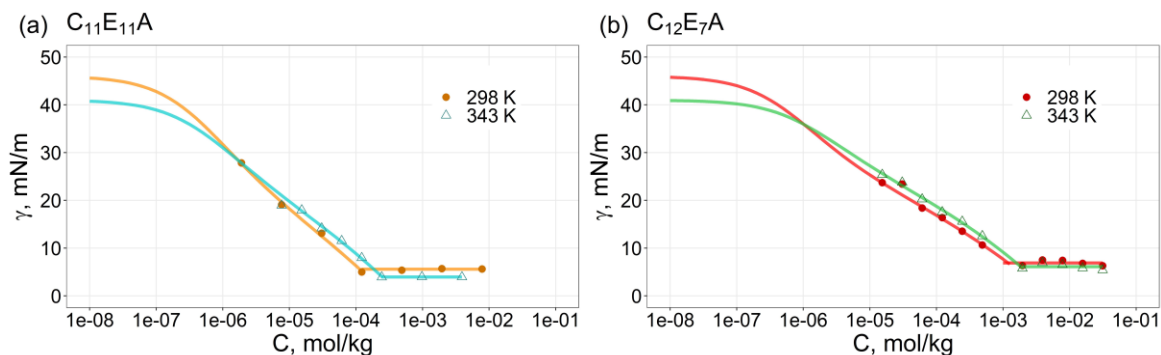
Figure 31. Experimental isotherms for $C_{11}E_{11}A$ (a) and $C_{12}E_7A$ (b) fitted with the RP model. Filled circles: $T = 298$ K; open triangles: $T = 343$K

Table 10. Summary of experimental and simulation results: surfactant properties (holecular mass, hydrophilic-lipophilic balance, critical micelle concentration), adsorption and interfacial tension at CMC determined from experimental data obtained in the paper, coefficients of the Redlich—Peterson equation obtained from the simulation, hypothetical adsorption that corresponds to zero IFT

Surfactant	M, g/mol	HLB	T, K	CMC, mmol/kg	γ_{CMC}, mN/m	Γ_{CMC}, nm^{-2}	A/B	β	Γ_0, nm^{-2}
$C_{11}E_0A$	222.3	20.9	298	-	-	-	-	0.49	3.7
$C_{11}E_4A$	398.5	26.1	298	-	-	-	-	0.73	2.2
$C_{11}E_5A$	442.6	27.4	298	-	-	-	-	0.77	1.8
$C_{11}E_7A$	530.7	29.9	298	-	-	-	-	0.80	1.6
$C_{11}E_{11}A$	706.9	35.2	298	0.11	5.6	1.3	3.4±0.3	0.87±0.03	1.4
			343	0.24	3.9		3.3±0.3	0.85±0.04	
$C_{11}E_{13}A$	795.0	37.8	298	-	-	-	-	0.79	1.5
$C_{11}E_{16}A$	927.2	41.7	298	-	-	-	-	0.75	1.5
C_4E_7A	432.5	33.3	298	-	-	-	-	0.70	2.0
C_8E_7A	488.6	31.4	298	-	-	-	-	0.80	1.6
$C_{12}E_7A$	544.7	29.5	298	1.50	6.9	1.5	1.9±0.4	0.88±0.02	1.6
			343	1.84	6.1		2.0±0.2	0.87±0.01	
$C_{16}E_7A$	600.8	27.6	298	-	-	-	-	0.81	1.6

3.3.3. Comparison of experimental data with simulated isotherms

Figure 32 relates the interfacial tension to the interfacial concentration of a surfactant. This dependence is pretty much linear, which is natural at higher Γ (see equation 4) and, correspondingly, low γ (the points with a disrupted interface where $\gamma \leq 0$ were

excluded from the fit). However, the almost linear $\gamma(\Gamma)$ dependence in the entire range is surprising. Such a dependence was observed for all surfactants in this work. It should be noted that the existing attempts to extract $\gamma(\Gamma)$ at liquid-liquid interfaces from experiments resulted in strongly non-linear $\gamma(\Gamma)$ at lower adsorption. Our fit of the RP isotherm to the experimental data is also shown in Figure 32. Then we obtained $\beta = 0.85$ for $C_{11}E_{11}A$ and $\beta = 0.85$ for $C_{12}E_7A$ at 25°C. Our values of β are very close to those fitted to the experimental data, within the error margin.
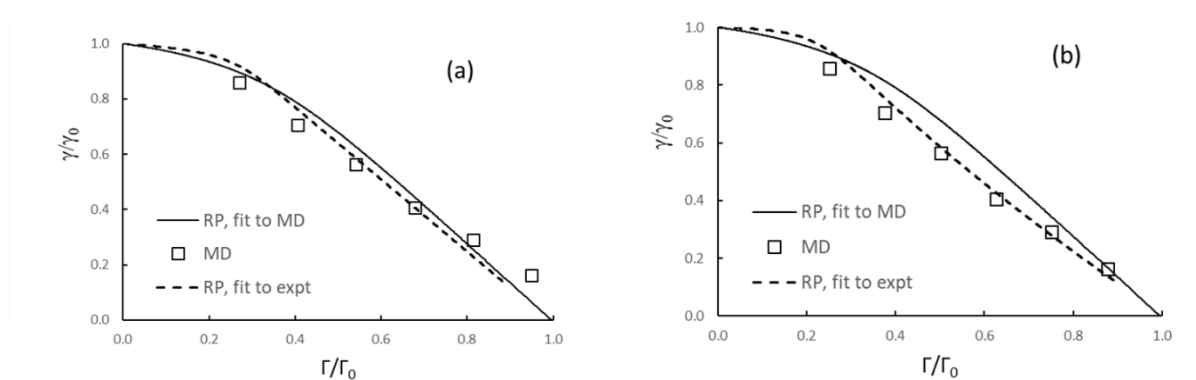
Figure 32. MD isotherms for $C_{11}E_{11}A$ (a) and $C_{12}E_7A$ (b) at 25 °C scaled by the IFT at zero surfactant concentration γ_0 and the estimated lateral density of the surfactant Γ_0 at which $\gamma=0$

3.3.4. Orientation of surfactant molecules at decane-water interface

Figure 33 demonstrates exemplary snapshots of the surfactant layer at the decane-water interface obtained with TraPPE forcefield using VMD package. As Γ increases, the interface becomes less sharp, and finally, at $\Gamma = 2.0$ nm^{-2} it is rough, and surfactant molecules leave the interfacial layer and move into the surrounding bulk phases, although the simulation box size and time are insufficient to model the equilibrium between the micellar solution and the interfacial layer. The value of γ obtained for this configuration is negative, which confirms that such high surface density is unphysical.

The configurations of AECs on water-decane interface obtained through molecular dynamics simulations support the hypothesis described in the part 2.3.2. and schematically

illustrated in Figure 20. The ethylene oxide chain is twisted at the interface and oriented to the water.
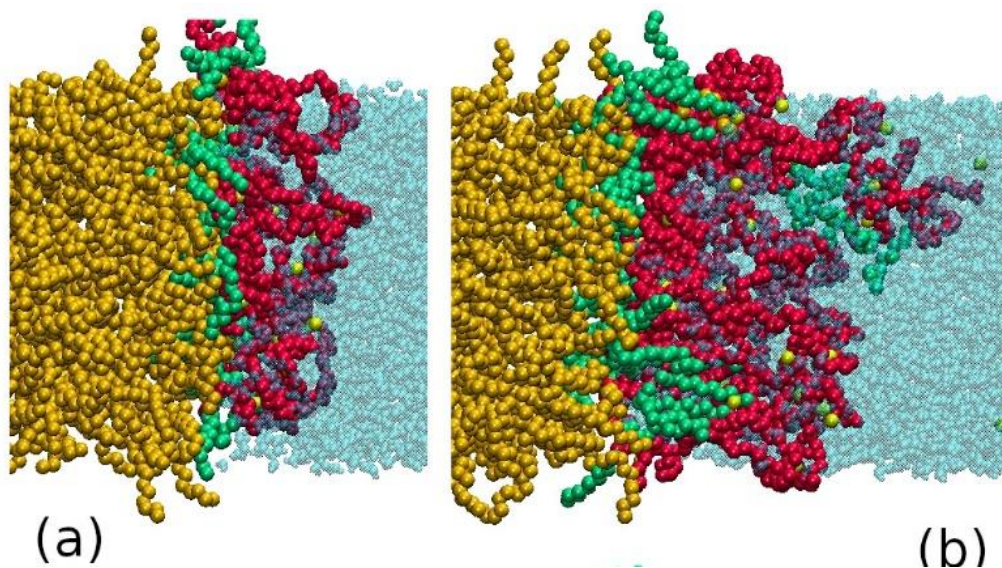
Figure 33. Snapshots of the equilibrated decane-water-$C_{11}E_{11}A$ system at $\Gamma = 1.0$ nm^{-2} (a) and $\Gamma = 2.0$ nm^{-2} (b). Water is cyan, decane is orange, surfactant tail is green, head is red, sodium is yellow

3.3.5. The effects of head and tail length on surfactant adsorption and the interfacial tension

In order to find the effects of the molecular structure on the adsorption behavior of AEC surfactants, we examine two series of model molecules with different ratios of the alkyl tail length n to the EO segment length m. We alter the head length for $C_{11}E_mA$ surfactants and the tail length for C_nE_7A surfactants. One can see the complete list of molecules in Table 10, where $m = 0$ corresponds to a fatty acid. The adsorption isotherms are calculated and analyzed for all considered surfactants in the decane-water system. Figure 34 shows the effect of the head length of the surfactant on the adsorption, interpreted with the compressibility parameter β and the adsorption limit Γ_0. All surfactants in this sequence have the same tail length of 11 C groups.

The EO segments interact with each other through entropic forces: the neighboring EO chains restrict the conformations available to each other and therefore experience soft repulsion, which should strengthen as EO chain length (m) increases. In polymer brushes with mobile attachment points, the repulsion increases proportional to $m^{1/3}$, and for

dependence on the brush density different scaling laws were proposed in the literature. It was expected that the layer becomes less dense and less compressible at constant c as the uncharged hydrophilic segment becomes longer. At low m the surfactant behaves according to the expectations: the adsorption limit Γ_0 decreases significantly with the head length, more than 2 times as m increases from 0 to 7. At the same time, β parameter increases as the head length increases, indicating that the adsorption mechanism is approaching the Langmuir isotherm. However, what is quite unexpected from the general theory is that both parameters reach a plateau after the head length in the molecule reaches about 8 groups. Even doubling the head length from 8 to 16 groups has no visible effect on the adsorption limit. However, the experiments showed a significant effect of EO chain length ($m = 7$ and $m = 11$) on the behavior of AECs that was discussed in details in Chapter 2.
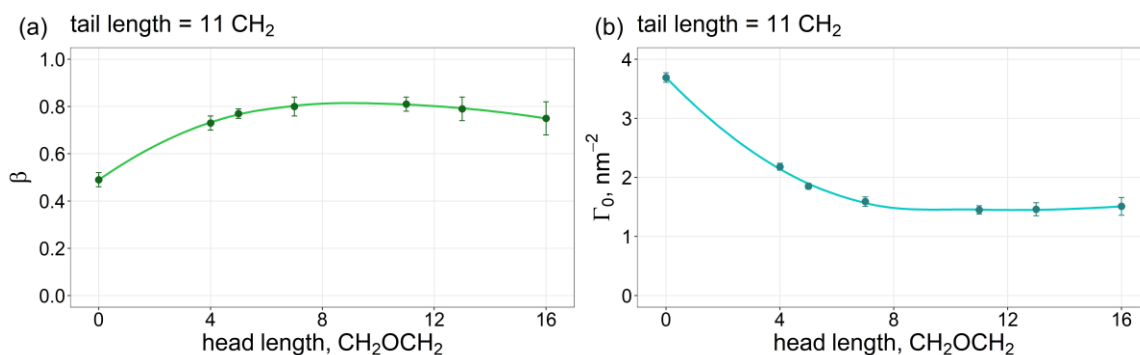
Figure 34. The dependence of the adsorption parameter β (a) and the adsorption limit Γ_0 (b) on the hydrophilic ethyleneoxide segment m of the AEC surfactants with the same alkyl tail length (C_{11}). The adsorbed monolayer becomes less compressible and the maximum adsorption decreases with m until the segment reaches approximately 8 ethyleneoxide monomers. At higher m, both β and Γ_0 become independent of the segment length

The other effect we studied was the effect of the tail length of the surfactant on the adsorption parameter β and the adsorption limit Γ_0. We chose the sequence of surfactant molecules with the same head length $m = 7$ and increased n from 4 to 16. Figure 35 shows that the tail length has only a tiny effect on AEC surfactants' adsorption behavior. Doubling

the tail length from 4 to 8 groups has qualitatively the same effects as increasing the head length: an increase in beta and a decrease in the adsorption limit, but quantitatively the effects of head and tail are not even comparable. Further increases in tail length over 8 groups have no effect at all.
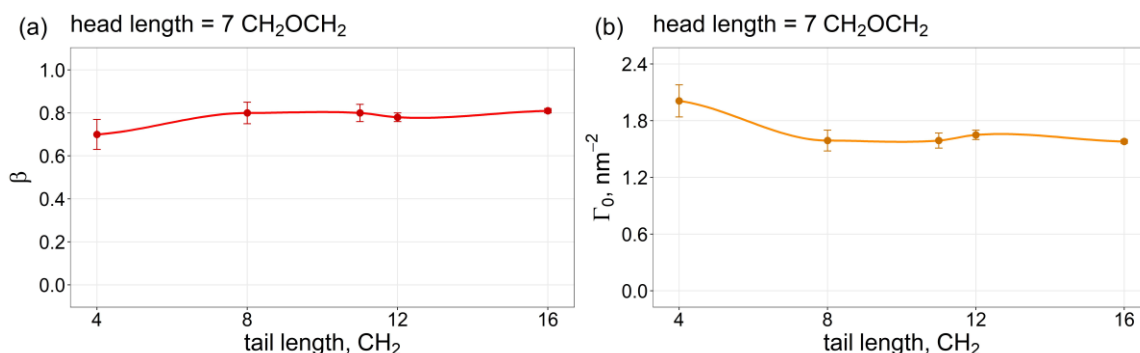
Figure 35. The dependence of the adsorption parameter β (a) and the adsorption limit Γ_0 (b) on the hydrophobic alkyl tail length n of the AEC surfactants at constant ethyleneoxide segment length of 7 monomers

3.4. Conclusions

Using combination of experiments and MD simulations, we explore the performance of AEC surfactants at the alkane-water interface. Two exemplary compounds, $C_{11}E_{11}A$ and $C_{12}E_7A$, were studied experimentally at 25 and 70°C, and a wider range of systems was modeled with MD. AECs display the behavior characteristic of ionic surfactants, with a reasonably linear relationship between the IFT and the logarithm of the bulk surfactant concentration about two decimal orders above CMC, indicating that the surfactant monolayer is close to saturation and adsorption nearly invariant of the bulk surfactant concentration. The CMC values are determined from the crossover from logarithmic dependence of the interfacial tension on the bulk concentration to constant, and the results are consistent with the earlier published data on AEC surfactants.

The effective interactions within the layer are interpreted in terms of the compressibility parameter β. The β values we obtain are visibly lower than 1 (β = 1 reduces the RP model to the Langmuir model). The compressibility is related to substantial freedom

90

of motion of the surfactants with respect to the decane-water interface, as the interactions between the EO and alkyl segments are reasonably favorable, while the dissociated carboxylates have a strong preference for water. Based on the interpretation of the MD results, we demonstrate the dependence of the surface concentration of the surfactant in the adsorbed layer and surfactant-surfactant interactions within the layer interactions the limiting surface concentration Γ_0 on the length of the hydrophobic and hydrophilic segments. Alkyl chain length has almost no influence on the monolayer properties since it is smaller or comparable in length to the solvent molecules. The alkyl tail strongly influences the CMC but causes almost no lateral forces within the monolayer. The EO segment length strongly influences the adsorbed monolayer properties: an increase in length reduces the compressibility and decreases the density, but only for $m < 8$. Then, the influence of the EO segment length becomes much weaker, which may be related to the interplay between steric repulsion between the EO segments and the electrostatic repulsion between the charged heads.

Despite the possibility of "digital screening" provided by MD, this method has significant limitations. Thus, a very short time may be considered (in ps to ns scale) and simulation box size is very small (nm scale) compared to real scale of oilfield or even a core sample. Besides this, unphysical results may be obtained in some cases when temperature or ions are added to the system. Concerning all above, the method currently cannot fully replace laboratory experiments.

Chapter 4. Rock-fluid interactions of alkyl ether carboxylate surfactants with carbonate rock: wettability alteration, zeta potential, and adsorption

4.1. Motivation

The previous chapters demonstrated that behavior of surfactants on the liquid-liquid interfaces is highly influenced by their molecular structure and reservoir conditions, mainly temperature and brine salinity. During the flooding process, injected compositions contact and interact with oil and with rock creating a system *"oil-brine (surfactant composition)-rock"*. Understanding of interaction mechanisms of surfactant molecules with rock is crucial for surfactant flooding design development. The wetting ability of surfactants inputs in capillary number reduction, and adsorption capacity determines economic feasibility of the project.

This part of work provides a set of experiments that characterize the behavior of AECs during the interactions with carbonate rock. Rock-fluid interactions of $C_{11}E_{11}A$ and $C_{12}E_7A$ in carbonates were evaluated: wetting ability, zeta potential, and adsorption capacity. Contact angle measurements with sessile drop technique were used as main test for wettability evaluation. To do this, core plates from a carbonate reservoir were used and evaluated as-is, after aging in oil and after treatment with surfactant compositions selected on the base of studies conducted in Chapter 2 and Chapter 3. Then, a novel approach of wettability alteration mechanism assessment through Rock-Eval pyrolysis was described and applied. Carbonate rock fine particles were used in static adsorption test and zeta potential measurements. The main goal of this experiment was to determine the maximum adsorption capacity and adsorption mechanism in deionized water and in the presence of ions. All mechanisms were analyzed, and the main governing forces were suggested and explained.

4.2. Materials and methods

4.2.1. Materials

Surfactant compositions. This chapter used two AECs, sodium laureth-11carboxylate $C_{11}E_{11}A$ and sodium trideceth-7 carboxylate $C_{12}E_7A$. $C_{11}E_{11}A$, with a molecular weight of 706 g/mol and 11 units in the oxyethylene chain, is a clear, viscous liquid. The molecular weight of $C_{12}E_7A$ is 544 g/mol, with seven EO units and appears as a yellowish clear, viscous liquid. Characteristics of surfactants were given in Table 3.

Six surfactant compositions in different brines were developed based on stability screening and interfacial behavior evaluation described in the previous part of the present work 2.3. The main characteristics of surfactant compositions are shown in Table 11.

Table 11. Surfactant compositions and IFT values on the boundary with oil

Surfactant	Surfactant concentration, wt%	Brine ID	Total salinity, wt%	NaCl, wt%	CaCl$_2$, wt%	MgCl$_2$, wt%	Na$_2$SO$_4$, wt%	IFT, mN/m (oil, 70°C)
$C_{11}E_{11}A$	0.25	DI	0	0	0	0	0	4.29±0.045
		Hard1	6.0	5	0.5	0.5	0	0.57±0.089
		Hard2	6.5	5	0.5	0.5	0.5	0.44±0.114
$C_{12}E_7A$	0.5	DI	0	0	0	0	0	7.32±0.085
		Soft1	5	5	0	0	0	1.45±0.158
		Soft2	5.1	5	0	0	0.1	1.16±0.001

Oil. Crude oil from a carbonate field with reservoir temperature of 70°C was used for the experiments; the main properties were summarized in Table 4.

Rock samples. Core samples of carbonate rock were obtained from an oilfield and represent the limestone. For wettability evaluation, two core cylinders with a diameter of 35 mm were cut into plates 5 mm thick and extracted with toluene in the Soxhlet apparatus for 7 days to remove free oil and contaminations. For the static adsorption test, the core was crushed until 250 μm. The size of fine particles for zeta potential measurements was 140 μm.

The mineralogy of rock samples was determined through an X-ray diffraction analysis (XRD) [172,173] using Huber G670 unit. The diffractogram of a crushed sample if given in the Appendix. The main peak observed indicates that the rock is 100% calcite $CaCO_3$, and no impurities are present in the sample.

4.2.2. Methods

Rock characterization. Rock microstructure and lithology were characterized through petrographical thin-section (30 μm) analysis with a ZEISS Axioscope 5 polarizing microscope. High-resolution 2D microstructural visualization of rock sample surface was done with a Thermo Fisher Scientific Quattro S scanning electron microscope (SEM) [172–174]. SEM images were done before aging, after aging in oil, and after treatment with surfactants to show the qualitative changes in wettability and explain the wettability alteration mechanism [32].

Rock-Eval pyrolysis studies. Rock-Eval (RE) pyrolysis studies were performed with a HAWK Resource Workstation (Wildcat technologies) according to a Classical Pyrolysis-TOC temperature program. RE pyrolysis is a decomposition (evaporation and cracking) of organic matter by heating in an inert atmosphere. It is typically used to estimate the oil-and-gas-generation potential and thermal maturity for organic matter in the rocks and to assess the hydrocarbon group composition in the reservoirs [175]. The grinded rock sample in a crucible was placed into the oven and stepwise heated up to 650°C with the constant heating rate of 25°C/min in an inert atmosphere of helium followed by oxidation in air. The output RE pyrolysis parameters were S0, S1, and S2 peaks measured in mg-HC/g rock according to the temperature output. S0 peak corresponds to gaseous hydrocarbons (100°C), S1 – to free oil (liquid hydrocarbons) (300°C), and the S2 peak was formed by HC of kerogen cracking in case of source rock or heavy oil components (including paraffins, resins and asphaltenes) in the reservoirs or unconventional resources [176–178]. Each sample was analyzed at least twice. In this work, a Rock-Eval pyrolysis technique was proposed for the qualitative characterization of rock wettability change and description of the surfactants' mechanism of action. The method can quantify the surface

94

action of the surfactant, namely, whether it washes away the adsorbed hydrocarbons or adsorbs on the rock itself.

First, we qualitatively and quantitatively compared the amount of organic matter on the surface of the original rock (after toluene cleaning) and samples aged in oil. Second, we obtained pyrograms of pure surfactants. In this step, a drop of surfactant dissolved in deionized water was placed on crushed pure calcite, pre-calcined in an oven at 550°C to remove all residual organic substances. Third, we obtained pyrograms of rock samples that were treated with surfactant compositions after being aged in oil. We compared them with pyrograms of pure surfactant and aged rock and got an insight into the mechanism of the rock-surfactant interactions.

Wettability studies (aging procedure and contact angles measurements). The wettability was assessed on the macro level through contact angle measurements. The workflow of the experiment is illustrated in Figure 36. Carbonates are known to be predominantly oil-wet or mix-wet [14], so the initial wettability of the samples plays a crucial role. Thus, the core slices were aged with oil to restore the original wettability according to the methodology proposed by Standnes and Austad [54]. After the slices were cleaned with toluene and dried, they were placed in jars with oil preheated until 70°C and stored for 14 days at 70°C. Next, each sample was washed with toluene to remove extra oil and dried at room temperature. Finally, the oil-wet calcite slices were soaked in surfactant solutions for 48 hours at 70°C to assess the wetting ability of AEC surfactants in different brines, the volume of surfactant solution was 20 mL in each jar. After soaking in surfactant solutions, core plates were washed with deionized water and dried in the oven for 1 hour [57,121]. It should be noted that polyoxyethylene units degrade in the presence of oxygen [60,179] under high temperatures, and it was removed from each surfactant composition by purging with nitrogen and creating a "nitrogen cap" [56].

Thus, three series of contact angle measurements were performed: before aging (as-is), after aging in oil, and after treatment with surfactants. The measurements were conducted with Kruss Drop Shape Analyzer 30S at ambient pressure and temperature. Deionized water was used as a wetting fluid. The water droplet volume in experiments was

95

4 µL. At least 10 drops of DI water were placed in random positions on the surface of each core plate, and the CA was measured after the equilibration. The contact angle value was calculated as an average mean, and the standard deviation was determined [24,180].
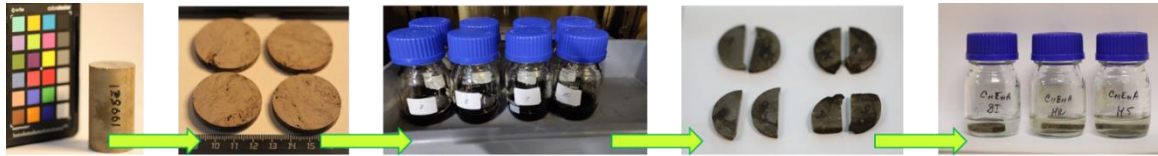
Figure 36. Workflow of wettability evaluation experiment

Zeta potential measurements. In this experiment, limestone fine particles with diameter of 140 µm were used. They were prepared according to the methodology illustrated in Figure 37. The sample from a carbonate field was crushed into particles of 1-4 mm first. Then, limestone was extracted with chloroform to remove oil and impurities in Dean-Stark apparatus. Further, the clean particles were crushed until 140 µm (for zeta potential measurements) and 250 µm (for static adsorption test). No aging procedure was applied for this experiment.
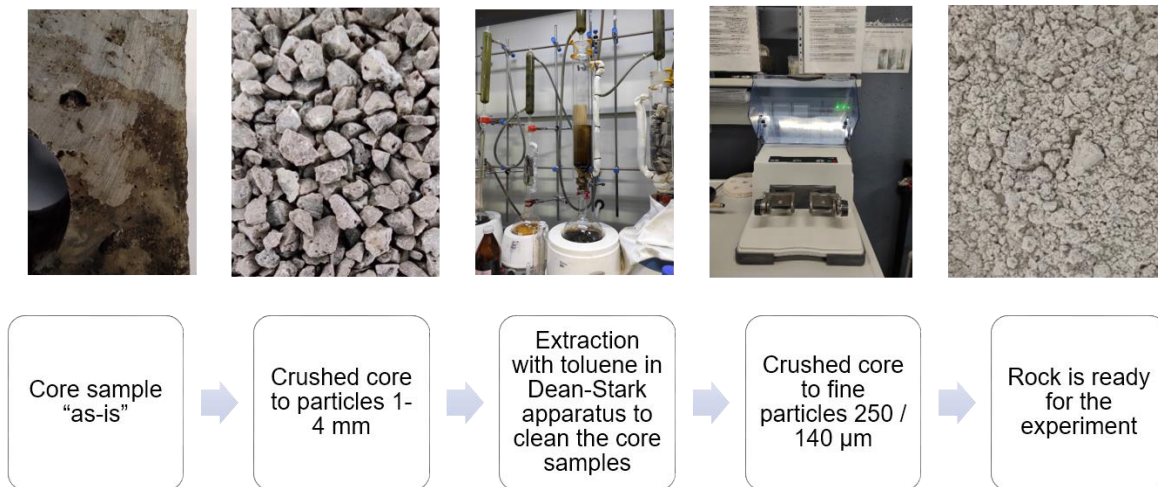
Figure 37. Methodology of limestone rock powder preparation

The methodology of zeta potential evaluation was developed based on Ding and Rahman [181] and Lara Orozco et al. [182]. To prepare a calcite suspension, 10 mL of brine/surfactant solution was placed into a 20-mL vial, and 0.1 g of rock powder was added.

No acid or base were introduced to adjust the pH. Then, the solutions were ultrasonicated for 30 minutes to obtain homogeneous dispersions and left to equilibrate for 48 hours at room temperature. After equilibration, 5 mL of the supernatant was transferred into another vial, and the zeta potential was measured with Zetasizer Nano ZS (Malvern Panalytical). The capillary cell DTS1070 was filled with 1 mL of the suspension and equilibrated for 3 minutes at 25°C. Each measurement was performed with 3 runs and 100 sub-runs. The operation temperature of the instrument is limited to 70°C, and the values obtained may have a significant standard deviation. Thus, all the measurements were performed at 25°C [183].

Static adsorption test. A static adsorption test was performed with crushed limestone from a carbonate field and surfactant compositions. The equilibrium concentration of surfactant remained in the aqueous phase after contact with rock was measured through potentiometric titration with sodium tetraphenyl borate (Na-TPB) as a titrant using an automatic titrator Mettler Toledo T5 Excellence. To prepare a sample for the analysis, 1 mL of surfactant solution was added to a titration breaker and diluted with ~40 mL of deionized water. Then, 2 mL of 0.1 mol/L $BaCl_2$ solution was added for sample activation, and 1 mL of polyvinyl alcohol solution was added to achieve a finely dispersed precipitate [184].

As the concentration of surfactant in a chemical composition for EOR is typically above CMC, the range of concentrations was selected in the post-CMC region. First, a calibration curve was built for each surfactant composition. Second, the equilibrium surfactant concentrations were determined to obtain adsorption isotherms.

In this experiment, 3 g (m_{rock}) of crushed rock was placed into a glass jar and 15 g (m_{surf}) of surfactant solution was added. The composition was purged with nitrogen to remove dissolved oxygen in order to prevent the oxidation of AECs under heating. Then the jars were sealed, manually shaken, and placed into an oven for 24 hours at 70°C. The solution was centrifuged for 30 minutes at 2500 rpm to separate the rock particles, and the supernatant was used for the analysis [56,185]. Knowing the surfactant concentrations in

the solution before (C_0) and after (C_{eq}) contact with the rock, the adsorption value (Γ) was determined using the formula below:

$$\Gamma = \frac{(C_0 - C_{eq}) \cdot m_{surf}}{m_{rock}} \quad , \tag{11}$$

4.2.3. Equilibrium adsorption models

Adsorption isotherms built based on static adsorption test results were fitted to two-parameter equilibrium adsorption models, namely Langmuir, Freundlich and Temkin. Langmuir isotherm was introduced to describe gas adsorption on solid surfaces and used to characterize the performance of bio-sorbents [186,187]. It supposes a monolayer adsorption, in which molecules are solely adsorbed at particular, homogeneous locations with no contact with each other. Once the adsorbate molecules have filled the active sites, no more adsorption is possible [114,186]. The Langmuir isotherm is described below [188]:

$$q_e = \frac{q_0 K_L C_e}{K_L C_e + 1} \quad , \tag{12}$$

The linear form of the mathematical expression is given in Eq. (13) [186]:

$$\frac{1}{q_e} = \frac{1}{q_0 K_L C_e} + \frac{1}{q_0} \quad , \quad , \tag{13},$$

where q_e is the amount of surfactant adsorbed (mg/g-rock), q_0 is the maximum adsorbed value (mg/g-rock), C_e is the equilibrium surfactant concentration in aqueous phase (mg/L), K_L is the Langmuir adsorption constant (L/mg). To determine the equation parameters, $\frac{1}{q_e}$ should be plotted versus $\frac{1}{C_e}$ and the straight line equation has to be obtained where $\frac{1}{q_0 K_L}$ corresponds to the slope, $\frac{1}{q_0}$ is the intercept.

Freundlich isotherm model is the earliest one introduced to describe the reversible polymolecular adsorption characterized with various types of active sites and formation of multilayers. The concept of this model is that the more amount of adsorbate is, the higher the adsorption than can be described with a power-law dependence [186]. This isotherm is

particularly often used in studies of adsorption on porous materials and powders and can be described with the Eq. 14 [189]:

$$q_e = K_F C_e^{\frac{1}{n}} \quad , \tag{14}$$

The linearized form of the Freundlich isotherm model expression can be written as in Eq. (15) [186]:

$$ln q_e = ln K_F + \frac{1}{n} ln C_e \qquad , \tag{15},$$

where K_F is the Freundlich adsorption constant (L/mg), and $\frac{1}{n}$ is a constant which shows the adsorption strength. To obtain the adsorption parameters, $\ln(q_e)$ should be plotted versus $\ln(C_e)$, where $\frac{1}{n}$ is the slope, and $ln K_F$ is the intercept.

Temkin adsorption isotherm was introduced to describe chemisorption processes and takes into account the adsorbent and adsorbate interactions [190]. According to Temkin model, the reduction in heat of adsorption as a function of temperature for all molecules present in the layer is assumed to be linear rather than logarithmic as surface coverage increases [187]. The Temkin isotherm is described in Eq. (16) [186]:

$$q_e = \frac{RT}{b_T} ln A_T C_e \quad , \tag{16}$$

The linearized form of the Temkin isotherm model expression can be presented as in Eq. (17) [186]:

$$q_e = \frac{RT}{b_T} ln A_T + \frac{RT}{b_T} ln C_e \quad , \tag{17},$$

where R is a universal gas constant 8.314 J/(mol K), T is temperature (K), b_T is the Temkin constant related to the heat of adsorption (J/mol), A_T is Temkin equilibrium binding constant (L/g). To obtain the model parameters, q_e should be plotted versus $\ln(C_e)$, where $\frac{RT}{b_T}$ is the slope, and $\frac{RT}{b_T} ln A_T$ is the intercept.

4.3. Results and discussion

4.3.1. Rock characterization and aging in oil

Calcite rock samples were characterized before and after aging with oil using different techniques: SEM images, contact angle measurements, and RE pyrolysis studies. The aging time with crude oil was selected as 14 days. The time of aging was set based on the analysis of the studies published previously. There was found no common methodology of core aging before wettability modification with wetting fluids. Yao et al. [71] summarized that the typical aging time for mineral plates is up to one week, and for core plugs, it is more than one week. Thus, Standnes and Austad [57] soaked calcite crystals for 30 minutes at room temperature in model oils that contained fatty acids. Deng et al. [191] reported that carbonate rock (Indiana limestone was used in their work) became oil-wet after 0.5 days of contact with oil at 90°C due to its strong tendency to oil-wetness. Das et al. [79] soaked Iceland Spar plates in oil at 120°C for 2-3 days. Sharma et al. [4] aged calcite mineral plates in oil for 5 to 7 days at 80°C. Souayeh et al. [121] aged Iceland Spar samples for 3 weeks at 75°C. Saputra et al. [192] performed a statistical analysis of core samples with different mineral compositions soaked in various oils. The authors observed no significant changes in contact angle values after 35 days of aging. However, after 14 days of aging, the rock surface becomes oil-wet with an average CA value higher than 105°.

The sample is represented by limestone (mudstone according to Dunham's classification of carbonate rock [193]). The rock thin-section microphotograph is shown in Figure 38. The rock is predominantly composed of microcrystalline calcite with local areas of recrystallization. Calcite matrix holds 95% of the structure, porosity is less than 5%, and single isolated cracks are noted. Samples with low porosity were chosen for the experiments to decrease the surface roughness during the CA measurements. Figure 39 demonstrates SEM images of carbonate rock samples before (b) and after (c) aging in oil. The samples are composed of fine calcite crystals with the size of 1-10 μm. Pores are not common, the size is within 0.5-2 μm. Recrystallization areas are characterized by the crystals larger than 50 μm. According to different scale SEM images in Figure 39 the

samples are characterized by comparable surface roughness, microstructure, and porosity. There are no any apparent differences in rock microstructure before and after aging. However, the results of RE pyrolysis analysis confirm the adsorption of hydrocarbons on calcite. It can be seen from Figure 40 that a negligible quantity of HCs was present in an initial rock sample cleaned with toluene. After soaking in oil for 14 days, a significant amount of liquid hydrocarbons that correspond to the S1 peak were observed in the oil film that covered the samples. Heavy oil components such as resins and asphaltenes that correspond to the S2 peak of the pyrogram were also present in the aged core sample. From the temperature profile of the heating rate: peak S1 (300°C) appears in the period between 4 to 9 mins, and peak S2 appears in the period between 9 and 15 minutes. It should be noted that polar oil components from heavy fractions mainly cause the hydrophobicity of carbonate rocks [13].
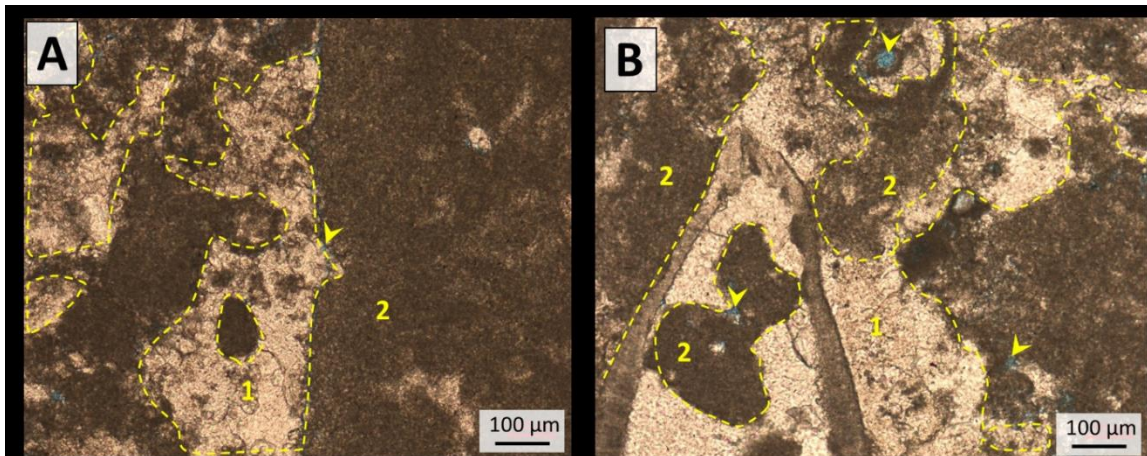
Figure 38. Microphotograph of thin-section, 1 – areas of calcite recrystallization, 2 – calcite matrix, arrows indicate single pores. A – local recrystallization of calcite micrite, B – area with single pores
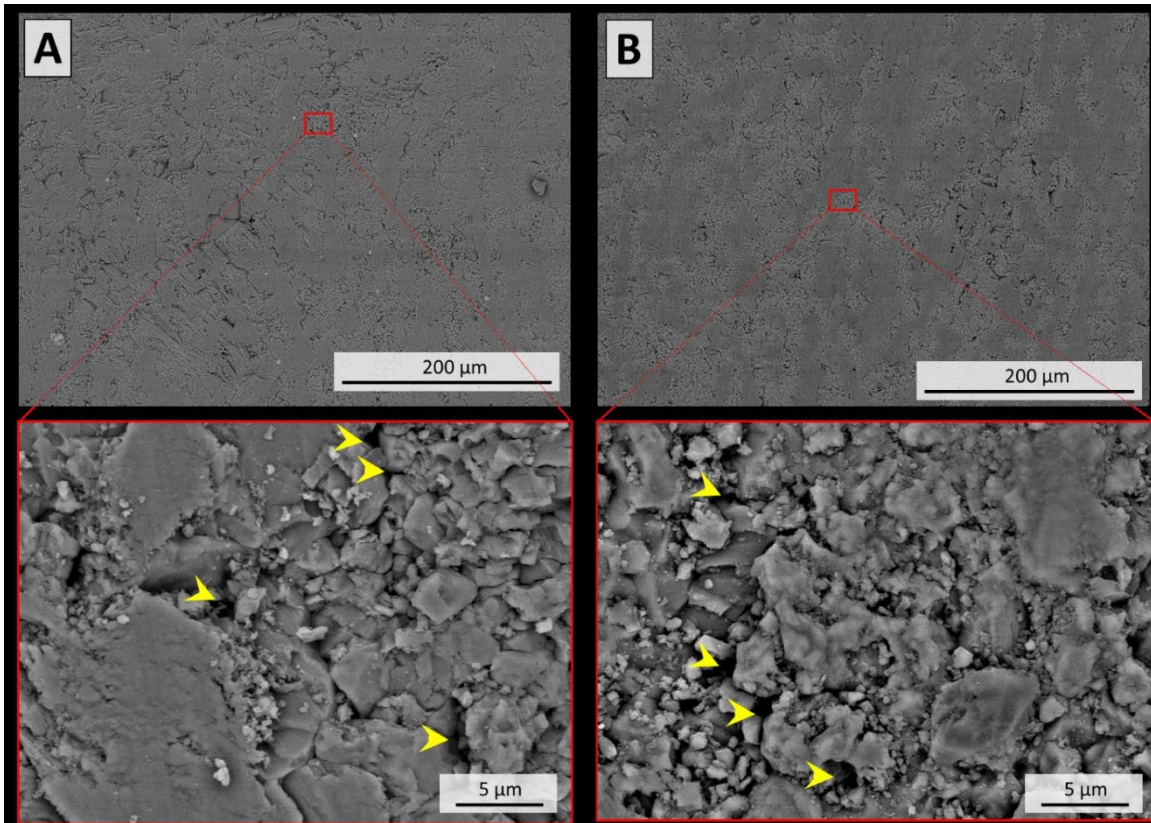
Figure 39. SEM images of calcite samples before (A) and after (B) oil aging. Arrows indicate pores. Microstructure is identical before and after aging
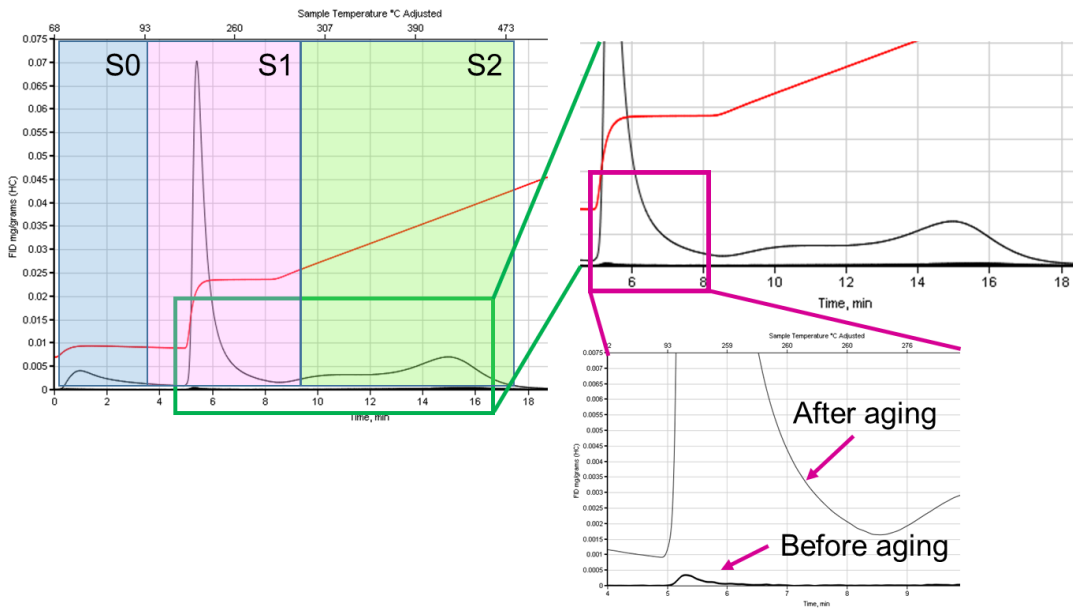
Figure 40. Pyrograms of calcite samples before and after aging in oil. Red line indicates temperature, black lines are pyrograms of samples

Contact angle measurements were performed to evaluate the wettability change before and after the treatment of carbonate rock samples with oil. As was reported before [31,191], the surface is classified as water-wet with CA values lower than 70°, intermediate-wet with CA ranging from 70° to 110°, and oil-wet starting from 110°. The results are shown in Figure 41. As one can see, the initial surface was intermediate-wet with contact angles ranging from 85° to 107°. After aging with oil, a stronger tendency to oil-wetness was observed, and the CA varied from 97° to 117°. The wettability of the samples became more uniform, thus allowing us to compare the effect of further surfactant treatment.
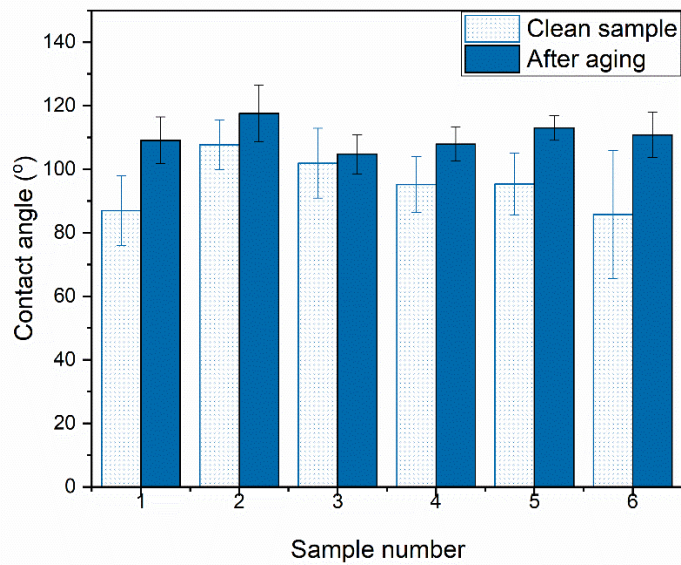
Figure 41. Contact angle values of initial core samples and aged in oil (rock-water-air contact, ambient conditions)

4.3.2. Wetting ability evaluation

Contact angle measurements were performed for carbonate rock surface wettability assessment at the macro level. The CA values after treatment with surfactant compositions were compared with contact angles after oil aging. As presented in Figure 42a and Table 12, sodium laureth-11 carboxylate $C_{11}E_{11}A$ is ineffective in deionized water. The average CA of the sample is $115\pm3°$, which is higher than before surfactant treatment, namely $109\pm7°$. This fact may be explained by the insufficient interaction of $C_{11}E_{11}A$ molecules with adsorbed oil components. When salts are present in brine, the CA decreases

significantly. Thus, when the solution contains 5 wt% of NaCl and 1 wt% of $CaCl_2$ and $MgCl_2$ (Hard1 artificial brine, Table 11), the rock surface becomes water-wet, characterized by a CA value of 44±5°. The addition of 0.5 wt% Na_2SO_4 (Hard2 artificial brine) has no significant effect on $C_{11}E_{11}A$ wetting ability resulting in a contact angle value of 51±11°. The CA values in Hard1 and Hard2 brines are close and compatible. The difference is within the limits of the instrument error and the entire method. It was reported that wettability alteration (WA) depends on brine salinity with the strongest ability of calcium Ca^{2+} and sulfate SO_4^{2-} ions to change the wetness towards a preferential water-wet state [17,194]. This hypothesis was supported by the results obtained in the present work. The wetting ability of $C_{11}E_{11}A$ correlates with its interfacial performance. When at least 5 wt% of NaCl and 1 wt% of $CaCl_2$ and $MgCl_2$ are added to the solution, the IFT on the boundary with oil decreases until the value less than 1 mN/m compared to 4.29 mN/m in DI water at 70°C, Table 11.

It can be seen from Figure 42b that sodium trideceth-7 carboxylate $C_{12}E_7A$ has a strong tendency to hydrophilize the surface. Likewise the performance of $C_{11}E_{11}A$, $C_{12}E_7A$ with a shorter EO chain is more active in the presence of salts. Thus, in deionized water, it decreases the CA value from 108±5° to 27±12°. In the presence of 5 wt% NaCl (brine Soft1), the contact angle changes from 113±4° to 17±5°. When 0.1 wt% of sodium sulfate Na_2SO_4 is added to the composition (brine Soft2, Table 11), the CA decreases from 111±7° to 20±9°, Table 12. Calcium ions were not added to the brine compositions due to the stability limitations of $C_{12}E_7A$. It can be concluded that 0.1 wt% of Na_2SO_4 is a negligible concentration and has no positive effect on the wetting ability of the surfactant. The comparison of contact angle profiles for $C_{11}E_{11}A$ in Hard1 brine and $C_{12}E_7A$ in Soft1 brine is shown in Figure 43a,b.
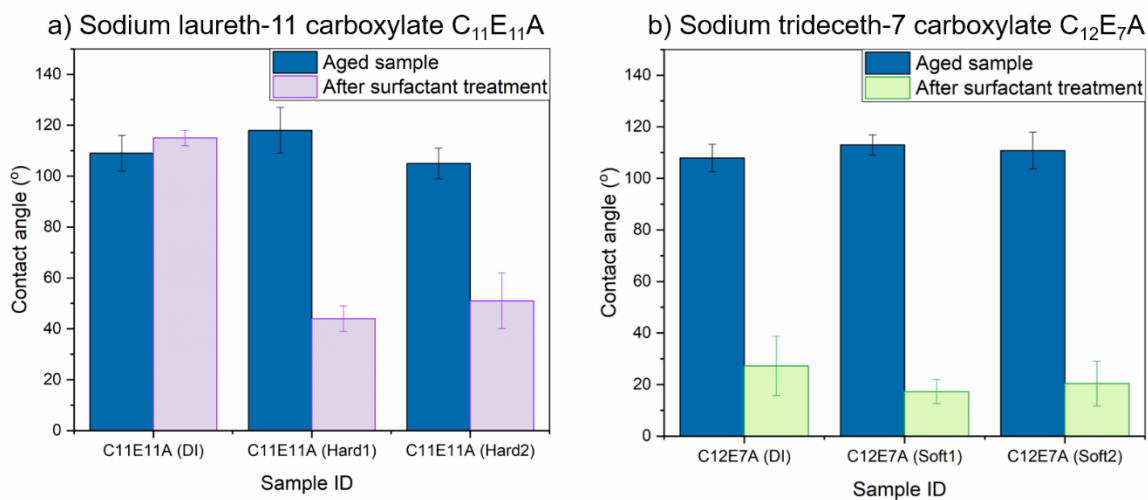
Figure 42. Contact angles values before and after treatment with surfactant compositions: (a) $C_{11}E_{11}A$, (b) $C_{12}E_7A$ (rock-water-air contact, ambient conditions)
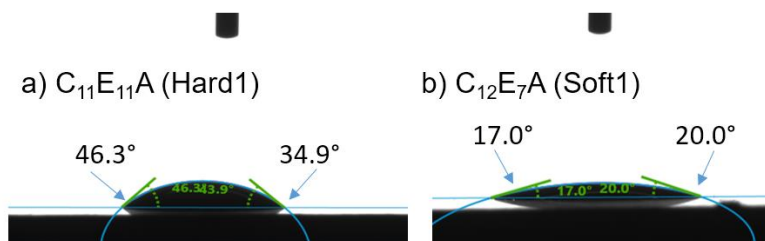
Figure 43. Contact angle profiles of DI water on the oil-aged calcite chips surface after soaking in (a) $C_{11}E_{11}A\_Hard1$ and (b) $C_{12}E_7A\_Soft1$ solutions (rock-water-air contact, ambient conditions)

As alkyl ether carboxylates contain an ethylene oxide chain, their behavior can be compared with that of nonionic ones. The wettability alteration by nonionic surfactants, namely ethoxylated alcohols, was studied by several researchers. Our results are in accordance with findings reported by Das et al. [17,79] that surfactants with fewer ethylene oxide units make the surface more water-wet. This can be explained by the capacity of surfactants to interact with adsorbed oil components. The shorter the EO chain, the more hydrophobic surfactant is. Thus, if a surfactant is well soluble in oil and interacts with oil components, it will be a good wetting agent. When the EO chain is longer, the surfactant is more hydrophilic and consequently better water-soluble. Therefore, the shorter the EO

fragment is, the better it hydrophilizes the rock [17]. A more detailed explanation of the WA mechanism is given in the next section.

Table 12. Contact angle values of clean carbonate rock samples, aged with oil and treated with surfactants

ID	Contact angle, °		
	Initial (as-is)	Oil-aged	Treated with surfactant
$C_{11}E_{11}A$ (DI)	87 ± 11	109 ± 7	115 ± 3
$C_{11}E_{11}A$ (Hard1)	108 ± 20	118 ± 9	44 ± 5
$C_{11}E_{11}A$ (Hard2)	102 ± 22	105 ± 6	51 ± 11
$C_{12}E_7A$ (DI)	95 ± 9	108 ± 5	27 ± 12
$C_{12}E_7A$ (Soft1	95 ± 10	113 ± 4	17 ± 5
$C_{12}E_7A$ (Soft2)	86 ± 14	111 ± 7	20 ± 9

4.3.3. Carbonate rock characterization after treatment with surfactants

It was reported that four techniques indicate qualitative wettability changes in the rock surface: SEM, infrared spectroscopy, thermogravimetric analysis, and atomic force microscopy [32]. TGA is an appropriate method to specify the amount of components adsorbed onto the rock surface [32,75]. It indicates the weight loss of the rock sample as a function of temperature. In past literature thermogravimetric analysis was applied for the analysis of rock wettability after the adsorption of organic acids [16,195–197], as well as after treatment with surfactants [75,80,198]. The results of TGA analysis point to the removal of physisorbed and chemosorbed compounds from the surface, and the decomposition of the rock [195]. In this work, we propose to use the pyrolysis method for qualitative WA analysis as a TGA alternative. Rock-Eval pyrolysis is a well-known approach for organic matter characterization [175,178]. However, it was not used for wettability alteration and surfactant adsorption investigation before. Thus, we suggest the application of the Rock-Eval pyrolysis method for the evaluation of the WA mechanism with surfactants. It allows determining the types and amount of hydrocarbons washed by surface active agents. Further, the method enables estimating whether the surfactant molecules have adsorbed onto the rock surface or not. The advantage of the RE pyrolysis

method over the TGA technique is that it allows for an indication of the temperature of hydrocarbon evaporation "washed" with surfactants.

First, a pyrogram of aged carbonate rock sample was obtained as a baseline, as shown in Figure 40. Second, pyrograms of surfactants in deionized water were captured for reference. For this purpose, a drop of surfactant solution was placed onto the rock sample calcined at 550°C to remove all hydrocarbons. The detailed methodology is explained in section 2.2.4. Figure 44 demonstrates the profiles of $C_{11}E_{11}A$ and $C_{12}E_7A$ surfactants. It can be observed that the temperature profiles are similar since the structure of the AECs used in this study differs only in the alkyl tail and ethylene oxide chain lengths. Third, rock samples after treatment with surfactants were analyzed. Finally, all results were analyzed and compared.
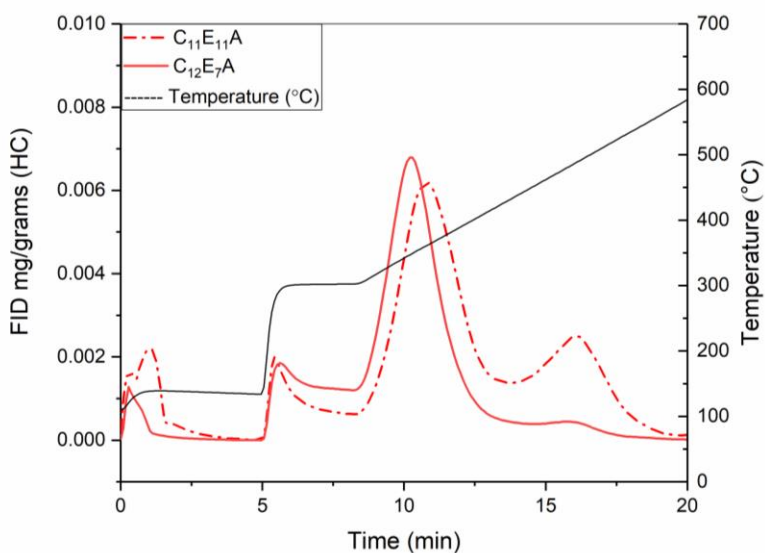
Figure 44. Pyrograms of surfactants on pure calcite (calcined at 550°C)

The comparison of $C_{11}E_{11}A$ pyrograms is shown in Figure 45, where the blue line corresponds to the initial core sample, and the red line corresponds to the surfactant profile. Green, lilac, and orange lines correspond to samples soaked in $C_{11}E_{11}A$ dissolved in DI, Hard1, and Hard2 (Table 11) artificial brines, respectively. It can be seen that all surfactant compositions remove a significant part of hydrocarbons. Particularly liquid hydrocarbons that correspond to the S1 peak, as well as heavy polar oil components such as resins and

asphaltenes (S2 peak on the pyrogram). However, no significant difference can be noted between the profiles of three core samples treated with different surfactant compositions (brine salinity varied). Only the $C_{11}E_{11}A$_Hard1 pyrogram (lilac line, Figure 45) is slightly lower than pyrograms that correspond to $C_{11}E_{11}A$_hard2 and $C_{11}E_{11}A$_DI, and it can be concluded that it washes more hydrocarbons. This is in agreement with contact angle values, Table 12 (except of $C_{11}E_{11}A$ in DI water case). Besides that, no surfactant adsorbed can be indicated in the temperature profile as no peak on the 10th minute is observed. Yet, it was found from the contact angle measurement results (Figure 42) that $C_{11}E_{11}A$ was not effective in deionized water. The observation can be explained by low interfacial activity of AECs with oil in the absence of salts that was discussed in the section 2.3.2.

Thus, it can be summarized that sodium laureth-11 carboxylate only washes a certain amount of hydrocarbons but does not adsorb onto the rock surface, forming a double layer via the "coating" mechanism. Despite quite good wetting ability in the presence of salt (the contact angle values were 44±5° and 51±11° in Hard1 and Hard2 brines, respectively), the water drop did not fully spread over the surface, Figure 43.

Figure 46 illustrates the pyrograms of $C_{12}E_7A$ surfactant. The blue line corresponds to the initial core sample, and the red line corresponds to the surfactant profile; purple, cyan, and orange lines conform to the core samples treated with $C_{12}E_7A$ in DI, Soft1, and Soft2 brines, respectively. According to the data obtained, each composition removes a particular amount of hydrocarbons, the forms of S1 and S2 peaks point to this. Unlike sodium laureth-11 carboxylate, $C_{12}E_7A$, with a shorter EO chain, adsorbs onto the rock surface. The profiles of samples soaked in surfactant composition based on Soft1 and Soft2 brines (cyan and orange lines, Figure 46) demonstrate this. A peak on minute 10 nearly reproduces the main peak of surfactant itself. Presumably, their shapes are not entirely identical due to some amount of heavy hydrocarbons that were not thoroughly washed by the surfactant, and thus remained on the sample surface. The $C_{12}E_7A$_DI temperature profile (purple line, Figure 46) demonstrates that the composition washes more HCs, but no surfactant has adsorbed onto the surface. The peak on minute 10 repeats the shape of the oil-aged core sample. These results are supported by the contact angle values (Table

12). The CA after calcite slice soaking in $C_{12}E_7A$ dissolved in deionized water is $27\pm12°$. The average CA values for samples treated with $C_{12}E_7A$ in the presence of salts are significantly lower, i.e. $17\pm5°$ and $20\pm9°$ for Soft1 and Soft2 brines, correspondingly. The better effectiveness of $C_{12}E_7A$ can be explained by its adsorption indicated by the pyrolysis results. It was reported that the wettability alteration and adsorption of surfactants are in direct correlation [199]. Specifically, the higher the adsorption, the lower the contact angle of wetting fluid onto the rock surface. Notably, ethoxylated surfactants with shorter EO chains are more likely to adsorb onto carbonate rock, provide high surface coverage and thus also demonstrate a better WA performance [17,199].
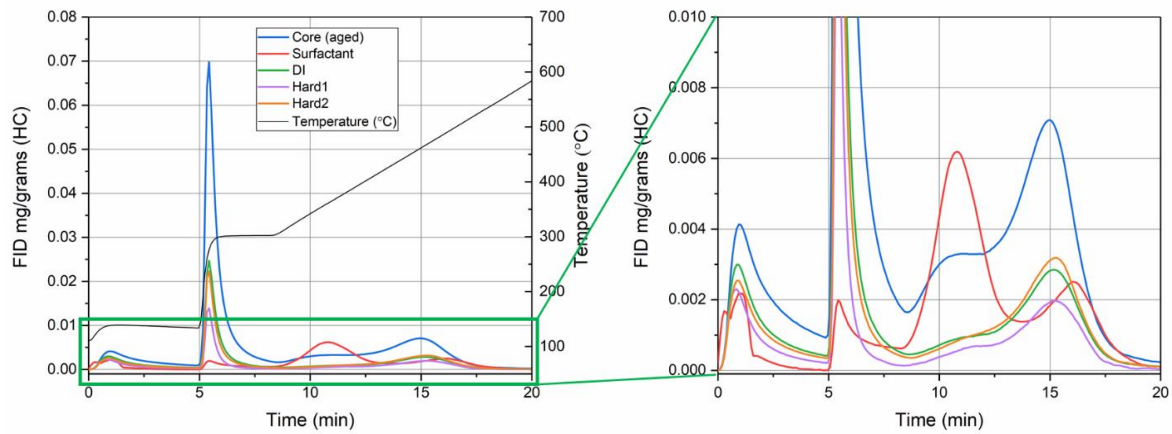
Figure 45. Pyrograms of carbonate rock samples before and after soaking in $C_{11}E_{11}A$ surfactant solutions
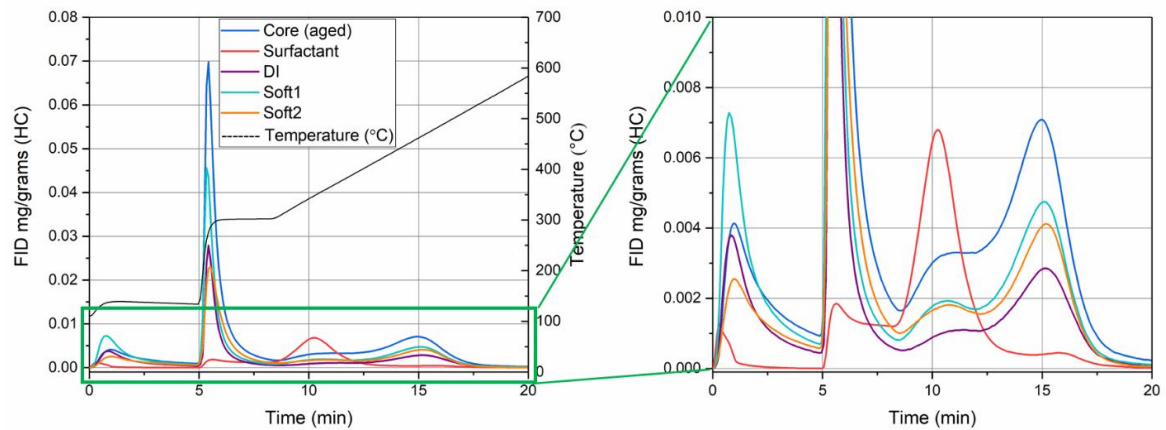
Figure 46. Pyrograms of carbonate rock samples before and after soaking in $C_{12}E_7A$ surfactant solutions

4.3.4. Mechanism analysis of wettability alteration with AECs

Hammond and Unsal [200,201] reported that surfactants might change the wettability towards water-wet through "coating" and "cleaning" mechanisms. The coating mechanism implies the adsorption of surfactant molecules onto the rock surface due to hydrophobic interactions with hydrocarbons. Cleaning means desorption or "washing" of oil components from the rock via complex formation with surfactant molecules. Hydrophobic interactions are significantly weaker than ion-pair formation [202], and it was considered that cationic surfactants (form ion pairs) are much more effective as wettability modifiers compared to anionic and nonionic ones [54]. Then, it was found that hydrophilization directly correlates with the adsorption of surfactant.

We suppose that AECs used in this work demonstrated both mechanisms. All surfactant compositions removed a certain amount of adsorbed hydrocarbons, but only $C_{12}E_7A$ surfactant in the presence of ions coated the rock surface (that was illustrated through pyrolysis analysis). The obtained results in Figure 42 and Table 12 demonstrated that the integrated mechanism of cleaning and coating could lead to a successful wettability alteration. Several researchers described the combined WA mechanism. Das et al. [17] introduced a model of wettability modification by ethoxylated nonionic surfactants that involved both cleaning and coating processes. First, surfactants covered the rock through the hydrophobic interactions between their tails and adsorbed oil components, forming a temporary water-wet surface. Then, water assisted by surfactant molecules swept the oil and thus cleaned the solid surface. After that, surfactant molecules occupied the cleaned area on the solid surface, creating a strong hydrophilic zone.

Jarrahian et al. [75] described the WA mechanism of a nonionic TritonX-100 evaluated through TGA analysis. The authors found that TritonX-100 adsorbed onto the rock surface via polarization of π electrons and ion exchange and desorbed the stearic acid from the surface. Then, the stearic acid molecules adsorbed on the surfactant layer through interactions with the hydrophobic tails. This resulted in a weak water-wet condition of dolomite. Since AECs have no benzene ring in their structure (consequently no π-electrons), the interactions with oil components may occur between $–CH_2\text{-}O\text{-}CH_2–$

110

ethylene oxide fragments through hydrogen bonding and the formation of bilayers or hydrophobic interactions [80,121]. In the present case, $C_{11}E_{11}A$ was presumably performed in accordance with the cleaning mechanism and removed a part of hydrocarbons from the rock surface. In contrast, $C_{12}E_7A$ demonstrated a combined mechanism. It washed a certain quantity of hydrocarbons and then occupied active sites of calcite through hydrogen bonding of ethoxy units with hydroxyl and carboxylic groups [80]. A brief summary of WA mechanisms with surfactants is shown in Table 13.

Table 13. Comparison of proposed wettability alteration mechanisms based on experimental and theoretical results

Reference	Surfactant	Rock	Experimental techniques	Mechanism proposed
[200]	_	_	Numerical simulations of coating mechanisms	There is no surfactant adsorption from the meniscus. It occurs when the meniscus passes through and depends on the driving velocity, i.e. the time for adsorption
[201]	_	_	Numerical simulations of cleaning mechanisms	When a surfactant able to alter wettability imbibes spontaneously and acts by a "cleaning" process, the meniscus propagates faster that when only "coating" mechanism takes place
[75]	Triton X-100 (nonionic)	Substance of crystalline dolomite	Contact angle measurements, TGA, AFM, FTIR, zeta potential measurements	Adsorption on rock surface due to polarization of π-electrons and ion exchange with stearic acid
[17]	Secondary alcohol ethoxylates, Nonylphenol ethoxylates (nonionic)	Iceland Spar	Contact angle measurements, kinetic analysis	Combination of "coating" and "cleaning" mechanisms leads to a better wettability alteration. WA is enhanced at high temperatures and short EO chain length
[80]	Polyethoxylated Surfactants (nonionic)	Iceland Spar	Contact angle measurements, TGA, FTIR, zeta potential measurements	Two possible mechanisms are proposed. (1) Adsorption of surfactant via hydrophobic interactions followed by surfactant double layer. (2) Hydrogen bonding between EO groups and hydroxyl or carboxylic groups of adsorbed oil components on the rock.
Present study	$C_{11}E_{11}A$ $C_{12}E_7A$ (anionic)	Limestone	Contact angle measurements, Rock-Eval pyrolysis, SEM	Combination of "coating" and "cleaning" mechanisms leads to a better wettability alteration and depends on surfactant structure. Both coating and cleaning with

111

				surfactants were detected with Rock-Eval pyrolysis

4.3.5. Zeta potential of carbonate rock particles

Zeta potential shows the rock surface charge, which is a key parameter in studying the mechanism of surfactant adsorption [203]. First, the ζ-potential of fine rock particles (140 μm) in deionized water and artificial brines was evaluated. It was found that the surface charge of the limestone in DI water was negative, namely -3.69 mV at a pH value of 5.6. In brines Hard1 and Hard2 the ζ-potential was positive in the range from +4 to +5 mV. This is supported by the data described in the literature [203,204]. Kasha et al. [204] reported that the ζ-potential of pure calcite powder in DI water was positive at pH values below 6 and became negative at pH=6 and higher. However, ζ-potential becomes positive in the presence of salts and higher pH values. This may be explained by the fact that Ca^{2+} ions are strong potential determining ions for calcite and thus change the charge of limestone rock particles [204].

In this work, zeta potential measurements were performed with clean rock powder that was not aged in oil. It should be noted that interactions between surfactant molecules and oil film are discussed in wettability evaluation experiments, and in adsorption and zeta potential measurements the interactions occurred between surfactants and clean rock. These conditions were created to simulate more clearly the processes of adsorption and wettability as the hydrophobicity of the rock surface is ensured by the adsorption of heavy oil components [13], and the highest adsorption of surfactants occurs on clean negatively charged calcite surface.

Figure 47 demonstrates the pH change after rock particles equilibration in surfactants compositions and ζ-potential values of rock. It was found that the pH values increased after the equilibration from 5-6 until 9-10. This occurs due to calcite dissolution and the release of hydroxyl ions OH^- that could increase the adsorption of surfactant molecules on the rock surface [80]. This is supported by the observation that in the presence of surfactants in water, limestone particles have a net negative charge. That indicates on the adsorption of anionic surfactant molecules on the limestone particles. After adding salts

112

into surfactant solutions, the zeta potential is still negative with the decreased magnitude. In the case of $C_{12}E_7A$, the zeta potential is -12.9 ± 0.5 mV in brine that contained 5 wt.% NaCl (Soft1) and -14 ± 0.5 mV in brine with 5 wt% NaCl and 0.1 wt.% Na_2SO_4 (Soft2). The difference in ζ-potential between these two compositions is due to the presence of Na_2SO_4 and consequently SO_4^{2-} ions in Soft2. As for $C_{11}E_{11}A$, ζ-potential was negative but close to 0. This can be explained by the high noise level of the zetasizer that took place because of high brine conductivity. However, sulfate ions SO_4^{2-} again have an input in ζ-potential value that was lower for Hard2 brine.
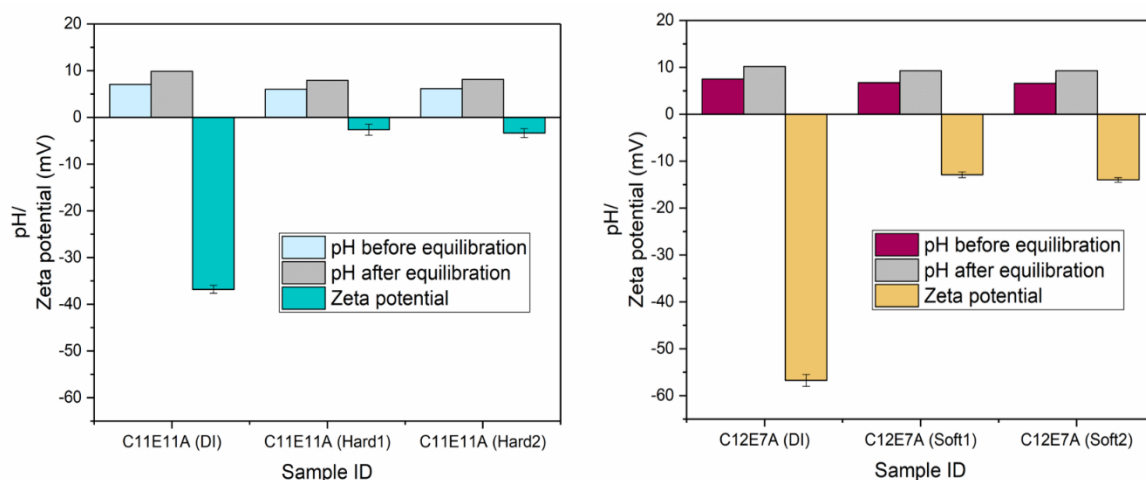
Figure 47. pH of surfactant solutions before and after equilibration with fine rock particles and zeta potential values (ambient conditions)

4.3.6. Static adsorption of AECs and mechanism evaluation

Static adsorption test was performed for 4 compositions discussed previously in this work (Table 11), namely $C_{11}E_{11}A$ in DI water and Hard1 brine, and $C_{12}E_7A$ in DI water and Soft1 brine. The main purpose was to compare the adsorption behavior of AECs with different EO chain lengths and the salinity effect. Surfactant concentrations in the post-CMC region were considered in this experiment ($0.1\div1$ wt%), and the adsorption isotherms obtained are given in Figure 48. The higher experimental adsorption value was achieved by $C_{11}E_{11}A$ in deionized water and was 9.23 mg/g-rock at an initial surfactant concentration of 0.75 wt%. Notably, both surfactants showed similar trends in deionized water and then comparably changed their behavior in the presence of salts despite the molecular structure

113

variations. Also, the adsorption values of $C_{12}E_7A$ with a shorter EO chain were significantly lower.

As shown in Figure 48, the adsorption of $C_{11}E_{11}A$ in deionized water (blue line) gradually increased until it reached a plateau at a value of ~9 mg/g-rock. At high concentrations, the adsorption slightly reduced, indicating a desorption process that took place due to full surface coverage and saturation. This phenomenon was described in past literature and was attributed to micellar exclusion at high surfactant concentrations in the post-CMC region. Thus, the active sites of the rock surface are charged similarly and repel the micelles from the rock-liquid interfacial area back to the solution volume resulting in an adsorption decrease [99,205]. In the case of $C_{12}E_7A$ in DI water (orange line), the adsorption pattern is close to $C_{11}E_{11}A$ in DI: it increases until a value of ~4 mg/g-rock and then slightly reduces. This behavior can be characterized as monomolecular adsorption with a monolayer formation [186]. The amount of adsorbed surfactant was lower for $C_{12}E_7A$ with fewer EO units in the structure. The EO chain length effect was discussed in the literature for nonionic ethoxylated surfactants C_mE_n. It was reported that increased EO fragment leads to higher adsorption onto silica at a fixed hydrophobic chain length [206,207]. However, the behavior of AECs is different, and it was found that the longer EO fragment caused higher adsorption onto crushed limestone. Presumably, this occurs due to the formation of hydrogen bonds between the ethoxy chain and the rock surface's OH- or COO- ions.

Salinity has a significant effect on the equilibrium adsorption profiles of both AECs. As shown in Figure 48, the behavior of $C_{11}E_{11}A$ in Hard1 brine (purple line) and $C_{12}E_7A$ in Soft1 brine (green line) changed similarly: the adsorption gradually increases and does not reach a plateau that indicates the formation of multilayers [208] and a change of the adsorption type from monomolecular in DI water to a polymolecular in brines. Again, the adsorption values of $C_{11}E_{11}A$ are significantly higher than of $C_{12}E_7A$. Similar adsorption profiles were obtained by Belhaj et al. [114] for an AEC-based surfactant blend onto quartz samples at 106°C and salinity of 32k ppm.

The adsorption of surfactants on minerals is significantly affected by the surface charge. The ζ-potential of limestone rock powder in deionized water was negative and negatively charged AECs were supposed to repulse from the rock surface resulting in lower adsorption. However, the adsorption values were higher in DI water in the considered range of concentrations (0.1 – 1 wt%) and it can be supposed that electrostatic interactions are not the leading force in the adsorption of ethoxylated surfactants. In the presence of cations Na^+, $Ca^{2+,}$ and Mg^{2+}, carbonate rock particles' zeta potential was positive, which means the reduced repulsive forces between rock and surfactant. Thus, higher adsorption of anionic-nonionic surfactants was expected. However, the amount of surfactant losses decreased, and the behavior (adsorption isotherm profile) changed. Jian et al. [207] found that the salinity did not affect the adsorption of nonionic ethoxylated surfactants on different minerals (calcite, dolomite) and explained that it was not governed by electrostatic interactions with minerals, but mainly occurred due to hydrogen bonding. As for charged AECs, the presence of ions can partially break the hydrogen bonds, and consequently, the electrostatic interactions contribute to the adsorption process leading to the formation of multilayers. The isotherms obtained (Figure 48) support this idea. The adsorption implies a complex of interactions that needs further investigation to be explained more appropriately.
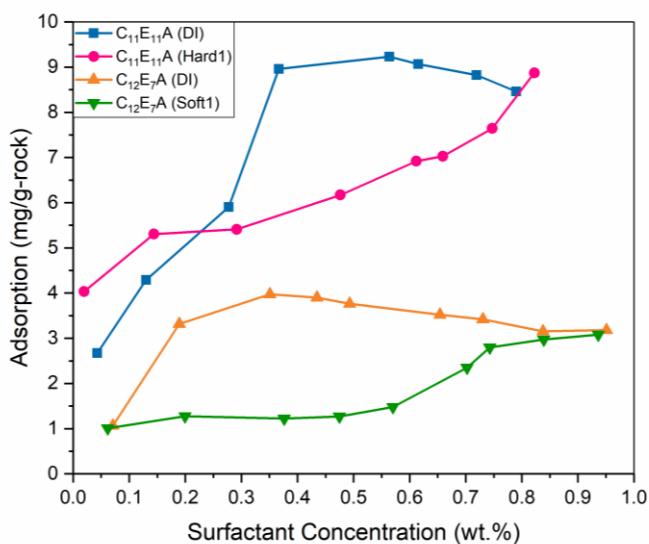
Figure 48. Adsorption isotherms of surfactant compositions at 70°C (titration was performed at ambient conditions)

4.3.7. Equilibrium adsorption models

The experimental data were analyzed with two-parameter equilibrium adsorption models: Langmuir, Freundlich, and Temkin. The results and model parameters are presented in Figure 49 and Table 14. The fittings for $C_{11}E_{11}A$ and $C_{12}E_7A$ in DI water showed a good agreement with the Langmuir model that describes the monolayer formation of the adsorbate as a finite process [186]. This is confirmed by the values of determination coefficient R^2 that is 0.9507 for $C_{11}E_{11}A$ and 0.8823 for $C_{12}E_7A$.

The fitting results for AECs in brines are different. $C_{11}E_{11}A$ in Hard1 brine that contained Na^+, Ca^{2+} and Mg^{2+} cations is better described by the Freundlich model with R^2=0.8516. The best R^2 value for $C_{12}E_7A$ in Soft1 brine was 0.6452, also obtained with the Freundlich model introduced for multilayer adsorption description with various active sites [186,208]. These results support our previous explanations of the salinity effect on the adsorption of AECs.

An inverse relationship was observed concerning the correlation of adsorption capacity and the wetting ability of AECs. $C_{11}E_{11}A$ has shown higher adsorption on crushed limestone samples, but the wetting ability was comparably low. $C_{12}E_7A$ demonstrated lower adsorption in a static test but strong hydrophilization properties of core plates aged in oil. This can be explained by the different surfaces involved in these processes. In the case of the wettability evaluation experiment, surfactant molecules first interacted with oil film components. It was discussed that a more hydrophobic surfactant ($C_{12}E_7A$ in this study) more likely dissolves in oil and thus leads to a wettability shift. Upon contact with crushed clean rock with a "fresh" (bare) surface, the interaction occurs more actively between $C_{11}E_{11}A$.

Table 14. Isotherm parameters for Langmuir, Freundlich, and Temkin models

Isotherm model	Parameter	Value			
		$C_{11}E_{11}A$ (DI)	$C_{11}E_{11}A$ (Hard1)	$C_{12}E_7A$ (DI)	$C_{12}E_7A$ (Soft1)
Langmuir	R^2	0.9507	0.7138	0.8823	0.4819
	K_L	8.3934	69.619	3.7694	13.416
	q_0	9.7656	6.8400	5.4142	2.0820
Freundlich	R^2	0.9051	0.8516	0.5400	0.6452

	K_F	10.4387	7.6612	4.1997	2.5008
	n	2.3912	5.5525	2.7816	2.4509
Temkin	R^2	0.8566	0.7546	0.4525	0.5717
	A	70.119	1470.8	235.30	32.030
	B	1260.2	2734.7	4031.8	3874.6
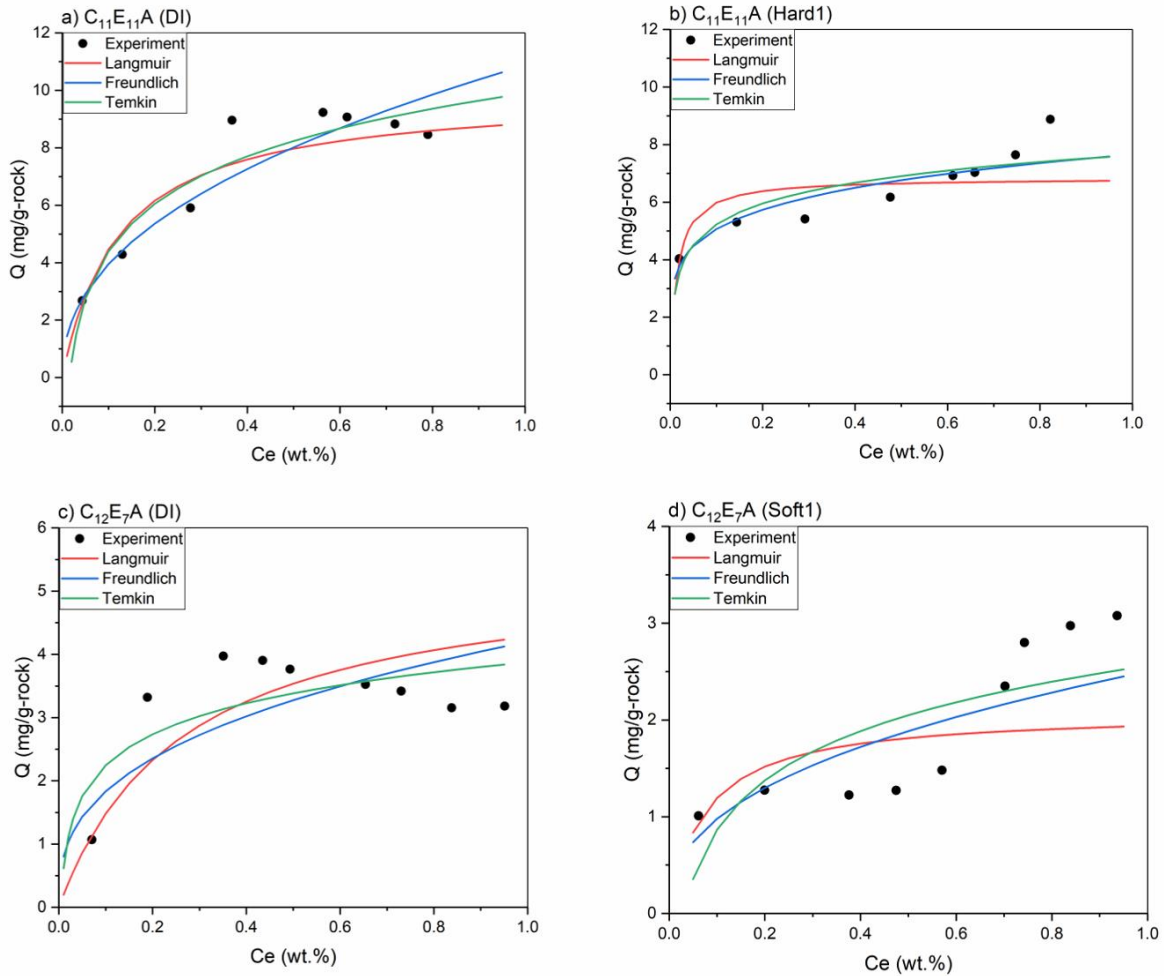
Figure 49. Adsorption isotherm models and experimental data

4.4. Conclusions

This work investigated the wetting ability and adsorption capacity of linear alkyl ether carboxylate surfactants in carbonates. The contact angle measurements showed that both sodium laureth-11 carboxylate $C_{11}E_{11}A$ and sodium trideceth-7 carboxylate $C_{12}E_7A$

decrease water CA until values are less than 60°. Thus, AECs have shown promising results in the wettability alteration of carbonate rock. These findings were supported by the Rock-Eval pyrolysis studies. In this study, RE pyrolysis was proposed as a technique for surfactant performance characterization after contact with rock as an alternative to thermogravimetric analysis. The static adsorption test showed that the adsorption values of $C_{11}E_{11}A$ were higher than of $C_{12}E_7A$ in both DI water and brines. The presence of salts caused the change in adsorption type from monomolecular to polymolecular for both AECs. The following conclusions can be drawn from the results:

• AECs washed some adsorbed oil compounds from the rock surface. All compositions removed a significant amount of free oil, as well as heavy oil components (resins, asphaltenes), according to the pyrolysis studies. This was indicated by the changes in S1 and S2 peaks on the pyrograms of rock samples treated with $C_{11}E_{11}A$ and $C_{12}E_7A$ surfactant compositions.

• The most effective rock hydrophilization is attributed to surfactant adsorption onto the rock surface. Presumably, the adsorption occurs due to hydrophobic interactions between remained oil components and surfactant tails. The full WA mechanism includes both cleaning and coating processes.

• The degree of ethoxylation has a strong effect on the wetting properties of AECs. $C_{12}E_7A$, with a shorter EO chain, demonstrated a better ability to wet the carbonate rock than $C_{11}E_{11}A$. This can be explained with a certain amount of $C_{12}E_7A$ adsorbed on calcite.

• According to interfacial analysis, salinity has a significant effect on the performance of AECs as wetting agents in carbonates. The wetting ability increases in the presence of ions, as well as the interfacial activity.

• The findings obtained in this study support the outcomes made by other researchers in previous works, namely, better performance was observed with surfactants that follow the coating mechanism adsorbing onto the rock surface.

• The suggested approach of WA mechanism analysis through RE pyrolysis method can be applied to different types of surfactants and their mixtures, and thus the performance of complex chemical compositions for enhanced oil recovery can be quantified effectively.

- The adsorption of $C_{11}E_{11}A$ with a longer EO fragment was found to be higher due to hydrogen bond formation between the ethoxy chain and OH^- or COO^- ions of the rock surface.

- Salinity has a significant effect on the adsorption behavior of AECs. In the presence of ions in brine, hydrogen bonds are partially destroyed, and electrostatic interactions contribute to the adsorption process making possible formation of polylayers when surfactant molecules interact with the rock surface and with each other.

- A better wetting ability of $C_{12}E_7A$ can be explained by a strong tendency to dissolve in oil film that covered the core plate as it is more hydrophobic because of the shorter EO chain. The higher adsorption of $C_{11}E_{11}A$ can be interpreted with its more likely interactions with the clean "fresh" surface of carbonate samples.

The findings reported in this work have shown that AECs have a good ability to decrease oil-water interfacial tension and modify the wettability of carbonate rock. Thus, this type of surfactants can be recommended for application in EOR compositions in moderate and harsh reservoir conditions. Besides that, the conclusions made in this study can be used as a basis for further research work.

Chapter 5. Core flooding test with X-ray saturation control

5.1. Motivation

In previous chapters, a sequence of tests was conducted aiming to determine main trends in the behavior of AEC surfactants depending on their molecular structure and surrounding conditions. Investigation of the ability of surfactants to decrease capillary number through

Core flooding is a commonly used method of water- and gas-based compositions displacement efficiency evaluation. The main goals of such experiments are (1) assessment of recovery factor achieved by a chemical or gas injection and (2) measurements of dynamic residual oil saturation during coreflooding to obtain relative permeability. This data is used in further reservoir simulations to predict the oil production in time and evaluate project economic feasibility.

For a high-quality study, precise fluid saturation control should be performed that is not always trivial. Such techniques as NMR and CT scanning of samples can be applied for this purpose after the samples are extracted from the core holder. Recently, in-situ saturation monitoring (ISSM) with X-rays has become a traditionally used method of fluid saturation determination in commercial core flooding tests. Typically, it is a 1D saturation measurement as a function of core model length and time. This method allows avoiding the systematic errors characteristic for mass balance method.

The present core flooding test was conducted with a most promising surfactant composition $C_{12}E_7A$ that demonstrated optimal set of properties, namely IFT, wetting ability and adsorption capacity. The water flooding stage was followed by surfactant flooding with a 48-hours shut-in for imbibition that resulted in additional amount of extracted oil. Typically, this stage is included in corefloding tests with low-permeability samples when huff-n-puff process is reproduced in the experiment. In the section of results interpretation, we compared two approaches of recovery factor calculation based on mass balance and X-ray scanning data.

5.2. Materials and methods

5.2.1. Materials

Oil. Crude oil (Table 4) was dehydrated and deasphalted by saturating with nitrogen at elevated pressure (12 MPa) and temperature (70°C) and then filtering the oil through a sequence of mechanical filters 7.0-2.0-0.5 µm. This procedure was done in order to avoid precipitation of asphaltenes under reservoir conditions during the experiment and possible damage of pore space. Then, oil was doped with 15% 1-iodooctane as a contrast for X-ray scanner. The oil density was measured with Anton Paar DMA 4200M under reservoir temperature of 70°C and ambient and reservoir pressures, Table 15.

Table 15. Density and viscosity of oil used in core flooding test under target conditions

Pressure, MPa	Temperature, °C	Density, g/mL	Viscosity, mPa·s
Degassed oil			
Atmospheric	70	0.8500	8.030
Reservoir, 12		-	-
Oil modified with 15 wt% 1-iodooctane			
Atmospheric	70	0.9353	5.790
Reservoir, 12		0.9133	2.920

Injected compositions. Based on wettability, IFT and adsorption studies, a surfactant composition was chosen for a core flooding test: brine – 5 wt% NaCl, surfactant – 0.5 wt% $C_{12}E_7A$ in 5 wt% NaCl. The rheological properties were measured at ambient and reservoir pressure and temperature of 70°C. The results are shown in Table 16.

Table 16. Density and viscosity of injected fluids used in core flooding test under target conditions

Pressure, MPa	Temperature, °C	Density, g/mL	Viscosity, mPa·s
Brine (5% NaCl)			
Atmospheric	25	1.0327	-
Atmospheric	30	1.0310	-
Atmospheric	40	1.027	0.800
Atmospheric	70	1.0004	0.500

Reservoir (12)		-	-
Surfactant solution (0.5% $C_{12}E_7A$ in 5% NaCl)			
Atmospheric	70	1.0004	0.500
Reservoir (12)		-	-

Core samples. Limestone core samples from a carrier were selected for the experiment as a representative model rock. The elemental composition was determined with a portable X-ray fluorescence spectrometer Olympus Vanta C [209]. It was found that the calcium is a predominant element and no impurities are present in the rock. Cylinders with the length of 60 mm and diameter of 30 mm were manufactured from the block, Figure 50. Then they were dried at 115°C until constant weight was achieved. The porosity and permeability were measured with an automated gas permeameter-porosimeter "PIK-PP" using helium as a probe gas as it does not cause washout of salts and hydrocarbons from the pore space. The main properties of rock samples are given in Table 17: dimensions, porosity, permeability and mass.
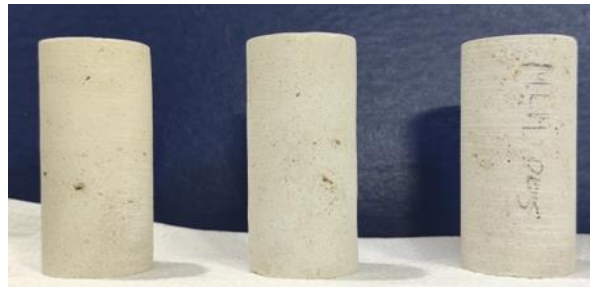
Figure 50. Limestone samples with diameter of 30 mm

Table 17. Main properties of limestone samples used in core flooding test

Sample	Mass (dry), g	Diameter, mm	Length, mm	Volume, cm^3	Porosity (He), %	Permeability (He), mD	Pore volume, cm^3
1	81.88	29.11`	60.58	40.31	23.59	32.74	9.51
2	76.35	28.96	59.94	39.47	27.63	38.99	10.91
3	81.51	29.17	59.73	39.91	23.03	28.19	9.19

Before the experiment, core samples were dried until constant mass and then vacuumed. After that, core cylinders were fully saturated with brine (5 wt% NaCl). To do this, water

was pressurized at 20 MPa in a saturator. To create residual water saturation (connate water), samples were loaded into Atmospheric Model AP-250-008-0 core holders and centrifuged for 48 hours at 40°C in capillary pressure refrigerated centrifuge RC 4500 (Vinci-Technologies). The program used was a capillary test, and the process contained 15 steps with different rotation speed: 300, 500, 700, 900, 1100, 1300, 1500, 1700, 1900, 2200, 2500, 3000, 3500, 4000 and 4500 rpm. Capillary pressure curves (capillary pressure vs water saturation) were obtained for each sample, and the maximum capillary pressure achieved was considered as one that corresponds to S_{wirr}. The residual water content was determined through mass balance, and the free pore volume was calculated. The results are given in Table 18. Thus, the pore volume of the whole core model was 27.52 cm^3. The main core model properties are specified in Table 19.

Table 18. Pore volume in core samples

Sample	Pore volume, cm^3	Residual water volume, cm^3	Free pore volume, cm^3
1	9.51	0.59	8.92
2	10.91	0.72	10.19
3	9.19	0.78	8.41
Total	**29.61**	**2.08**	**27.52**

Table 19. Core model characterization data

Parameter	Value
Length (cm)	18.03
Cross-sectional area (cm^2)	6.64
Porosity (%)	24.75
Abs gas permeability (mD)	32.73
Pore volume (cm^3)	29.61
Free pore volume (cm^3)	27.52
Connate water (cm^3 / PV)	2.08 / 0.07

5.2.2. Methods

Experimental setup. The laboratory setup for core flooding tests was a PIK-OFP/EP apparatus from Geologika equipped with an X-ray transparent core holder PIK-CP. The setup was designed to experimentally determine the residual oil saturation, relative phase permeability, displacement efficiency by X-ray method. The main units are three high-pressure pumps, pressure and differential pressure sensors, pressure gauges, a backpressure regulator (to maintain reservoir pressure at the outlet), valves, and a controlling computer with signal transducers. A graduated (0.2 mL) test tube and scales were used to measure the volume and mass of liquid fluids at the backpressure regulator (BPR) outlet. Continuous supply of fluids is ensured by a system of pneumatic valves and pressure sensors under computer control. A core holder was placed into X-ray apparatus with a help of mobile hydraulic crane. The in-situ saturation monitoring was performed with a linear X-ray scanner (a source and detector moving along the core). A simplified scheme of the core holder is demonstrated in Figure 51.
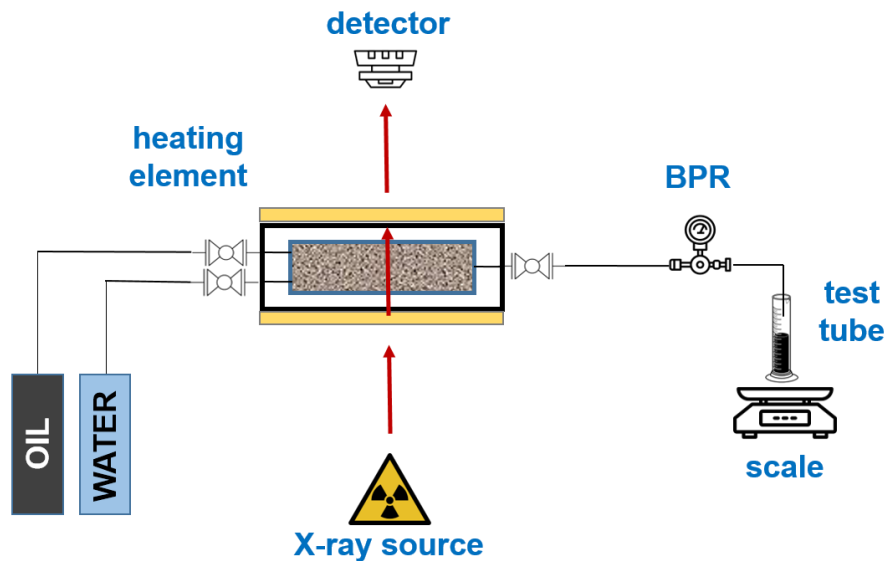
Figure 51. Scheme of X-ray transparent core holder connection with a heating element to PIK-OFP/EP hydraulic system

124

The setup general scheme is shown in Figure 52, where 1 – heat chamber, 2 – three groups of two-piston pumps, 3 – piston column with water, 4 – piston column with oil, 5 – pressure sensor and manometer at the core holder inlet, 6 – pressure sensor and manometer at the core holder outlet, 7 – differential pressure sensors with a pneumatic valve system, 8 – bypass pneumatic valve, 9 – core holder, 10 – heating system of X-ray transparent core holder, 11 – PIK-CP block (lead-steel chamber with X-ray linear scanning system), 12 – BPR, 13 – separator, 14 – crimp pressure maintenance pump, 15 – scale. The general view of the setup is shown in Figure 53.
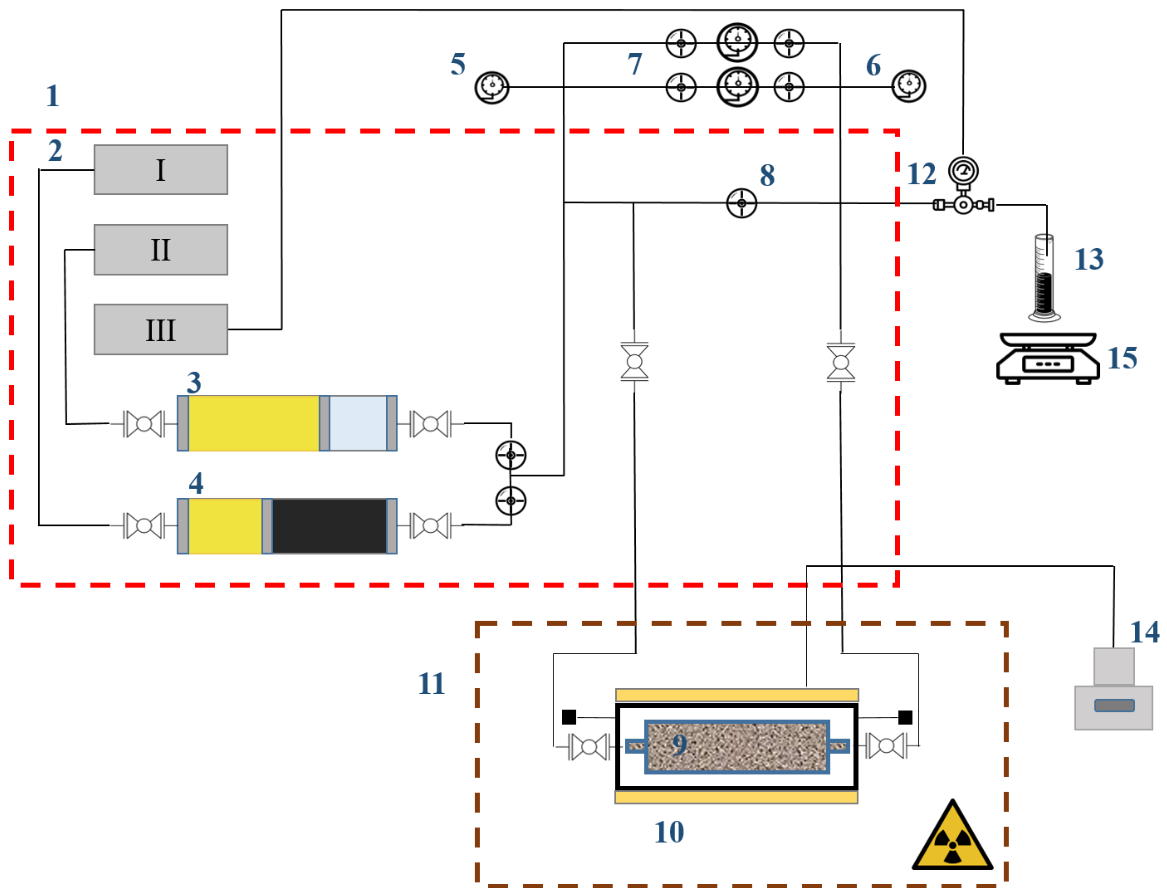
Figure 52. Scheme of experimental setup
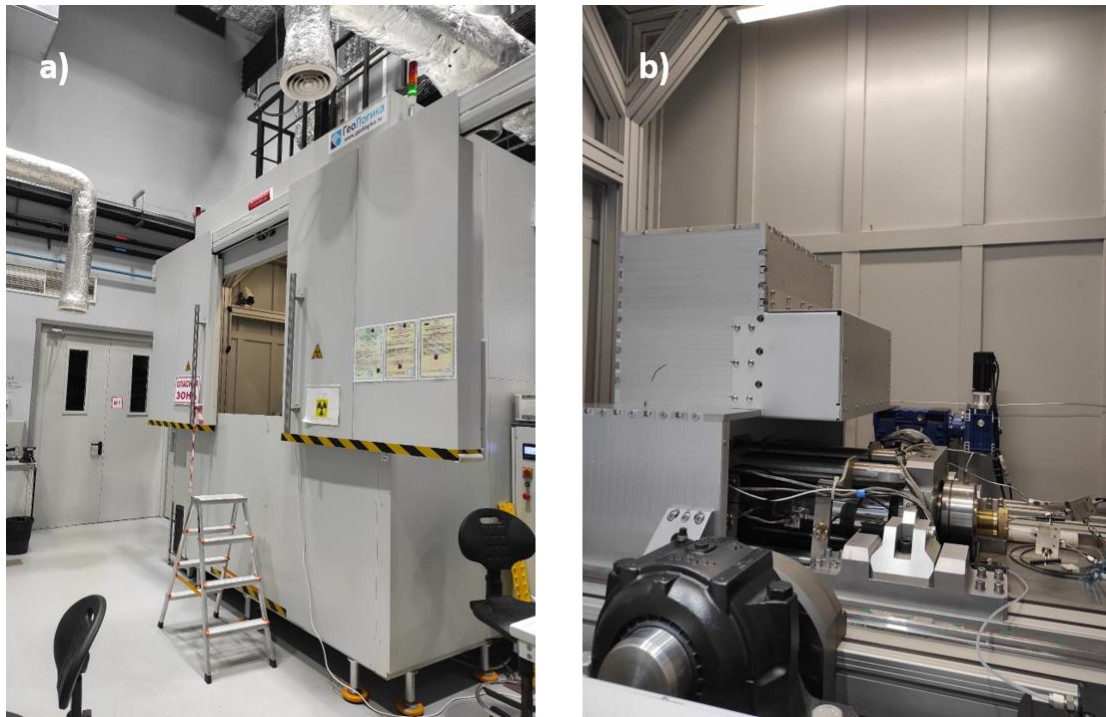
Figure 53. Experimental setup for core flooding experiment: (a) the general view, (b) core holder with X-ray scanner

Experimental design. Core samples were placed in a core holder in order of decreasing permeability, namely sample 2 (38.99 mD) – sample 1 (32.74 mD) – sample 3 (28.19 mD). The coreflood test consisted of five main steps. (1) The first stage included core model preparation, core holder assembly and loading into setup, and thermostatting. Then, the core model was fully saturated with oil. After the reservoir temperature of 70°C was achieved, the system was aged at reservoir pressure of 12 MPa for 1 day to create the hydrophobic wettability of the carbonate rock. (2) On stage 2, brine (5% NaCl) was injected with the rate 0.1 mL/min until steady state, indicated by stabilization of pressure drop stabilization and X-ray scanner indications. (3) Surfactant solution was injected with the rate 0.1 mL/min until steady state. (4) Then, system was shut-in for 48 hours under reservoir conditions (70°C, 12 MPa) to facilitate surfactant imbibition. (5) Surfactant injection was continued with the rate of 0.1 mL/min until steady state. (6) Surfactant was injected with an increased rate of 0.5 mL/min until steady state. The scheme of coreflood

experiment is depicted in Figure 54. The confinement pressure was 22 MPa, and the backpressure 12 MPa.

The time of 1 day for core model aging was chosen based on our previous experience of conducting experiments with this oil. A coreflooding test was performed in an X-ray computed tomography scan (General Electric v|tome|x L240 CT system) using core cylinders of 8 mm diameter. The main purpose was to inject oil in the sample, then displace it with brine and evaluate the wettability change on pore level. It was found that the core surface became hydrophobic after 1 day of contact with oil and no significant changes were observed during further aging. The results are published by Kumar et al. [210]

After the injection of fluids was finished, the core model was washed by benzene-alcohol injection, dried and vacuumed. Then, it was filled with artificial brine (5 wt% NaCl) and scanned to obtain the reference X-ray profile by water.

Saturation control. When applying ISSM method, the saturation is determined not directly. The attenuation of X-rays or gamma rays as they pass through the core holder, the core plug, and the fluids within is used to infer the saturation of the core samples rather than directly measuring it [127,202]. The attenuation of X-ray beams can be defined as follows:

$$\frac{I}{I_0} = e^{-\mu d} \quad , \tag{18}$$

Where I_0 is the intensity of the original X-ray source, I is the intensity measured during the flooding procedure at the detector, μ is the attenuation coefficient of the material (typically known for standard materials used in coreflood tests) between source and detector, d is the thickness of the material [128].

To obtain accurate saturation profiles, the long scanning is performed with the step of 2 mm when an X-ray source and detector are moving along the core model when the injection is stopped. The full scanning takes ~2 hours. Short scans are made every 10 mm

to check for stabilization are measure saturation at certain flooding points. They are made during injection and take about 20 minutes.
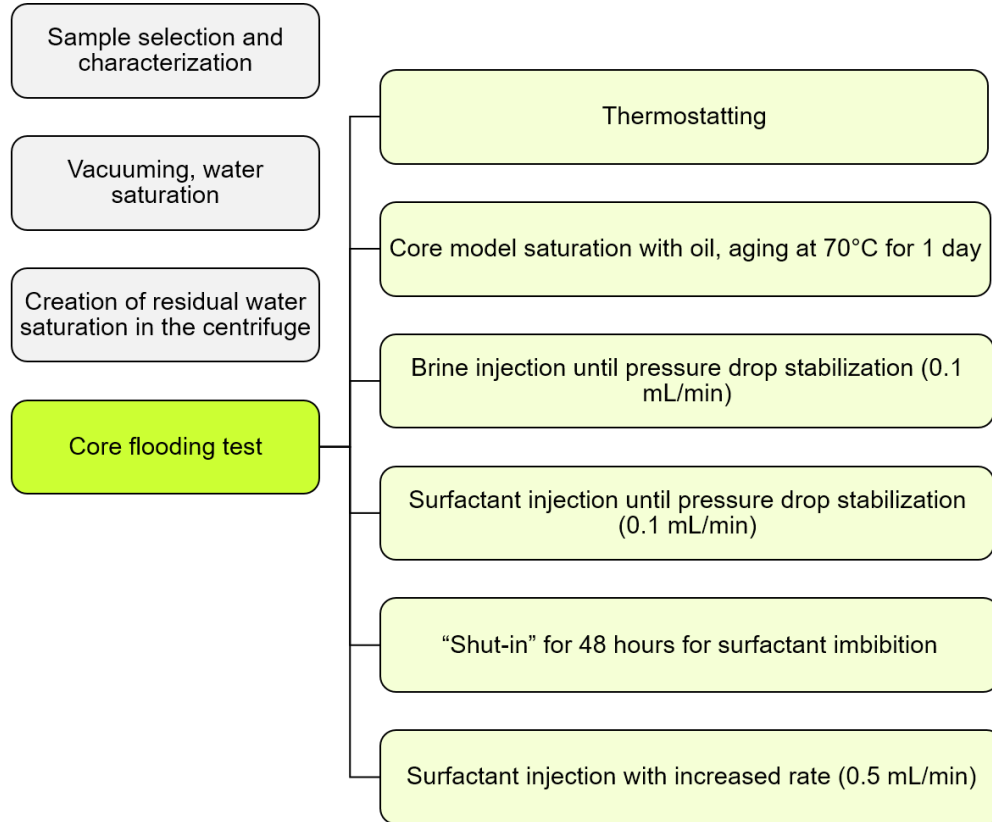
Figure 54. Scheme of core flooding experimental design

Injection rate selection. The injection rate of oil on the first stage of experiment was calculated using the formula below taking into account the value of linear rate of the fluid in the reservoir is 1 m/day [212]:

$$V_{linear} = \frac{864 \cdot Q}{F \cdot \varphi \cdot (1 - S_{wr} - S_{or})} \; ,$$
(19)

Where V_{linear} is linear injection rate (set as 1 m/day), Q is injection rate, F is cross section area of the core model, φ is porosity, S_{wr} is residual water saturation and S_{or} is residual oil saturation. Thus, the injection rate Q was set as 0.1 cm^3/min.

Oil recovery factor determination. In this study, two approaches were applied for RF determination, first based on mass balance and second based on core model saturation analysis. The first method used for oil recovery factor determination was based on mass balance, working well with degassed oil. Oil recovery coefficient (K_{OR}, %) was calculated after the formula:

$$K_{OR} = \frac{m_{oil\ out}}{m_{oil\ in}},\qquad (20)$$

$m_{oil\ out}$ – mass of the oil degassed oil displaced from the core sample during flooding;

$m_{oil\ in}$ – mass of the oil remained in the core sample after flooding; determined by the difference between the masses of oil-saturated and core after flooding.

For better accuracy two additional coefficients were added to the formula:

- ω_{water}, mass.% – mass fraction of water in oil, determined through Karl Fischer titration;

- ω_{LHC}, mass.% – mass fraction of light hydrocarbon components evaporated during filtration under reservoir conditions, determined by chromatography.

Thus, the true $m_{oil\ out}$ was calculated as:

$$m_{oil\ out\ (true)} = m_{oil\ out} - m_{oil\ out} * \omega_{water} + m_{oil\ out} * \omega_{LHC} \quad (21)$$

The second method of recovery factor determination was based on saturation analysis. The water saturation was determined using the formula [128]:

$$S_w = S_{wr} + (1 - S_{wr}) \cdot \frac{\ln(I_{exp}) - \ln(I_{oil})}{\ln(I_w) - \ln(I_{oil})}, \qquad (22)$$

Where S_w is water saturation, S_{wr} is residual water saturation, I_{exp} is the intensity (brightness) measured at the detector during the experiment, I_{oil} is the intensity of oil reference, I_w is the intensity of water reference.

5.3. Results and discussion

5.3.1. Fluid flow dynamics in the core model

In this experiment, limestone samples with typical porosity-permeability relationship for carbonates were used. The porosity-permeability range compared with literature data demonstrated in Figure 55. The full pore volume of the core model (three 60 mm length samples) was determined as 29.605 cm^3. The connate water volume after the samples were centrifuged was 2.083 cm^3, so the initial oil saturation after the samples were filled with oil was 92.96 %. The fluid flow was mainly characterized with the pressure drop (PD) dynamics [213]. PD significant increase indicates plugging of the porous medium or rock components swelling and is unfavorable.
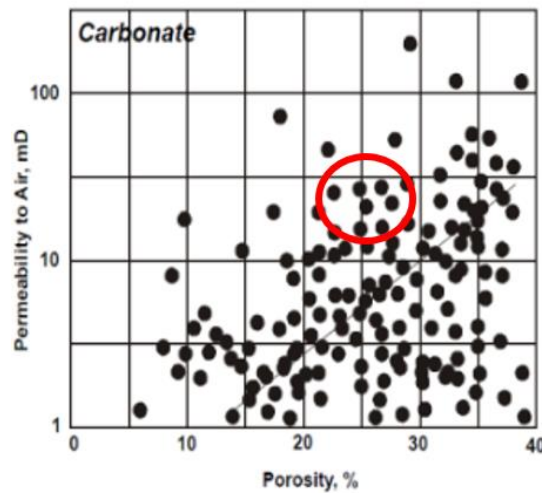
Figure 55. Porosity and permeability range in relation to typical porosity-permeability relationship [11]

The core model permeability was determined during the experiment by calculation applying the Darcy law:

$$k = \eta \cdot \frac{Q \cdot L}{\Delta P \cdot F} \qquad (23)$$

Where η is injected fluid dynamic viscosity (Pa·s), Q is injection rate (m³/s), L is core model length (m), ΔP is pressure drop difference (Pa), and F is cross-sectional area (m²).

The main parameters obtained during oil injection into the core model are given in Figure 56, namely pressure drop dynamics, injection rate and oil permeability. The initial injection rate was set as 0.5 mL/min (30 mL/hour), and then was gradually decreased until 0.2 mL/min. The pressure drop stabilization was achieved, and the average PD was calculated as 0.23 MPa. The core model oil permeability was 22.53 mD. It should be noted that average gas (helium) permeability of dry samples was 32.73 mD.
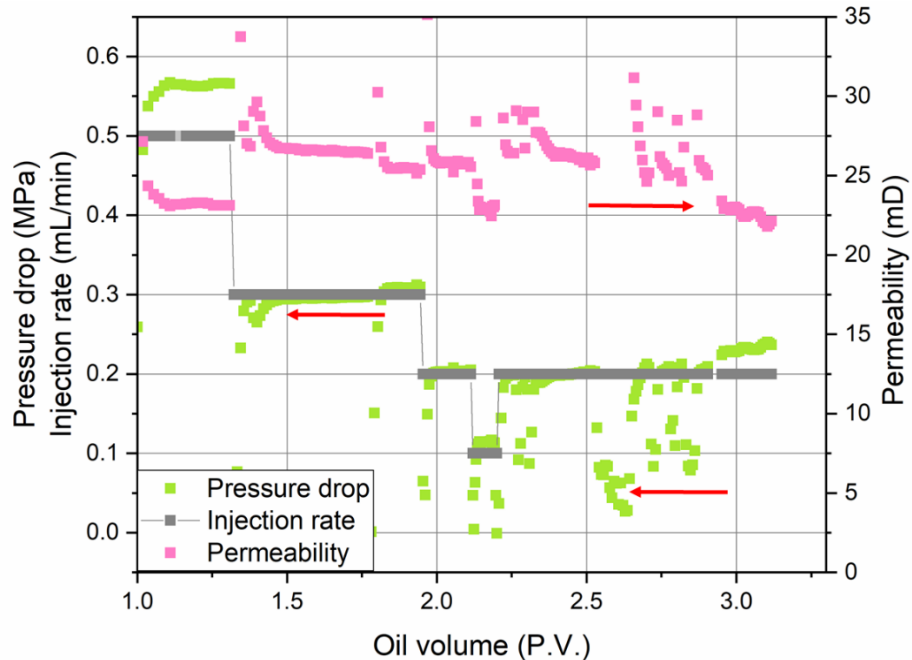
Figure 56. Pressure drop dynamics during core model saturation with oil

After the core model was fully saturated with oil and scanned with the X-ray device, brine injection started with the rate of 0.1 mL/min. The pressure drop and water permeability profiles during brine and surfactant solution injection are shown in Figure 57a,b. It can be seen that the pressure drop stabilized after ~2.5 PV of brine was injected and was 0.084 MPa. In Figure 57b, pressure drop stabilization was achieved faster, i.e. after 0.5 PV of surfactant solution was injected and was 0.074 MPa. Concerning the

131

permeability dynamics, its value depends on pressure drop dynamics according to Darcy law. Thus, the permeability stabilization occurred after ~2.5 PV of injected brine and 0.5 PV of injected surfactant solution, respectively. The water permeability value after brine injection was 2.18 mD, and after surfactant flooding (Q = 0.1 mL.min) it achieved 2.15 mD. Consequently, the data obtained show that surfactant does not lead to any permeability damage, associated with channel blockage or precipitation.
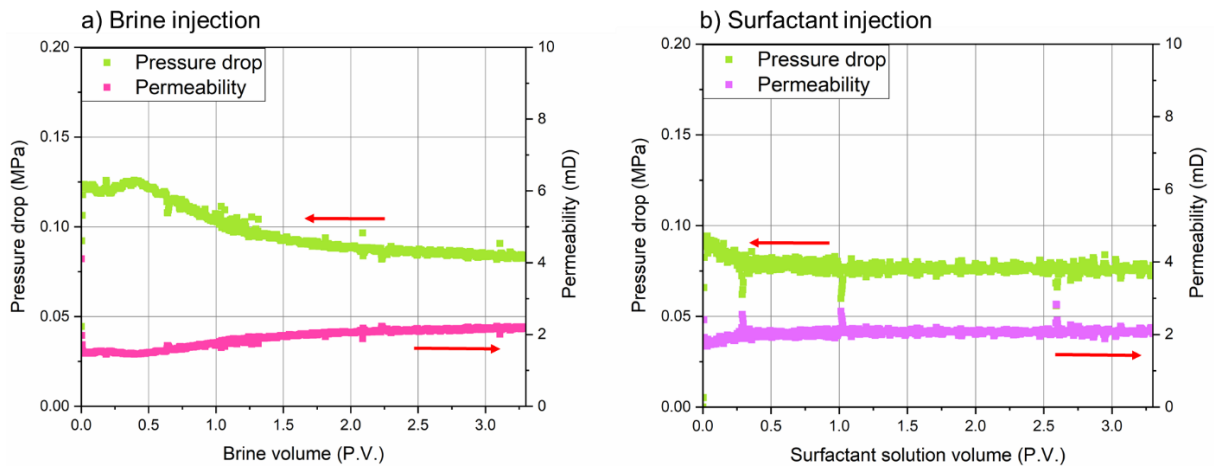
Figure 57. Pressure drop dynamics during oil displacement by (a) brine and (b) surfactant solution (Q = 0.1 mL/min)

As $C_{12}E_7A$ showed good wetting ability (please see section 4.3.2.) it was decided to shut in the system for 48 hours and let spontaneous imbibition in porous media occur. After the shut-in, surfactant injection started with the rate of 0.1 mL/min, and then the injection rate was increased by 5 times until 0.5 mL/min. Pressure drop and permeability profiles are shown in Figure 58a,b.
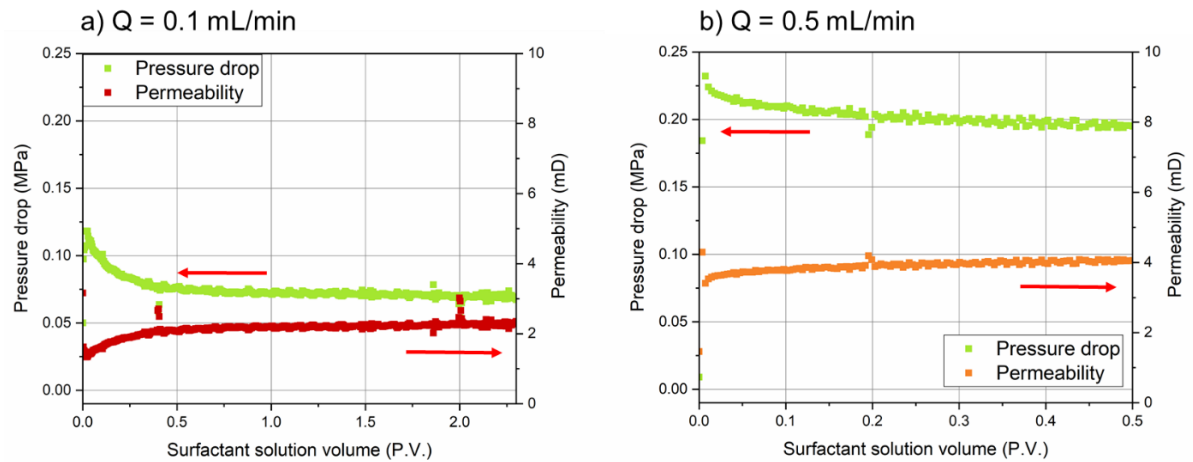
Figure 58. Pressure drop dynamics during oil displacement by surfactant after 48-hour shut-in with (a) Q = 0.1 mL/min and (b) Q = 0.5 mL/min

As one can see, the injection characteristics dynamics stabilize fast. The PD and permeability did not change compared to brine and surfactant injection before shut-in in the case of injection with the rate of 0.1 mL/min. When Q was increased, the permeability growth was observed by ~2 times and was 3.911 mD. Besides that, injection rate increase led to recovery factor improvement that will be discussed in next section.

5.3.2. X-ray scanning and saturation maps. Recovery factor determination

Figure 59 demonstrates X-ray images that represent the fluid distribution in the porous medium of core model, where oil is colored with yellow, and water phase is colored with red. The images were taken after water injection, after surfactant injection and after 48-hour shut-in.

The first image (Figure 59a) was obtained at the end of water flooding stage after 3.5 PV (~87 mL) brine injection. The oil recovery profile by brine is shown in Figure 60a and it can be seen that the RF gradually increased during the injection of first brine PV and reached the value of 44 %. Then, the oil recovery came out on a plateau and reached 55 % after 3.5 PV brine injection. This result is supported with the past literature. For example, Sofla et al. [214] described brine (only NaCl was present) injection followed by surfactant injection in carbonate rock samples at 70°C resulted in ~50 % oil recovered after waterflooding stage.

133
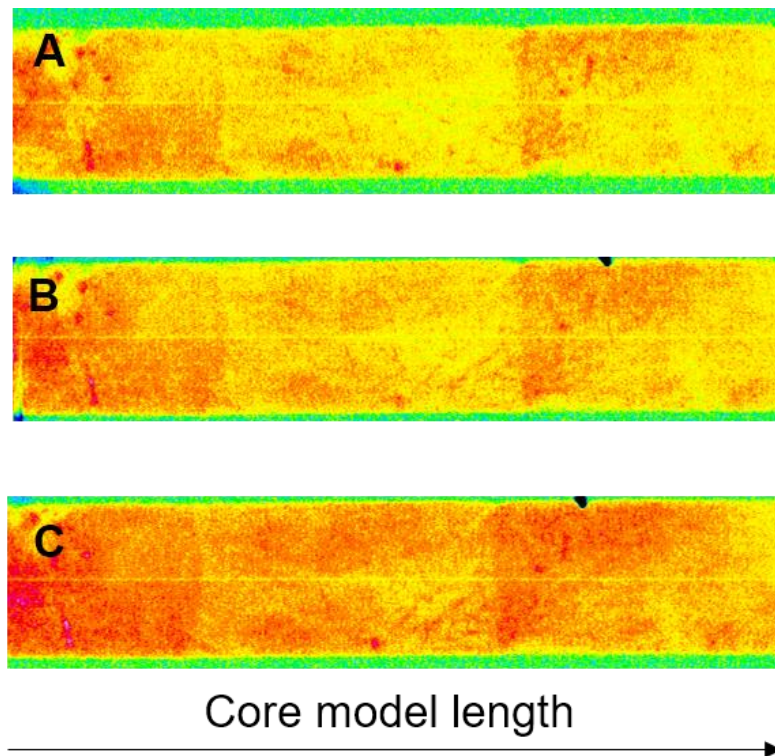
Figure 59. 2D fluid distribution in core model (a) after water flooding, (b) after surfactant flooding, (c) after 48-hour shutdown. Yellow – oil, red – water phase, green – core model coverage (rubber sleeve)

Second image (Figure 59b) was taken after 5 PV surfactant injection with the rate of 0.1 mL/min, and one can see that surfactant had a positive effect on extra oil recovery. In the end of this stage, RF achieved 60 % and it was decided to shut-in the system for 48 hours to ensure water phase imbibition into the porous medium. As it was shown before, $C_{12}E_7A$ demonstrated a strong ability to hydrophilize the surface, please see Figure 42 and Figure 43. The oil recovery profile of surfactant flooding stage is shown in Figure 61.

Thus, third image (Figure 59c) was obtained after surfactant imbibition and additional 4 PV solution injection that resulted in 70 % oil recovery and a more uniform aqueous phase distribution. It is most prominently in first and third samples in the model. This indicates on trapped oil displacement that was impossible without surfactant imbibition and capillary forces decrease. Generally, the additional oil recovery produced

by surfactant was 18.28 %. RF values after each stage of the experiment are specified in Table 20.

Comparative results were reported by Kornilov et al. [215]. The authors tested a commercial surfactant blend based on AEC surfactant for a carbonate field. The recovery factor achieved at waterflood stage was 52.4 %, and additional recovery by surfactant was 22 %.
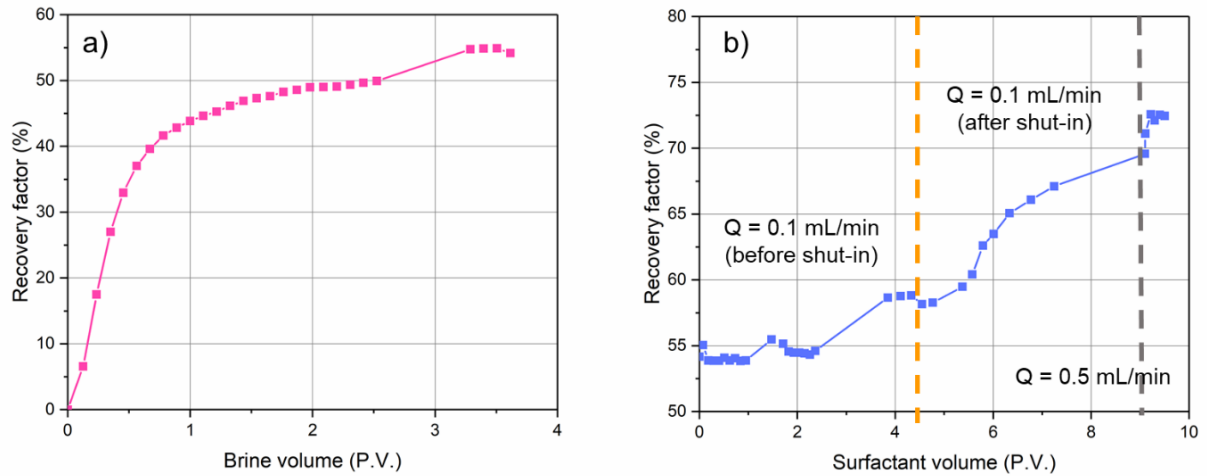
Figure 60. Brine (a) and surfactant (b) flooding RF profiles determined through X-ray saturation control
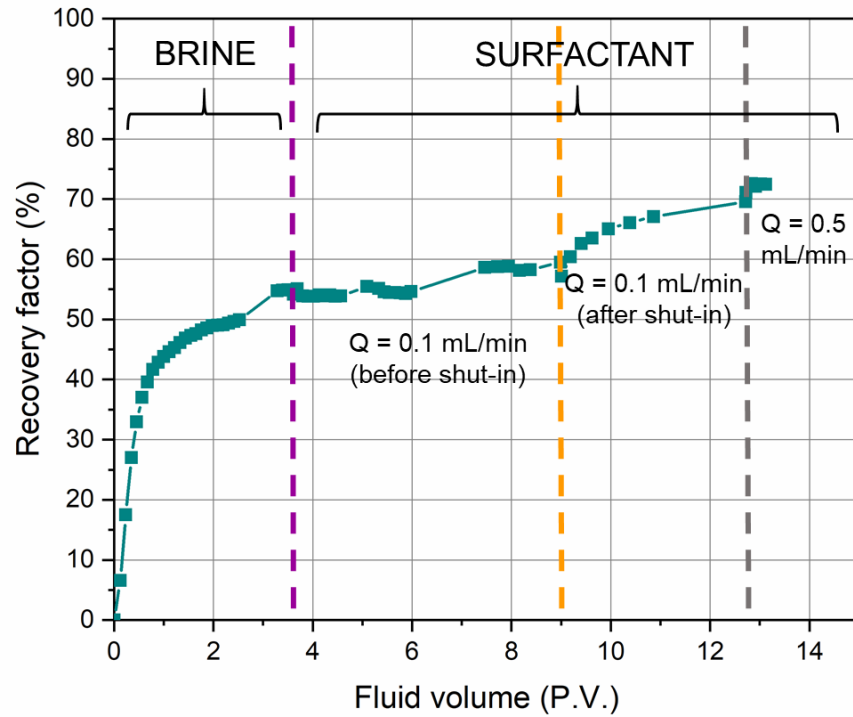
Figure 61. General RF determined through X-ray saturation control

Table 20. Oil recovery factor values after each stage of core flooding test

Stage	Recovery Factor
Water flooding	54.1
Surfactant flooding	59.5
Surfactant flooding after imbibition	69.6
Surfactant flooding after injection with high rate	72.5

The recovery factor values were calculated through two methods (ISSM and mass balance) on the stage of brine injection to be compared. The results obtained are given in Figure 62. Notably, the trends are similar, but the RF values differ by ~10 % and are higher when obtained by ISSM. This difference may be explained by several reasons and was discussed by Cense et al. [127,207]:

1. The volume of inflow and outflow lines of core holder is significant and inputs into mass balance calculations;

2. Heterogenity of rock matrix that may be interpreted as a change in water saturation;

3. Calibration of scans may be not perfect as core samples contain not 100 % brine or oil;

4. The change in ambient temperature that can have impact on X-ray detector;

5. The change in the injected fluids within one experiment.

Despite all these factors and not perfect convergence of recovery factor values, the results are fairly reliable and can spotlight the additional oil produced in the result of surfactant injection.
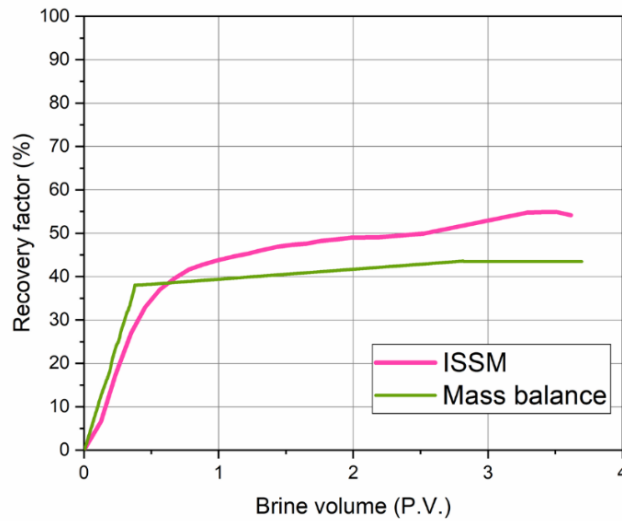
Figure 62. Comparison of recovery factor profiles obtained through ISSM and mass balance methods

5.4. Conclusions

In this chapter, oil displacement efficiency of $C_{12}E_7A$ linear AEC surfactant was investigated. Surfactant composition was selected based on optimal set of properties (IFT, wetting ability and adsorption capacity). Brine injection was followed by injection of surfactant composition that included a 48-hours shut-in for better spontaneous imbibition. Two approaches of recovery factor determination were implemented: in situ saturation

monitoring using X-ray and mass balance. The main outcomes from this study can be drawn:

- RF after brine injection stage achieved 54.2 % that is comparable with the data published in past literature.

- Additional amount of oil recovered by surfactant is 22 % that is a promising result for anionic-nonionic surfactants.

- The shut-in of the system for spontaneous imbibition resulted in increased oil recovery that was demonstrated visually and by calculations. This fact correlates the wettability evaluation results obtained in section 4.3.2. This stage may be considered as an obligatory in future coreflooding tests design that aim to evaluate the wetting ability of a chemical composition or low-salinity water.

- Recovery factor profiles obtained through two methods differ, but still provide a reliable data.

Chapter 6. Optimization of a commercial AEC-based surfactant blend

6.1. Motivation

This chapter presents an optimization of a commercial surfactant composition for application in a real carbonate field. The surfactant used in the experiments described below is different from AECs employed in previous chapters.

Adsorption of surfactants onto rock surface is one of main parameters that determine economic feasibility of chemical flooding. It is commonly known that surfactant and ASP flooding are traditionally carried out in sandstone reservoirs and not in carbonate ones because of the high adsorption of surfactant onto carbonate rock and, therefore, economic limits. One of the strategies to reduce surfactants adsorption is the application of adsorption inhibitors. Alkalis are the commonly used as such sacrificial agents, but their use is limited with brine salinity due to precipitation.

This chapter evaluates the performance of a novel anionic-nonionic commercial surfactant composition designed for a particular carbonate field with high temperature (70°C) and salinity (201 g/L). Under such harsh reservoir conditions alkalis precipitate and thus alternative chemicals should be selected.

The study focuses on the adsorption behavior of surfactant onto the rock surface through a static adsorption test using high-performance liquid chromatography (HPLC) for surfactant concentrations determination. To find the chemicals able to decrease the adsorption loss, a list of alkalis and polyelectrolytes was tested for compatibility and thermal stability, pH and interfacial performance in composition with surfactant. Then, the effectiveness of agents that passed the screening criteria was examined.

6.2. Materials and methods

6.2.1. Materials

Surfactant. A commercial anionic-nonionic surfactant blend based on alkoxylated fatty alcohol (alkyl ether carboxylate) with 43.1 wt% active matter content was used. This composition was designed and synthesized especially for application in a particular field and it is effective in a narrow range of conditions, i.e., fixed salinity (~200 g/L) and

temperature interval of 68-72°C. This surfactant has been shown as a promising chemical to be used in a carbonate reservoirs with high temperature and salinity [215].

Salts. Inorganic salts sodium chloride, calcium chloride dihydrate, magnesium chloride hexahydrate, and sodium sulfate of chemical grade were used for model brine preparation in accordance with the field data. The total salinity of brine is 201 g/L, and its composition is shown in Table 21.

Table 21. Composition of model brine

Salt	Mass, g/L
NaCl	159.26
CaCl$_2$	32.08
MgCl$_2$	9.41
Na$_2$SO$_4$	0.94
Total salinity:	201.7

Adsorption inhibitors. A list of chemicals that were tested in this work is shown in Table 22. Their main properties are also specified. All chemicals in this study were used as received without further purification.

Oil. Crude oil from a carbonate field was used for IFT measurements. Detailed characteristics of oil were reported in Table 4.

Rock samples. Natural carbonate core samples (100% CaCO$_3$, Figure 38) from the oilfield were used for adsorption studies. The rock was treated prior to use in the static adsorption experiment as described in section 4.2.2. and illustrated in Figure 37. Zeta potential of rock powder was measured in artificial brine and surfactant solution according to the methodology given in section 4.2.2.

Table 22. Brief characteristic of tested "sacrificial agents"

Chemical		Structure	Appearance	Manufacturer	Reference
Inorganic alkali	Sodium metaborate tetrahydrate (MB)	$NaBO_2 \cdot 4H_2O$	White crystals	Sigma Aldrich	[105,217]
	Sodium tetraborate decahydrate (TB)	$Na_2B_4O_7 \cdot 10H_2O$	White powder	Sigma Aldrich	[95]
	Ammonium hydroxide	NH_4OH	Clear liquid with a characteristic odor	Chimmed	[94,102]
	Sodium silicate	Na_2SiO_3	White granules	Chimmed	[104]
Organic alkali	Ethanolamine	C_2H_7NO	Clear liquid with a characteristic odor	Chimmed	[106,107]
Polyelectrolyte	Sodium polystyrene sulfonate (70 kDa)	$(C_8H_7SO_3Na)_n$	Yellow powder	Sigma Aldrich	[109]
	Sodium polyacrylate (Flosperse 1000)	$[-CH_2-CH(COONa)-]_n$	Clear, viscous liquid	SNF	[88,89,108]
	Sodium polyacrylate (Flosperse 3000)	$[-CH_2-CH(COONa)-]_n$	Clear, viscous liquid	SNF	
	Sodium polyacrylate Alcomer DP 1	$[-CH_2-CH(COONa)-]_n$ modified with hydrolyzed protein	Yellow to brown viscous liquid	BASF	-

6.2.2. Methods

Compatibility and thermal stability test. The compatibility of selected sacrificial agents with brine and surfactant was performed in two stages. The first batch of adsorption inhibitors was prepared based on model brine. The second batch was prepared based on surfactant dissolved in brine. The surfactant concentration was fixed in all compositions and equal to 1 wt% (higher that critical micelle concentration) while the concentrations of adsorption inhibitors varied.

To prepare a synthetic brine, each salt was dissolved in deionized water separately (to dissolve Na_2SO_4, we used an ultrasonic bath) and then mixed in a flask. A specified amount of surfactant was dissolved in brine with a magnetic stirrer for at least 2 hours to make homogeneous surfactant solutions. Adsorption inhibitors were dissolved in brine or surfactant solution with a magnetic stirrer, only sodium metaborate and sodium tetrahydrate were dissolved with ultrasound.

The surfactant may oxidize at the high reservoir temperature and lose its stability and activity. Thus, oxygen control is critical in laboratory experiments, and it is required to reproduce anaerobic reservoir conditions. The surfactant solutions were prepared following the modified methodology described by Belhaj et al. [60] and Zulkifli et al. [142] (see also sections 2.2.2. and 4.2.2.). First, all glass flasks and vials were "washed" with nitrogen before work. Then, synthetic brine was purged with nitrogen for at least 1 hour to remove the dissolved oxygen. This brine was used in surfactant solutions preparation. Further, each solution was also treated with nitrogen for at least 10 minutes and nitrogen "cap" was created. Then all compositions were placed in a thermostat preheated to 70°C. The heating continued for 14 days, the solutions were periodically evaluated visually, and changes were noted.

pH measurements. pH measurements were performed with a Mettler Toledo Seven Compact Duo S213 unit at room temperature 23°C. The pH-meter was calibrated before each series of measurements using calibration standards 4.01, 7.00, and 9.21 supplied by the manufacturer. Each measurement was repeated three times, and then the arithmetic mean was calculated.

Interfacial tension measurements. The IFT between crude oil surfactant compositions was measured in dynamic mode at 70°C with a Kruss Spinning Drop Tensiometer (please see sections 2.2.2.).

Static adsorption test. The static adsorption of surfactant on the rock was determined by measuring its equilibrium concentration in an aqueous solution after contact with crushed rock using high-performance liquid chromatography. The experiment consisted of three parts: calibration curve set, adsorption isotherm, and evaluation of sacrificial agents performance.

To obtain a calibration curve, solutions with the following surfactant concentrations were prepared: 0.05, 0.1, 0.25, 0.5, 0.75, 1 wt%. The post-CMC range of concentrations was considered in this work, as it is of interest in the following experiments and pilot tests. After the analysis, the characteristic chromatographic peaks were determined, and a calibration curve in the coordinates "Peak area (mV) – Surfactant concentration (wt%)" was plotted (shown in Appendix). A quadratic function with $R^2 = 0.9997$ was obtained.

Then, the adsorption test was performed with the following surfactant concentrations: 0.1, 0.25, 0.5, 0.75, 1 wt%. For adsorption experiments 3 g of crushed rock (m_{rock}) and 9 g of solution (m_{surf}) were placed into a 20 mL glass vial, purged with nitrogen and put in a heat chamber to achieve the adsorption-desorption equilibrium for 24 hours at 70°C [124,185,187,218].The solutions were periodically shaken manually to update the contact area of the surfactant with the rock. After 24 hours expired, the solutions were centrifuged for 20 minutes at 2500 rpm to remove rock particles. Then the supernatant was filtered through a PTFE (polytetrafluoroethylene) syringe filter, placed into a 2 mL vial and analyzed with HPLC. Knowing the surfactant concentrations in the solution before (C_0) and after (C_{eq}) contact with the rock, the adsorption value (Γ) was determined using the Eq. (11).

After the adsorption isotherm was obtained, the compositions with selected stable sacrificial agents were prepared. The surfactant concentration was fixed (1 wt%), and the concentrations of additives varied. The procedure of the adsorption test was the same as described previously.

Surfactant concentration determination with HPLC. The surfactant concentration in the water phase after the contact with rock was determined with high-performance liquid chromatography using Shimadzu Nexera XR. The unit was equipped with an evaporative light scattering detector ELSD-LT II and Thermo Scientific Acclaim Surfactant Plus column. The column temperature was 35°C, the evaporative temperature in the detector was 50°C. Mobile phase A was ammonium acetate, and mobile phase B was acetonitrile. The flow rate was 0.6 mL/min. The injection volume of the sample was 20 μL. Each measurement was repeated twice to obtain more accurate results [187,219].

The surfactant was detected between 16 and 33 minutes, fully analyzed within the measurement time range. The sacrificial agents were identified to have a different yield time and had no affect the shape of the surfactant peak, hence did not influence the analysis of its concentration, and additional calibration curves were not required. The obtained chromatograms were analyzed, the static adsorption was calculated, and the inhibition efficiency was evaluated.

6.3. Results and Discussion

6.3.1. Compatibility and thermal stability tests of surfactants with different adsorption inhibitors

The compatibility of surfactant and artificial brine (Table 21) and stability of adsorption inhibitors were tested at reservoir temperature – 70°C. The concentration of surfactant in all experiments was 1 wt%. The samples were visually assessed after 1, 7, and 14 days of heating in the following way: C – clear, O – opalescent, T – turbid, P – precipitation, S – stratification. The detailed results of the stability test are given in Appendix (day 14 with surfactant).

The concentrations of sodium metaborate tetrahydrate and sodium tetraborate decahydrate were 0.05 wt%, 0.1 wt%, 0.2 wt%, 0.3 wt%, 0.5 wt% and 1 wt% due to limited solubility of these alkalis in the synthetic brine with salinity 201 g/L. The solutions of MB with low concentrations 0.05 wt% and 0.1 wt% were clear. In the range of concentrations from 0.2 wt% to 0.5 wt% a light opalescence was observed, and precipitation was noticed

in 1 wt% solution after 14 days of heating. Thus, MB was selected as one of the potential surfactant adsorption inhibitors in the range of concentrations from 0.05 to 0.5 wt%. Our results support the previous findings regarding sodium metaborate high salinity tolerance. Sharma et al. [95] described the effectiveness of sodium metaborate and its tolerance towards 1604 ppm of Ca^{2+} ions. Flaaten et al. [220] reported that sodium metaborate demonstrated tolerance towards 6000 ppm Ca^{2+} and Mg^{2+} hardness ions.

In the solutions of TB precipitations were observed in almost all solutions except 0.05 wt%, which was turbid. As it was reported previously [99,220], monomeric borate ion ($B(OH)_4^-$) which is produced by the hydrolysis of sodium metaborate is the most stable form at high pH. This finding was proved by the stability results obtained in the present work.

Another seven sacrificial agents were considered in a wider concentration scale: 0.05 wt%, 0.1 wt%, 0.25 wt%, 0.5 wt%, 0.75 wt%, 1 wt%, 1.5 wt% and 2 wt%. Ammonium hydroxide and sodium silicate precipitated in a whole range of concentrations; a similar situation was noticed for ethanolamine, and all these chemicals were eliminated from the screening program. Although sodium polystyrene sulfonate was compatible with brine, it showed opalescence in the surfactant composition, and thus was excluded. Two sodium polyacrylates of the Flosperse series showed similar behavior: gel-like sediment was observed in vials with the solutions when the concentrations were higher than 0.1 wt%. This result is not in agreement with findings reported by He et al. [221]. The authors demonstrated that polyelectrolytes could not only decrease surfactant adsorption, but also perform as scale inhibitors. However, the type of polyelectrolytes was not specified. Alcomer DP 1 was clear in each solution, and thus showed the best salinity and temperature resistance. As a result of the bottle test, two chemicals with different mechanisms of action were selected for the next stage of study: polyacrylate Alcomer DP 1 and alkali sodium metaborate tetrahydrate, their solutions are shown in Appendix.

6.3.2. pH measurements and zeta potential

Zeta potential values of carbonate rock fine particles with a diameter <140 μm were measured in synthetic brine and surfactant solution. As shown in Table 23, zeta potential in brine is positive with a low value (+4.01 – +5.55 mV) that is typical for carbonate rock in high salinity water. Our results are similar to ones reported by Mahani et al. [222]: the zeta potential was about +5 mV in a formation brine with mineralization ⁓180 g/L and pH about 6. Zeta potential was positive in a wide pH range and increased with the pH growth [222].

When the surfactant was present in the solution, the zeta potential became negative with a higher value of -11.4 – -13.3 mV. These results indicated that anionic surfactant molecules adsorbed on positively charged calcite surface and created a negative surface charge by carboxylic and hydroxyl groups [223,224].

It is worth noting that during the measurements, the instrument showed results with a significant error due to the high mineralization of the water and its high conductivity. When attempting to measure formulations with adsorption inhibitors, the values were close to 0, and there was a high noise level, i.e., the results were not reliable.

Table 23. Zeta potential values of carbonate rock in the water phase

Zeta potential	Synthetic brine	Surfactant solution 1 wt.% in brine
Measurement 1	+4.01 mV	-13.3 mV
Measurement 2	+5.55 mV	-11.4 mV
Average	+4.78 mV	-12.35 mV
pH	5.27	5.1

The pH values were measured for concentrations selected in the previous stage of the study: sodium polyacrylate Alcomer DP 1 and sodium metaborate tetrahydrate The

146

measurements were performed on 1, 7, and 14th days of heating; the results are shown in Figure 63.

The addition of sodium metaborate in an amount higher than 0.05 wt% keeps the pH of the solutions in the alkaline range (pH is about 8.2, Figure 63a) and prevents it from dropping back to its original level. It creates a negative charge on the rock surface and can lead to the repulsion of anionic surfactants that preferably adsorb onto positively charged minerals. Although the pH values of the surfactant compositions with MB are below recommended (more than 9) [95,225], MB effectiveness as an adsorption inhibitor was tested. The higher concentrations of sodium metaborate and the application of more strong alkalis are limited due to stability issues.

A wider range of polyacrylate Alcomer DP 1 concentrations was studied in pH measurements. The values are in slightly acidic range close to the neutral one from 5 to 6.7 (Figure 63b). Alcomer DP 1 is not an alkali, and thus does not maintain the alkaline pH, performing as a more active adsorbate in the competitive adsorption process. In contrast to sodium metaborate alkali, the pH values of surfactant compositions with Alcomer DP 1 decreased over time, which may stemmed from gradual oxidation of the surfactant despite the removal of oxygen.
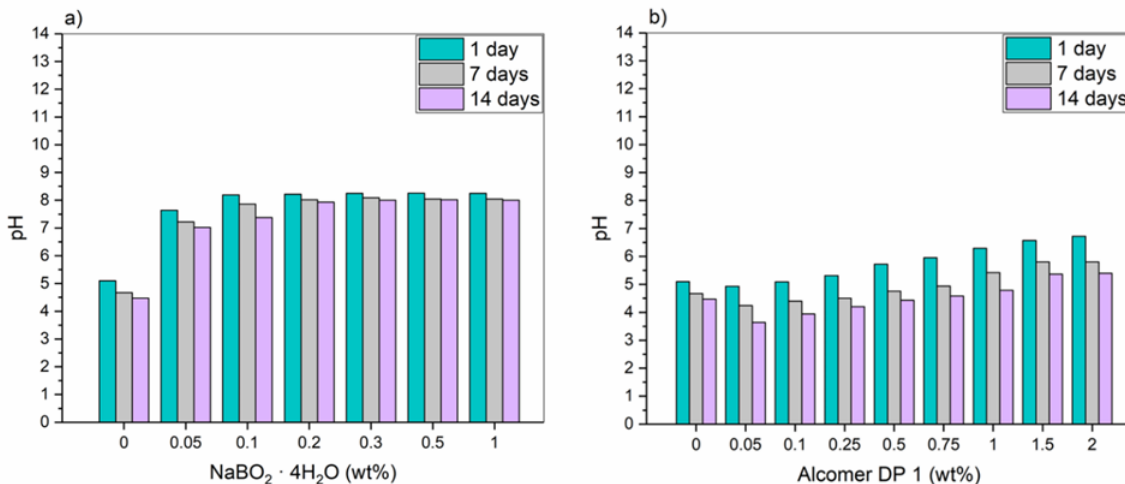
Figure 63. pH values of sodium metaborate tetrahydrate (a) and Alcomer DP 1 (b) in 1 wt% surfactant solution in brine

6.3.3. Interfacial tension measurements

The initial interfacial tension between brine and oil without surfactant at a reservoir temperature of 70°C was measured – 20.98 ± 2.98 mN/m. Then, IFT values were measured with the range of surfactant concentrations from 0.005 to 1 wt.% in order to determine the CMC value and the concentration of optimum interfacial activity [114]. Solutions were prepared in artificial brine (Table 21), and the temperature of each experiment was 70°C. As shown in Figure 64a, a typical "L-shaped" IFT profile was earned in the coordinates "IFT (mN/m) – Surfactant concentration (wt%)" [157]. The IFT sharply decreases in the pre-CMC region, reaches CMC, and then slightly reduces in the post-CMC region. The experimental CMC value was determined as 0.025 wt% with the IFT value of 0.155 ± 0.006 mN/m, and the minimum IFT was found to be at 1 wt% surfactant concentration and is 0.032 ± 0.0054 mN/m. According to Liu et al. [66] and Rosen [49], with the increase of surfactant concentration, more surfactant molecules adsorb at the oil-water boundary and replace the solvent molecules, thus reducing the interfacial tension in the pre-CMC region. It is generally accepted that once the CMC is reached, any further addition of surfactants should not lead to IFT reduction as the surface layer between the two phases is already in the saturated state at which the maximum reduction in IFT is observed [49]. However, this is not always true in practice and depends on the surfactant molecular structure as one can see in Figure 64a.

It was reported in the literature that alkyl ether carboxylate surfactants could reach ultralow IFT values of 10^{-2}–10^{-3} mN/m orders of magnitude in the presence of electrolytes [60,66,118,226]. This can be explained by the fact that the solubility of surfactants in water decreases, and they tend to further partition in oil phase. Besides that, electrolytes decrease electrostatic repulsion between heads of surfactants, and thus lead to a more dense molecular arrangement at the interface. Furthermore, bivalent cations such as calcium Ca^{2+} and magnesium Mg^{2+} are more effective in reducing the attractive forces between surfactant polar groups than monovalent sodium Na^+ cations [63,64,66]. In this study, the brine contains a considerable amount of mono- and bivalent cations, and the surfactant shows excellent performance under these conditions.

148

The IFT values between oil and surfactant compositions with adsorption inhibitors were measured to evaluate their influence on surfactant interfacial performance. The experiment results are shown in Figure 64b and Table. As it can be seen from the data no significant effect of sacrificial agents on the IFT was found. Alkali sodium metaborate leads to a gradual IFT decline with its concentration growth and achieves 0.022 ± 0.01 mN/m when added 1 wt% of MB. It was reported that alkalis react with carboxylic acids present in crude oil and form in-situ surfactants, reducing the IFT [227,228]. On the contrary, polyacrylate Alcomer DP 1 leads to an IFT increase within one order of magnitude up to 0.066 ± 0.005 mN/m.
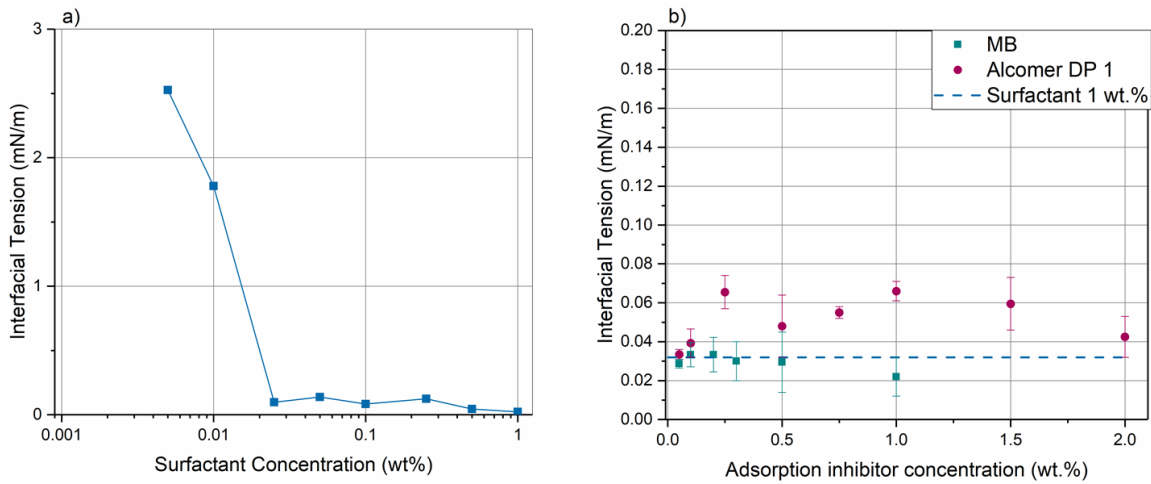
Figure 64. IFT in dependence of surfactant concentrations (a) and IFT values between oil and surfactant compositions with adsorption inhibitors sodium metaborate and Alcomer DP 1 (b)

6.3.4. Adsorption isotherm of surfactant onto carbonate rock

As this work aimed to evaluate the performance of different surfactant adsorption inhibitors, it was first critically important to characterize the behavior of AEC surfactant under conditions reproducing the reservoir ones (70°C) to understand the character of adsorption process. The adsorption was evaluated in a post-CMC region in the range of concentrations 0.1 wt% – 1 wt%. By analyzing surfactant adsorption it is possible to estimate potential surfactant losses and the economic efficiency of surfactant flooding. The adsorption isotherm was obtained by plotting the amount of surfactant adsorbed per 1 gram

of rock in dependence of surfactant concentrations remained in water phase after equilibration (Figure 65). As it can be seen, the maximum adsorption capacity was 2.23 mg/g-rock at initial surfactant concentration of 1 wt%. The appearance of the obtained adsorption isotherm on carbonate rock is similar to the surfactant isotherm on sandstone described by Belhaj et al. [123,187], where a carboxylate surfactant with an analogous structure was studied. The authors reported that the maximum adsorption capacity of the AEC was ~2 mg/g-rock at initial concentration of 1 wt% [187]. Besides that, the authors evaluated the adsorption of AEC in mixture with an alkylpolyglucoside (APG) in the presence of crude oil. It was observed that the adsorption value increased significantly, and the main income into the adsorption belonged to the AEC [123]. Jian et al. [179] compared the adsorption of two anionic and one amphoteric surfactant onto different minerals: calcite, dolomite, silica, and kaolin in different brines. One of anionic surfactants used was C_{13}-alcohol polyethylene glycol ether carboxylic acid L38 (otherwise, AEC). It was found that the adsorption value of L38 was less than 1 mg/m^2 in deionized water and significantly raised in the presence of 5 wt% $CaCl_2$ due to increased positive zeta potential of the rock surface. Besides that, the adsorption of L38 on calcite decreased by ~4 times when it was mixed with an amphoteric betaine.
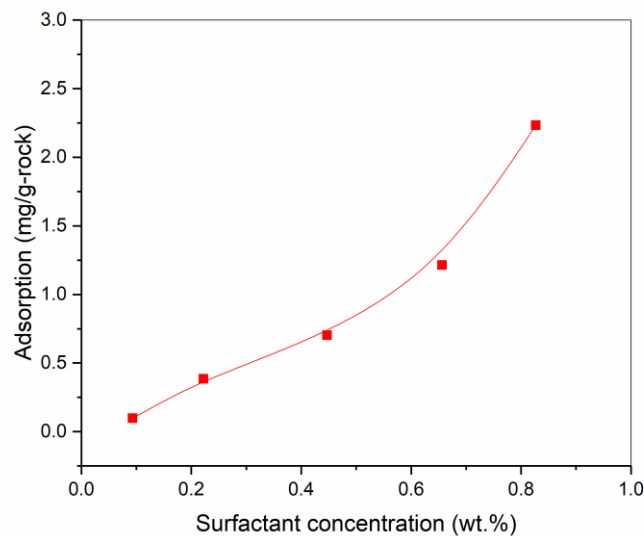
Figure 65. Adsorption isotherm of surfactant (Equilibrium adsorption profile)

According to Giles classification of the solute adsorption isotherms [229], this one belongs to L-type and subtype 3 (Langmuir isotherms). The initial curved area along the concentration axis indicates that as the amount of occupied adsorption sites increases, it is more difficult for adsorbent molecules to find a vacant spot. As the surfactant concentration increased, adsorption has not reached its limit but progressed after filling the monolayer. This may result from polymolecular adsorption or repositioning of molecules or their associates relative to the rock surface. It should be noted that Langmuir's conception of adsorption reaching a plateau significantly approximates and simplifies the actual adsorption process [186,230]. In fact, the surface of most adsorbents is not homogeneous, the adsorbate molecules interact with each other on the adsorbent surface, and adsorption often does not end up forming a monomolecular layer. In this case, the adsorption isotherm equation becomes more complicated. There are several accepted statements in polymolecular adsorption, which is different from monomolecular adsorption (Langmuir). According to one of them, each molecule of the previous layer is considered to represent a possible active site for the adsorption of the molecule of the next adsorption layer [208,229,231]. This process is schematically shown in Figure 66.

Thus, considering the "S" shape of the adsorption isotherm, it can be concluded that the adsorbed molecules may interact with the adsorbate. According to Polanyi and BET (Brunauer, Emmet and Teller) theory of polymolecular adsorption [208,231], it can be assumed that in this case, physical forces cause the adsorption. As follows, there is no chemical interaction between surfactant molecules and carbonate rock surface and only intermolecular electrostatic forces between ions, dipoles or other charged particles occur.
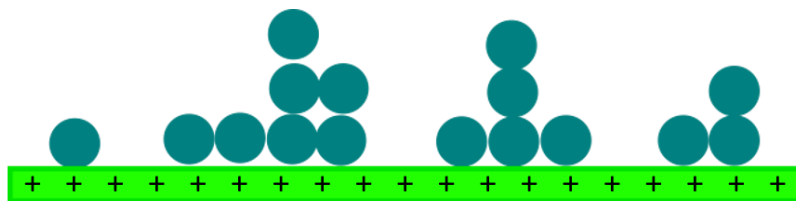
Figure 66. Scheme of the adsorption layer structure for multilayer adsorption on carbonate rock

The obtained adsorption isotherm was fitted to two-parameter Langmuir and Freundlich equilibrium adsorption models that were described in section 4.2.3. The fitting of adsorption data is shown in Figure 67 and the parameters are listed in Table 24. The comparison of adsorption isotherm models and experimental data are illustrated in Figure 68. We can conclude that the Freundlich model fits experimental data. This finding supported the above discussion on polymolecular adsorption of AEC surfactant onto the carbonate rock and the formation of multilayers.
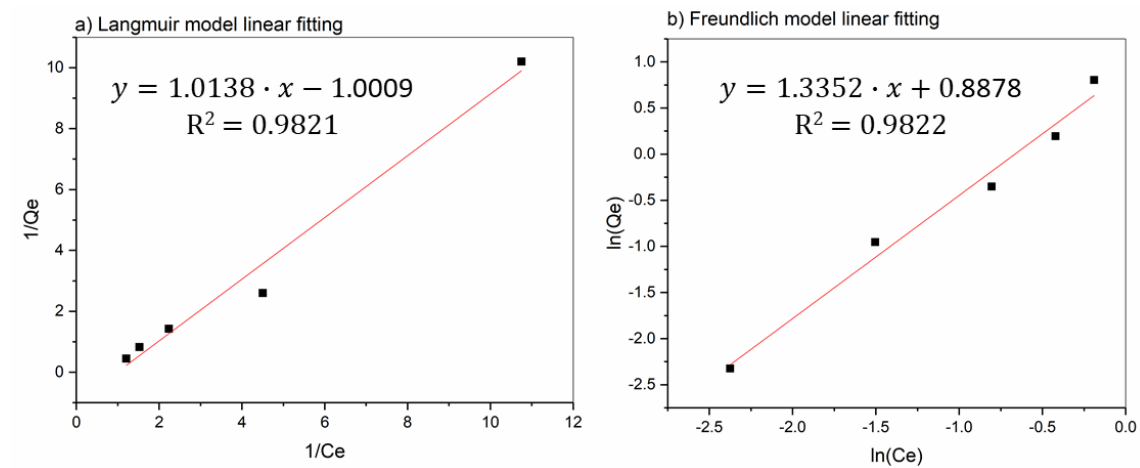
Figure 67. Fitting of adsorption isotherms with Langmuir (a) and Freundlich (b)

Table 24. Isotherm parameters for Langmuir and Freundlich models

Isotherm model	Parameter	Value
Langmuir	R^2	0.9821
	K_L	-0.9873
	q_0	-0.9991
Freundlich	R^2	0.9822
	K_F	2.4232
	n	0.7489
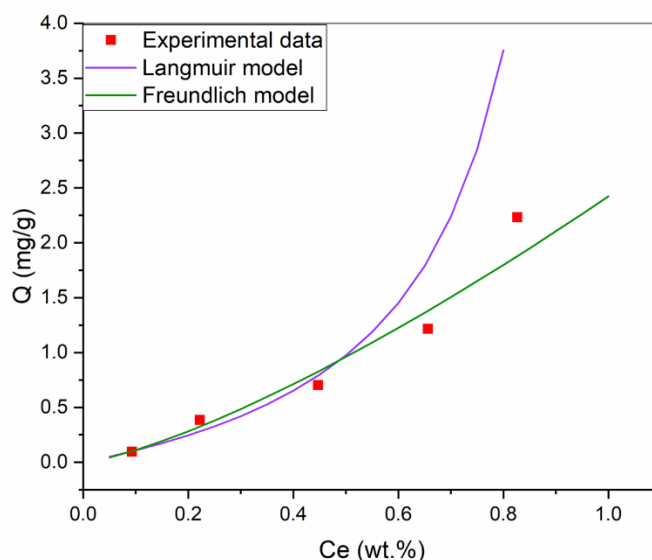
Figure 68. Adsorption isotherm models and experimental data

6.3.5. Effect of different additives on surfactant adsorption onto carbonate rocks

Once the adsorption mechanism of surfactant was investigated, it becomes possible to study the effect of different adsorption inhibitors selected in the previous sections. For this purpose, a weak alkali sodium metaborate tetrahydrate and an anionic modified polyacrylate Alcomer DP 1 were tested.

Figure 69 shows the equilibrium adsorption values obtained in the result of the static test, which lasted for 24 hours at 70°C, the effectiveness of adsorption inhibitors is shown in Table 25. It can be seen in Figure 69a,b that both sacrificial agents showed a similar behavior when the concentration in the surfactant solution was increased. Basically, the inhibitions efficiency raised to a particular concentration, and then a decrease was observed.

Reducing adsorption by adding MB to the surfactant composition led to a 2 times lower adsorption. Notably that adsorption is slightly dependent on MB concentration. This may be caused by close pH values (pH=9) that MB is able to maintain.

The introduction of Alcomer DP 1 resulted in a more significant reduction in adsorption losses in comparison with MB. It showed maximum efficiency at a concentration of 1 wt%, and the adsorption of the surfactant in this composition was 0.23

mg/g-rock, which was an order of magnitude lower than the reference value of 2.23 mg/g-rock without the addition of inhibitors. This is due to the fact that Alcomer DP 1 is a polyelectrolyte that blocks the adsorption sites on the carbonate surface, and thus repels the negatively charged surfactant anions due to electrostatic repulsion, resulting in adsorption reduction [88].

It is interesting to point out that all inhibitors showed significant impact on surfactant adsorption on carbonate rocks. However, the effect was more pronounced when competitive adsorption between inhibitors and surfactant molecules took place rather than creation of additional negative charge near surface.
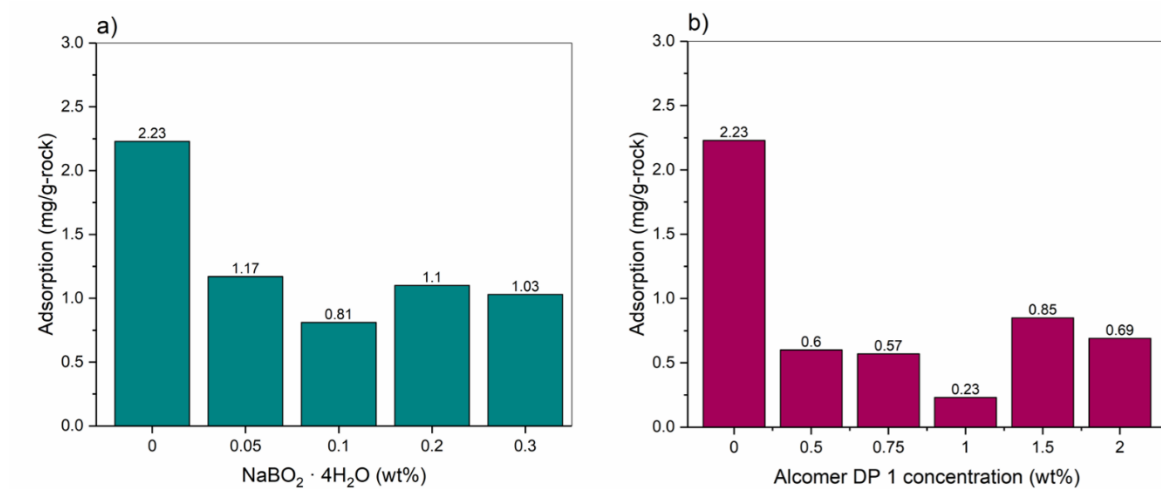
Figure 69. Static adsorption values of AEC surfactant in the presence of sodium metaborate tetrahydrate (a) and Alcomer DP 1 (b)

Table 25. Static adsorption test results

Inhibitor concentration, wt%	Adsorption, mg/g-rock	Effectiveness, %
Sodium metaborate tetrahydrate		
0	2.23	-
0.05	1.17	48
0.1	0.81	64
0.2	1.10	51
0.3	1.03	54
Alcomer DP 1		

0	2.23	-
0.5	0.60	73
0.75	0.47	79
1	0.23	90
1.5	0.85	62
2	0.69	69

6.4. Conclusions

The present work performs a study of the adsorption inhibitors that can reduce the adsorption loss of a novel anionic ethoxylated carboxylate surfactant onto carbonate rock under harsh reservoir conditions – 70°C and salinity of 201 g/L. The effectiveness of all main types of adsorption inhibitors was evaluated, i.e. alkalis and polyelectrolytes. The following conclusions can be drawn from the study:

• The CMC of the surfactant is 0.025 wt%, and the operation surfactant concentration was selected as 1 wt% (the IFT value is 0.032 ± 0.054 mN/m). The addition of adsorption inhibitors has not lead to significant IFT changes: the alkali MB slightly decreased, and the polyacrylate increased the IFT within one order of magnitude.

• The static adsorption tests were conducted (1) to describe the adsorption isotherm of the surfactant and (2) to evaluate the effect of sacrificial agents. It was found that the isotherm obtained is of L-type according to Giles classification, and the adsorption value was 2.23 mg/g-rock at 1 wt%. The Freundlich model ($R^2 = 0.9822$) optimally described the data obtained, indicating that the adsorption was polymolecular and characterized by the formation of multilayers.

• A number of alkalis and polyelectrolytes were listed to find suitable adsorption inhibitors, and a weak alkali sodium metaborate tetrahydrate and an anionic modified sodium polyacrylate Alcomer DP 1 were selected as stable agents. MB was stable in the narrow range of concentrations under the present conditions, namely $0.05 \div 0.3$ wt%. It maintained the pH of the surfactant compositions at the level $8 \div 9$ (a mildly alkaline environment). MB reduced the static adsorption by about a half. The highest inhibition efficiency was achieved at sodium metaborate concentration of 0.1 wt% and was 63.68 %.

-     Alcomer DP 1 (a polyacrylate modified with protein) was applied as a surfactant adsorption inhibitor for the first time. It was stable in the whole range of the concentrations examined (0.05 ÷ 2 wt%), and the amounts from 0.5 to 2 wt% were selected as they were comparable to surfactant content in the composition (1 wt%). It showed maximum efficiency at a concentration of 1 wt%, and the adsorption of the surfactant in this composition was 0.23 mg/g-rock, which is an order of magnitude lower than the reference value 2.23 mg/g-rock without the addition of inhibitors.

This work tries to solve the problem of high surfactant adsorption in carbonates and subsequent economic losses. The findings reported put forward the application of surfactant flooding in carbonate reservoirs with harsh conditions and can be used as a basis for further experiments.

Chapter 7. Summary, Conclusions and Recommendations

7.1. Summary

It was stated in numerous industrial and scientific reports that carbonate oil reservoirs hold more than a half of oil and natural gas reserves in the world. The main difficulties associated with oil production from carbonates are their heterogeneity and oil-wetness. Effective development of the majority of carbonate fields requires application of various enhanced oil recovery methods that should be comprehensively selected and estimated in appliance with oil and reservoir properties. One of the reasons that explains low recovery factor values is high residual oil saturation caused by adsorbed or trapped oil. To decrease residual oil saturation on the pore level, surfactant flooding may be implemented, but it should be designed in a proper way before pilot test and subsequent full-fledged project.

This thesis focuses on study of alkyl ether carboxylate surfactants as agents for chemical flooding in carbonate reservoirs. A complex of laboratory and computational techniques was applied to characterize the properties of AEC surfactants and draw the main trends in their behavior. Interfacial behavior of AECs on the liquid-liquid interface was studied through combination of IFT measurements and molecular dynamics simulations. Then, rock-fluid interactions of AECs with carbonate rock were analyzed and a composition was selected for a coreflooding test based on the main factors that determine the efficiency of a surfactant: interfacial tension, wetting ability and adsorption capacity. The work was completed with an optimization of a commercial AEC-based surfactant blend designed for particular conditions. The main conclusions were made and are given below.

7.2. Conclusions

1. The molecular structure of AECs, i.e. the length of alkyl chain and ethoxy fragment, has a significant effect on main properties of surfactants: stability, interfacial performance, wetting ability, and adsorption.

2.   A consisted study of interfacial behavior of two AECs' was studied in the presence of main cations and anions present in reservoir brines separately and in mixtures under two temperatures. It was concluded that temperature rise has a more significant effect on an AEC with longer EO chain, and salinity impact is stronger in the case of a shorter EO fragment. Anions do not change the interfacial behavior of AECs significantly in contrast to cations, particularly hardness ions Ca^{2+} and Mg^{2+} that had a similar effect on $C_{11}E_{11}A$, but different on $C_{12}E_7A$ that partially lost stability in the presence of Ca^{2+} ions.

3.   Molecular dynamics simulations allowed to scale up the experimental data. It was found that alkyl chain length has almost no influence on the monolayer properties since it is smaller or comparable in length to the solvent molecules. EO segment length strongly influences the adsorbed monolayer properties: an increase in length reduces the compressibility and decreases the density, but only for number of $EO < 8$. MD simulations support the idea about orientation of AECs on water-hydrocarbon interface. However, the MD method has some limitations and cannot replace the laboratory experiments.

4.   Wettability evaluation showed that AEC surfactants have a strong wetting ability in carbonate rocks (reduce contact angle of water until values less than 60°) that increases in the presence of electrolytes. As the hydrophobicity of carbonates is mainly caused by the adsorption of polar oil components on the rock surface, a better wettability shift by surfactants is caused by a combination of "cleaning" and "coating" mechanisms. It was achieved by $C_{12}E_7A$ surfactant that is more hydrophobic and is more likely to dissolve in adsorbed oil film and interact with oil components than $C_{11}E_{11}A$. Adsorption of AECs is relatively high and achieved ~9 mg/g-rock for $C_{11}E_{11}A$. To apply AEC surfactants in field projects, adsorption inhibitors should be used to reduce the adsorption loss and support economic feasibility of the project. Similarly to wetting ability, adsorption of AECs is highly influenced by water salinity. According to the results obtained, the adsorption mechanism changes from monomolecular in deionized water to polymolecular after adding salts.

5.   A core flooding experiment with X-ray in situ saturation monitoring was conducted with an optimal AEC composition that was selected based on IFT, wetting ability and

adsorption properties. A 48-hours system shutd-in was performed to promote spontaneous imbibition of surfactant into the pore space of core model. An additional oil recovery was achieved that confirmed a good wetting ability of $C_{12}E_7A$ surfactant.

6. Generally, alkyl ether carboxylate surfactants demonstrated a strong wetting ability and good tendency to decrease oil-water interfacial tension. A strong wetting properties were demonstrated by a pause during the injection process that allowed the surfactant composition to imbibe into porous media and resulted in additional sufficient oil recovery.

7. A novel commercial anionic-nonionic surfactant blend was evaluated and optimized for application in a carbonate field. A list of adsorption inhibitors (alkalis and polyelectrolytes) was selected and successfully tested under harsh reservoir conditions. This selection of chemicals alternative to traditionally used NaOH and Na_2CO_3 and stable in the presence of high salinity and temperature demonstrate the possibility of chemical flooding implementation in reservoirs with challenging conditions.

8. The findings made in this thesis may be applied in future surfactant and ASP flooding design for real field projects.

7.3. Scientific novelty

1. The effect of main ions present in reservoir brines was examined and compared for two AEC surfactants. Such a detailed study was not reported in past literature, to the best of our knowledge.

2. The effect of AECs head and tail length on the arrangement of the whole molecules was described using molecular dynamics simulation. Such "digital screening" was reported for the first time *for linear alkyl ether carboxylates*.

3. A novel approach of wettability alteration mechanism studies through Rock-Eval pyrolysis analysis was proposed and applied in this work. It can be used as an alternative for thermogravimetric analysis typically used for the analysis of wettability alteration mechanism by surfactants. The proposed method showed semiquantitative results and can be applied for different classes of surfactants.

4.   A coreflooding test with conventional carbonate rock samples included a shut-in stage. Such methodology is typically used for low-permeability (mainly shale) types of rock for huff-n-puff process simulation, where imbibition is crucial. This technique allowed to demonstrate a strong wetting ability of AEC surfactant because a boost in oil recovery was observed after the injection was restarted. This stage can be included in future coreflooding experiments with carbonate samples as an additional method of wetting ability examination.

5.   Adsorption inhibitors suitable for application under harsh reservoir conditions (temperature of 70°C and salinity ~200 g/L) were tested. Polyacrylate Alcomer DP 1 was not reported in literature before as a chemical applied in EOR, and now it can be introduced as a "sacrificial agent".

7.4. Contribution to Knowledge

A meticulous study of alkyl ether carboxylate surfactants gave the understanding of the main mechanisms underlying their performance in contact with brine, oil and rock. Understanding of the molecular structure effect allows choosing right compositions for target conditions in future chemical flooding design. It was demonstrated that AEC surfactants may be employed as EOR agents in moderate and harsh reservoir conditions, but some additives that optimize their effectiveness and cost are needed and should be selected properly.

7.5. Future Recommendations

The results described in this work answered a number of questions, but also laid the foundation for further research, both methodological and scientific. Here are some recommendations:

1.   Coreflooding experiment results should be coupled with microfluidic tests in transparent chips for visualization and better understanding of fluid flow process and phases distribution. 2.5-Dimensional models should be developed based on X-ray

computed tomography of core samples that were used for the coreflooding, taking into account porosity, permeability, pore and pore throat size distribution, tortuosity and aspect ratio.

2. As AEC surfactants demonstrated a strong wetting ability, it should be evaluated more detailed. X-ray micro-tomography coreflood test should be performed for rock surface wettability evaluation in dynamic mode.

3. 3-Dimensional core models should be built based on tomography scanning. Two-phase fluid filtration in porous media using these models may be simulated in GeoDict software (or alternative) for better understanding of the flow process on pore level.

4. Hydrodynamic simulation on the scale of a real field has to be conducted to more deeply analyze the effect of injection shut-in that leads to oil recovery increase.

5. Study of complexation reactions of AEC surfactants with carbonate rock ($CaCO_3$).

6. Evaluation of surfactant dynamic adsorption.

Bibliography

[1]   M. Chavan, A. Dandekar, S. Patil, S. Khataniar, Low-salinity-based enhanced oil recovery literature review and associated screening criteria, Pet. Sci. 16 (2019) 1344–1360. https://doi.org/10.1007/s12182-019-0325-7.

[2]   Z.X. Xu, S.Y. Li, B.F. Li, D.Q. Chen, Z.Y. Liu, Z.M. Li, A review of development methods and EOR technologies for carbonate reservoirs, Pet. Sci. 17 (2020) 990–1013. https://doi.org/10.1007/s12182-020-00467-5.

[3]   F. Pashapouryeganeh, G. Zargar, A. Kadkhodaie, A. Rabiee, A. Misaghi, S.J.S. Zakariaei, Experimental evaluation of designed and synthesized Alkaline-Surfactant-polymer (ASP) for chemical flooding in carbonate reservoirs, Fuel. 321 (2022) 124090. https://doi.org/10.1016/j.fuel.2022.124090.

[4]   G. Sharma, K.K. Mohanty, Wettability Alteration in High-Temperature and High-Salinity Carbonate Reservoirs, SPE J. (2013). https://doi.org/https://doi.org/10.2118/147306-PA.

[5]   Schlumberger, Characterization of Fractured Reservoirs, 2008.

[6]   Schlumberger, Carbonate Advisor, 2008.

[7]   P.H. Nadeau, Petroleum reservoir porosity versus depth : Influence of geological age, (2009). https://doi.org/10.1306/06120908163.

[8]   M. Shepherd, Carbonate Reservoirs, Oil F. Prod. Geol. (2020) 301–309. https://doi.org/10.1306/13161226m913372.

[9]   M. Laugié, J. Michel, A. Pohl, E. Poli, J. Borgomano, Global distribution of modern shallow-water marine carbonate factories : a spatial model based on environmental parameters, Sci. Rep. (2019) 29–31. https://doi.org/10.1038/s41598-019-52821-2.

[10]   K.H. Singh, R.M. Joshi, L. Elucidations, W. Forward, Petro-physics and Rock Physics of Carbonate Reservoirs, Springer Singapore, 2020.

[11]   S. Arwini, Porosity - Permeability Relationship of Libyan Carbonate Reservoir in Defa Oil Field, World Acad. J. Eng. Sci. (2021).

[12]   N. Kasiri, A. Bashiri, Wettability and its effects on oil recovery in fractured and conventional reservoirs, Pet. Sci. Technol. 29 (2011) 1324–1333. https://doi.org/10.1080/10916460903515540.

[13]   J.S. Buckley, Y. Liu, S. Monsterleet, P. Recovery, Mechanisms of Wetting Alteration by Crude Oils, SPE J. (1998) 54–61. https://doi.org/https://doi.org/10.2118/37230-PA.

[14]   P. V Brady, G. Thyne, Functional Wettability in Carbonate Reservoirs, Energy & Fuels. (2016). https://doi.org/10.1021/acs.energyfuels.6b01895.

[15]   A. Ivanova, N. Mitiurev, A. Cheremisin, A. Orekhov, R. Kamyshinsky, A. Vasiliev, Characterization of Organic Layer in Oil Carbonate Reservoir Rocks and its Effect on Microscale Wetting Properties, Sci. Rep. 9 (2019) 1–10. https://doi.org/10.1038/s41598-019-47139-y.

[16]   M.M. Thomas, J.A. Clouse, J.M. Longo, Adsorption of organic compounds on carbonate minerals 1 . Model compounds and their influence on mineral wettability, Chem. Geol. 109 (1993) 201–213. https://doi.org/https://doi.org/10.1016/0009-

2541(93)90070-Y.

[17]   S. Das, Q. Nguyen, P.D. Patil, W. Yu, R.T. Bonnecaze, Wettability Alteration of Calcite by Nonionic Surfactants, Langmuir. (2018). https://doi.org/10.1021/acs.langmuir.8b02098.

[18]   R.A. Salathiel, Oil Recovery by Surface Film Drainage In Mixed-Wettability Rocks, J. Pet. Technol. 25 (1973) 1216–1224. https://doi.org/https://doi.org/10.2118/4104-PA.

[19]   L. Xu, K. He, J.P. Rane, X. Yin, K. Neeves, Spontaneously imbibed fluids for increasing contact area between hydraulic fracturing fluids and formation matrix in liquids-rich shale plays, Soc. Pet. Eng. - SPE Liq. Basins Conf. - North Am. LRBC 2015. (2015). https://doi.org/10.2118/175536-ms.

[20]   S. Strand, T. Puntervold, T. Austad, Water based EOR from clastic oil reservoirs by wettability alteration: A review of chemical aspects, J. Pet. Sci. Eng. 146 (2016) 1079–1091. https://doi.org/10.1016/j.petrol.2016.08.012.

[21]   J.J. Sheng, Surfactant Enhanced Oil Recovery in Carbonate Reservoirs, First Edit, Elsevier Inc., 2013. https://doi.org/10.1016/B978-0-12-386545-8.00012-9.

[22]   J.J. Sheng, Review of Surfactant Enhanced Oil Recovery in Carbonate Reservoirs, Adv. Pet. Explor. Dev. 6 (2013) 1–10. https://doi.org/10.3968/j.aped.1925543820130601.1582.

[23]   J.J. Sheng, Surfactant Enhanced Oil Recovery in Carbonate Reservoirs, First Edit, Elsevier Inc., 2013. https://doi.org/10.1016/B978-0-12-386545-8.00012-9.

[24]   A. Ivanova, A. Orekhov, S. Markovic, S. Iglauer, P. Grishin, A. Cheremisin, Live imaging of micro and macro wettability variations of carbonate oil reservoirs for enhanced oil recovery and - CO_2 trapping / storage, Sci. Rep. (2022) 1–13. https://doi.org/10.1038/s41598-021-04661-2.

[25]   M. Puerto, G.J. Hirasaki, C.A. Miller, J.R. Barnes, Surfactant systems for EOR in high-temperature, high-salinity environments, SPE J. 17 (2012) 11–19. https://doi.org/10.2118/129675-PA.

[26]   J.J. Sheng, Surfactant Flooding, in: Mod. Chem. Enhanc. Oil Recover., 2011: pp. 239–335. https://doi.org/10.1016/b978-1-85617-745-0.00007-3.

[27]   A. Seethepalli, B. Adibhatla, K.K. Mohanty, Physicochemical interactions during surfactant flooding of fractured carbonate reservoirs, SPE J. 9 (2004) 411–418. https://doi.org/10.2118/89423-PA.

[28]   K. Al-azani, S. Abu-khamsin, R. Al-abdrabalnabi, M.S. Kamal, S. Patil, X. Zhou, S. Muhammad, S. Hussain, E. Al Shalabi, Oil Recovery Performance by Surfactant Flooding : A Perspective on Multiscale Evaluation Methods, Energy & Fuels. (2022). https://doi.org/10.1021/acs.energyfuels.2c02544.

[29]   P. Gould, Smart , clean surfaces, (2003) 44–48.

[30]   John R. Fanchi, Shared Earth Modeling: Methodologies for Integrated Reservoir Simulations, Gulf Professional Publishing, 2002.

[31]   W.G. Anderson, Wettability Literature Survey- Part2 : Wettability Measurement, J. Pet. Technol. 38 (1988) 1246–1262. https://doi.org/https://doi.org/10.2118/13933-PA.

[32]   X. Deng, M.S. Kamal, S. Patil, S.M.S. Hussain, X. Zhou, A Review on Wettability

Alteration in Carbonate Rocks: Wettability Modifiers, Energy and Fuels. 34 (2020) 31–54. https://doi.org/10.1021/acs.energyfuels.9b03409.

[33] W.W. Owens, A Laboratory Evaluation of the Wettability of Fifty Oil-Producing Reservoirs, Soc. Pet. Eng. J. 12 (1972) 531–540.

[34] E.J. Gelissen, C.W.M. Van Der Geld, M.W. Baltussen, J.G.M. Kuerten, Modeling of droplet impact on a heated solid surface with a diffuse interface model, Int. J. Multiph. Flow. 123 (2020) 103173. https://doi.org/10.1016/j.ijmultiphaseflow.2019.103173.

[35] M. Sagir, M. Mushtaq, M.S. Tahir, M.B. Tahir, A.R. Shaik, Surfactants for enhanced oil recovery applications, 2020. https://doi.org/10.1007/978-3-030-18785-9.

[36] W. Chen, D.S. Schechter, Surfactant selection for enhanced oil recovery based on surfactant molecular structure in unconventional liquid reservoirs, J. Pet. Sci. Eng. 196 (2020) 107–702. https://doi.org/10.1016/j.petrol.2020.107702.

[37] M. Saadat, J. Yang, M. Dudek, Ø. Gisle, P. Amy, Microfluidic investigation of enhanced oil recovery : The effect of aqueous floods and network wettability, J. Pet. Sci. Eng. 203 (2021). https://doi.org/10.1016/j.petrol.2021.108647.

[38] V. Alvarado, E. Manrique, Enhanced Oil Recovery: An Update Review, Energies. 3 (2010) 1529–1575. https://doi.org/10.3390/en3091529.

[39] M.S. Kamal, A.S. Sultan, U.A. Al-mubaiyedh, I.A. Hussein, Review on Polymer Flooding : Rheology , Adsorption , Stability , and Field Applications of Various Polymer Systems Review on Polymer Flooding : Rheology , Adsorption , Stability , and Field Applications of Various, Polym. Rev. 3724 (2015). https://doi.org/10.1080/15583724.2014.982821.

[40] A. Mohsenatabar, H. Reza, Review on chemical enhanced oil recovery using polymer flooding : Fundamentals , experimental and numerical simulation, Petroleum. 6 (2020) 115–122. https://doi.org/10.1016/j.petlm.2019.09.003.

[41] J.J. Sheng, Status of surfactant EOR technology, Petroleum. 1 (2015) 97–105. https://doi.org/10.1016/j.petlm.2015.07.003.

[42] S. Pal, M. Mushtaq, F. Banat, A.M. Al Sumaiti, Review of surfactant-assisted chemical enhanced oil recovery for carbonate reservoirs: challenges and future perspectives, Pet. Sci. 15 (2018) 77–102. https://doi.org/10.1007/s12182-017-0198-6.

[43] C. Negin, S. Ali, Q. Xie, Most common surfactants employed in chemical enhanced oil recovery, Petroleum. 3 (2017) 197–211. https://doi.org/10.1016/j.petlm.2016.11.007.

[44] M.S. Kamal, I.A. Hussein, A.S. Sultan, Review on Surfactant Flooding: Phase Behavior, Retention, IFT, and Field Applications, Energy and Fuels. 31 (2017) 7701–7720. https://doi.org/10.1021/acs.energyfuels.7b00353.

[45] A.O. Gbadamosi, R. Junin, M.A. Manan, A. Agi, A.S. Yusuff, An overview of chemical enhanced oil recovery: recent advances and prospects, Int. Nano Lett. 9 (2019) 171–202. https://doi.org/10.1007/s40089-019-0272-8.

[46] L.W. Delshad, M., Bhuyan, D., Pope, G. A., & Lake, Effect of Capillary Number on the Residual Saturation of a Three-Phase Micellar Solution, in: SPE Enhanc. Oil Recover. Symp., OnePetro, 1986.

[47]   X. Deng, Z. Tariq, M. Murtaza, S. Patil, M. Mahmoud, M.S. Kamal, Relative contribution of wettability alteration and interfacial tension reduction in EOR: A critical review, J. Mol. Liq. 325 (2021) 115–175. https://doi.org/10.1016/j.molliq.2020.115175.

[48]   J. Lu, A. Goudarzi, P. Chen, D.H. Kim, M. Delshad, K.K. Mohanty, K. Sepehrnoori, U.P. Weerasooriya, G.A. Pope, Enhanced oil recovery from high-temperature, high-salinity naturally fractured carbonate reservoirs by surfactant flood, J. Pet. Sci. Eng. 124 (2014) 122–131. https://doi.org/10.1016/j.petrol.2014.10.016.

[49]   M.J. Rosen, Surfactants and Interfacial Phenomena: Third Edition, 2004. https://doi.org/10.1002/9781118228920.

[50]   E. by K. Holmberg, Handbook of Applied Surface and Colloid Chemistry, 2002. https://doi.org/10.1108/prt.2006.12935eac.007.

[51]   S. Chowdhury, S. Shrivastava, A. Kakati, J.S. Sangwai, Comprehensive Review on the Role of Surfactants in the Chemical Enhanced Oil Recovery Process, Ind. Eng. Chem. Res. 2022 (2021). https://doi.org/10.1021/acs.iecr.1c03301.

[52]   A.A. Olajire, Review of ASP EOR (alkaline surfactant polymer enhanced oil recovery) technology in the petroleum industry: Prospects and challenges, Energy. 77 (2014) 963–982. https://doi.org/10.1016/j.energy.2014.09.005.

[53]   D.C. Standnes, T. Austad, Wettability alteration in chalk 1. Preparation of core material and oil properties, J. Pet. Sci. Eng. 28 (2000) 111–121. https://doi.org/10.1016/S0920-4105(00)00083-8.

[54]   D.C. Standnes, T. Austad, Wettability alteration in chalk 2. Mechanism for wettability alteration from oil-wet to water-wet using surfactants, J. Pet. Sci. Eng. 28 (2000) 123–143. https://doi.org/10.1016/s0920-4105(00)00084-x.

[55]   S. Kalam, S.A. Abu-Khamsin, M.S. Kamal, S. Patil, A review on surfactant retention on rocks: mechanisms, measurements, and influencing factors, Fuel. 293 (2021). https://doi.org/10.1016/j.fuel.2021.120459.

[56]   A. Scerbacova, A. Ivanova, P. Grishin, A. Cheremisin, E. Tokareva, I. Tkachev, G. Sansiev, G. Fedorchenko, I. Afanasiev, Application of alkalis, polyelectrolytes, and nanoparticles for reducing adsorption loss of novel anionic surfactant in carbonate rocks at high salinity and temperature conditions, Colloids Surfaces A Physicochem. Eng. Asp. 653 (2022). https://doi.org/10.1016/j.colsurfa.2022.129996.

[57]   D.C. Standnes, T. Austad, Wettability alteration in carbonates: Interaction between cationic surfactant and carboxylates as a key factor in wettability alteration from oil-wet to water-wet conditions, Colloids Surfaces A Physicochem. Eng. Asp. 216 (2003) 243–259. https://doi.org/10.1016/S0927-7757(02)00580-0.

[58]   G. Bourdarot, S. Ghedan, Modified EOR Screening Criteria as Applied to a Group of Offshore Carbonate Oil Reservoirs, in: SPE Reserv. Characterisation Simul. Conf. Exhib., 2011: pp. 1–21.

[59]   G. Alvarez Jürgenson, C. Bittner, V. Kurkal-Siebert, G. Oetter, J. Tinsley, Alkyl ether carboxylate surfactants for chemically enhanced oil recovery in harsh field conditions, Soc. Pet. Eng. - SPE Asia Pacific Enhanc. Oil Recover. Conf. EORC 2015. (2015) 288–298. https://doi.org/10.2118/174589-ms.

[60]   A.F. Belhaj, J. Aris B M Shuhli, K.A. Elraies, S.M. Mahmood, B. Maulianda, M.S.

Alnarabiji, Partitioning behaviour of novel surfactant mixture for high reservoir temperature and high salinity conditions, Energy. 198 (2020). https://doi.org/10.1016/j.energy.2020.117319.

[61] S. Chen, M. Han, A.M. Alsofi, M.M. Fahmi, Experimental evaluation of non-ionic mixed surfactant formulations at high-temperature and high-salinity conditions, J. Pet. Sci. Eng. 219 (2022) 111084. https://doi.org/10.1016/j.petrol.2022.111084.

[62] F.K. Veedu, D. Nebrigic, A. Smallwood, J. Hickey, P. Wang, EOR Pilot Design Through an Integrated Laboratory Evaluation and Reservoir Modeling Study for a Large Carbonate Field in Kuwait, (2015) 1–20.

[63] S. Pandey, R.P. Bagwe, D.O. Shah, Effect of counterions on surface and foaming properties of dodecyl sulfate, J. Colloid Interface Sci. 267 (2003) 160–166. https://doi.org/10.1016/j.jcis.2003.06.001.

[64] Y. Cao, L. Zhang, R.H. Zhao, L. Zhang, Z.C. Xu, Z.Q. Jin, L. Luo, S. Zhao, Effect of electrolyte and temperature on interfacial tensions of alkylbenzene sulfonate solutions, Energy and Fuels. 26 (2012) 2175–2181. https://doi.org/10.1021/ef201982s.

[65] Z.-Y. Liu, Z.Q. Li, X.-W. Song, J.-C. Zhang, L. Zhang, L. Zhang, S. Zhao, Dynamic interfacial tensions of binary nonionic-anionic and nonionic surfactant mixtures at water-alkane interfaces, Fuel. 135 (2014) 91–98. https://doi.org/10.1016/j.fuel.2014.06.031.

[66] Z. Liu, L. Zhang, X. Cao, X. Song, Z. Jin, L. Zhang, S. Zhao, Effect of electrolytes on interfacial tensions of alkyl ether carboxylate solutions, Energy and Fuels. 27 (2013) 3122–3129. https://doi.org/10.1021/ef400458q.

[67] S.S. Sheng, X.L. Cao, Y.W. Zhu, Z.Q. Jin, L. Zhang, Y. Zhu, L. Zhang, Structure-activity relationship of anionic-nonionic surfactant for reducing interfacial tension of crude oil, J. Mol. Liq. 313 (2020). https://doi.org/10.1016/j.molliq.2020.112772.

[68] J.J. Sheng, Comparison of the effects of wettability alteration and IFT reduction on oil recovery in carbonate reservoirs, Asia-Pacific J. Chem. Eng. (2018). https://doi.org/10.1002/apj.1640.

[69] Y. Yao, M. Wei, B. Bai, Descriptive statistical analysis of experimental data for wettability alteration with surfactants in carbonate reservoirs, Fuel. 310 (2022) 122–110. https://doi.org/10.1016/j.fuel.2021.122110.

[70] S. Das, A. Katiyar, N. Rohilla, R.T. Bonnecaze, Q. Nguyen, A methodology for chemical formulation for wettability alteration induced water imbibition in carbonate reservoirs, J. Pet. Sci. Eng. 198 (2021) 108–136. https://doi.org/10.1016/j.petrol.2020.108136.

[71] Y. Yao, M. Wei, W. Kang, A review of wettability alteration using surfactants in carbonate reservoirs, Adv. Colloid Interface Sci. 294 (2021) 102–477. https://doi.org/10.1016/j.cis.2021.102477.

[72] S. Strand, D.C. Standnes, T. Austad, Spontaneous Imbibition of Aqueous Surfactant Solutions into Neutral to Oil-Wet Carbonate Cores: Effects of Brine Salinity and Composition, Energy & Fuels. 17 (2003) 1133–1144. https://doi.org/https://doi.org/10.1021/ef030051s.

[73] Z. Qi, M. Han, A. Fuseni, A. Alsofi, S. Aramco, F. Zhang, Y. Peng, Laboratory

Study on Surfactant Induced Spontaneous Imbibition for Carbonate Reservoir, in: SPE Asia Pacific Oil Gas Conf. Exhib., Perth, Australia, 2016. https://doi.org/https://doi.org/10.2118/182322-MS.

[74] M. Han, A.B. Fuseni, A.A. Yousef, S.L. Kokal, S. Al-saleh, S. Aramco, Effect of Surfactants on Water Imbibition into Heterogeneous Carbonate Rocks at an Elevated Temperature, in: SPE Middle East Oil Gas Show Conf. MEOS, Proc., Manama, Bahrain, 2011. https://doi.org/https://doi.org/10.2118/141205-MS.

[75] K. Jarrahian, O. Seiedi, M. Sheykhan, M.V. Sefti, S. Ayatollahi, Wettability alteration of carbonate rocks by surfactants: A mechanistic study, Colloids Surfaces A Physicochem. Eng. Asp. 410 (2012) 1–10. https://doi.org/10.1016/j.colsurfa.2012.06.007.

[76] P. Chen, K.K. Mohanty, Wettability Alteration in High Temperature Carbonate Reservoirs, in: Eighteenth SPE Improv. Oil Recover. Symp., Tulsa, Oklakhoma, USA, 2014. https://doi.org/https://doi.org/10.2118/169125-MS.

[77] P. Chen, K.K. Mohanty, Surfactant-Enhanced Oil Recovery from Fractured Oil-Wet Carbonates: Effects of Low IFT and Wettability Alteration, in: SPE Int. Symp. Oilf. Chem., The Woodlands, Texas, USA, 2015. https://doi.org/https://doi.org/10.2118/173797-MS.

[78] Y. Wu, P.J. Shuler, M. Blanco, Y. Tang, W.A.I. Goddard, An Experimental Study of Wetting Behavior and Surfactant EOR in Carbonates With Model Compounds, SPE J. (2008). https://doi.org/https://doi.org/10.2118/99612-PA.

[79] S. Das, A. Katiyar, N. Rohilla, Q.P. Nguyen, R.T. Bonnecaze, Wettability Alteration and Adsorption of Mixed Nonionic and Anionic Surfactants on Carbonates, Langmuir. 36 (2020) 15410–15422. https://doi.org/10.1021/acs.langmuir.0c03022.

[80] M. Souayeh, R.S. Al-maamari, M. Aoudia, M. Karimi, M. Hadji, Experimental Investigation of Wettability Alteration of Oil-Wet Carbonates by a Non-ionic Surfactant, Energy & Fuels. 32 (2018). https://doi.org/10.1021/acs.energyfuels.8b02373.

[81] L.L. Schramm, Foams: Fundamentals and Applications in the Petroleum Industry, (1994).

[82] A.F. Belhaj, K.A. Elraies, S.M. Mahmood, N.N. Zulkifli, S. Akbari, O.S.E. Hussien, The effect of surfactant concentration, salinity, temperature, and pH on surfactant adsorption for chemical enhanced oil recovery: a review, J. Pet. Explor. Prod. Technol. 10 (2020) 125–137. https://doi.org/10.1007/s13202-019-0685-y.

[83] R. Zhang, P. Somasundaran, Advances in adsorption of surfactants and their mixtures at solid/solution interfaces, Adv. Colloid Interface Sci. 126 (2006) 213–229. https://doi.org/10.1016/j.cis.2006.07.004.

[84] Z. Chang, X. Chen, Y. Peng, The adsorption behavior of surfactants on mineral surfaces in the presence of electrolytes – A critical review, Miner. Eng. 121 (2018) 66–76. https://doi.org/10.1016/j.mineng.2018.03.002.

[85] Y. Shi, C. Miller, K. Mohanty, Surfactant-aided low-salinity waterflooding for low-temperature carbonate reservoirs, SPE J. 26 (2021) 2214–2230. https://doi.org/10.2118/201754-PA.

[86] P. Somasundaran, G.E. Agar, The Zero Point of Charge of Calcite, J. Colloid

Interface Sci. 440 (1967).

[87] B. Hou, Y. Wang, Y. Huang, Applied Surface Science Mechanistic study of wettability alteration of oil-wet sandstone surface using different surfactants, Appl. Surf. Sci. 330 (2015) 56–64. https://doi.org/10.1016/j.apsusc.2014.12.185.

[88] H. ShamsiJazeyi, R. Verduzco, G.J. Hirasaki, Reducing adsorption of anionic surfactant for enhanced oil recovery: Part I. Competitive adsorption mechanism, Colloids Surfaces A Physicochem. Eng. Asp. 453 (2014) 162–167. https://doi.org/10.1016/j.colsurfa.2013.10.042.

[89] H. Shamsijazeyi, R. Verduzco, G.J. Hirasaki, Colloids and Surfaces A : Physicochemical and Engineering Aspects Reducing adsorption of anionic surfactant for enhanced oil recovery : Part II . Applied aspects, Colloids Surfaces A Physicochem. Eng. Asp. 453 (2014) 168–175. https://doi.org/10.1016/j.colsurfa.2014.02.021.

[90] H. Shamsijazeyi, G.J. Hirasaki, R. Verduzco, Sacrificial Agent for Reducing Adsorption of Anionic Surfactants, in: 2013: pp. 8–10.

[91] Y.E. Volokitin, I.N. Koltsov, M.Y. Evseeva, O.A. Nurieva, I.S. Akhatov, L.A. Kovaleva, R.R. Zinnatullin, M. V. Mavletov, F.H. Kudasheva, Experimental studies of surfactant adsorption under conditions of ASP flooding at West Salym field, Soc. Pet. Eng. - SPE Russ. Oil Gas Explor. Prod. Tech. Conf. Exhib. 2014, RO G 2014 - Sustain. Optimising Prod. Challenging Limits with Technol. 1 (2014) 694–706. https://doi.org/10.2118/171223-ms.

[92] M.A. Bataweel, A. Texas, SPE 141451 Minimizing Scale Precipitation in Carbonate Cores Caused by Alkalis in ASP Flooding in High Salinity / High Temperature Applications, (2011).

[93] A.O. Gbadamosi, R. Junin, M.A. Manan, A. Agi, A.S. Yusuff, An overview of chemical enhanced oil recovery: recent advances and prospects, Springer Berlin Heidelberg, 2019. https://doi.org/10.1007/s40089-019-0272-8.

[94] H. Sharma, J. Lu, U.P. Weerasooriya, G.A. Pope, K.K. Mohanty, Adsorption in chemical floods with ammonia as the alkali, SPE - DOE Improv. Oil Recover. Symp. Proc. 2016-Janua (2016).

[95] H. Sharma, S. Dufour, G.W.P.P. Arachchilage, U. Weerasooriya, G.A. Pope, K. Mohanty, Alternative alkalis for ASP flooding in anhydrite containing oil reservoirs, Fuel. 140 (2015) 407–420. https://doi.org/10.1016/j.fuel.2014.09.082.

[96] B.N. Tackie-Otoo, M.A. Ayoub Mohammed, N. Yekeen, B.M. Negash, Alternative chemical agents for alkalis, surfactants and polymers for enhanced oil recovery: Research trend and prospects, J. Pet. Sci. Eng. 187 (2020). https://doi.org/10.1016/j.petrol.2019.106828.

[97] A.K. Flaaten, Q.P. Nguyen, G.A. Pope, J. Zhang, A systematic laboratory approach to low-cost high-performance chemical flooding, SPE Reserv. Eval. Eng. 12 (2009) 713–723. https://doi.org/10.2118/113469-PA.

[98] J. Zhang, Q.P. Nguyen, A.K. Floaten, G.A. Pope, Mechanisms of enhanced natural imbibition with novel chemicals, SPE Reserv. Eval. Eng. 12 (2009) 912–920. https://doi.org/10.2118/113453-PA.

[99] W. Lv, B. Bazin, D. Ma, Q. Liu, D. Han, K. Wu, Static and dynamic adsorption of

anionic and amphoteric surfactants with and without the presence of alkali, J. Pet. Sci. Eng. 77 (2011) 209–218. https://doi.org/10.1016/j.petrol.2011.03.006.

[100] M.R. Azam, I.M. Tan, L. Ismail, M. Mushtaq, M. Nadeem, M. Sagir, Static adsorption of anionic surfactant onto crushed Berea sandstone, J. Pet. Explor. Prod. Technol. 3 (2013) 195–201. https://doi.org/10.1007/s13202-013-0057-y.

[101] M.R. Azam, I.M. Tan, L. Ismail, M. Mushtaq, M. Nadeem, M. Sagir, Kinetics and Equilibria of Synthesized Anionic Surfactant onto Berea Sandstone, J. Dispers. Sci. Technol. 35 (2014) 223–230. https://doi.org/10.1080/01932691.2013.783491.

[102] H. Sharma, U. Weerasooriya, G.A. Pope, K.K. Mohanty, Ammonia-based ASP processes for gypsum-containing reservoirs, Proc. - SPE Annu. Tech. Conf. Exhib. 5 (2014) 3365–3381.

[103] S. Kumar, A. Mandal, Studies on interfacial behavior and wettability change phenomena by ionic and nonionic surfactants in presence of alkalis and salt for enhanced oil recovery, Appl. Surf. Sci. 372 (2016) 42–51. https://doi.org/10.1016/j.apsusc.2016.03.024.

[104] J.S. Falcone, P.H. Krumrine, G.C. Schweiker, The use of inorganic sacrificial agents in combination with surfactants in enhanced oil recovery, J. Am. Oil Chem. Soc. 59 (1982). https://doi.org/10.1007/BF02634449.

[105] M. a Bataweel, H. a Nasr-El-Din, T. a&M Univ, Minimizing Scale Precipitation in Carbonate Cores Caused By Alkalis in Asp Flooding in High Salinity/High Temperature Applications, Spe Int. Symp. Oilf. Chem. (the Woodlands, Tx, 4/11-13/2011) Proc. (2011). http://search.ebscohost.com/login.aspx?direct=true&db=pta&AN=1085791&site=ehost-live.

[106] L. Fu, G. Zhang, J. Ge, K. Liao, H. Pei, P. Jiang, X. Li, Study on organic alkali-surfactant-polymer flooding for enhanced ordinary heavy oil recovery, Colloids Surfaces A Physicochem. Eng. Asp. 508 (2016) 230–239. https://doi.org/10.1016/j.colsurfa.2016.08.042.

[107] Y. Bai, C. Xiong, X. Shang, Y. Xin, Experimental study on ethanolamine/surfactant flooding for enhanced oil recovery, Energy and Fuels. 28 (2014) 1829–1837. https://doi.org/10.1021/ef402313n.

[108] H. ShamsiJazeyi, G.J. Hirasaki, R. Verduzco, Sacrificial agent for reducing adsorption of anionic surfactants, Proc. - SPE Int. Symp. Oilf. Chem. 1 (2013) 214–229.

[109] M. Budhathoki, S.H.R. Barnee, B.J. Shiau, J.H. Harwell, Improved oil recovery by reducing surfactant adsorption with polyelectrolyte in high saline brine, Colloids Surfaces A Physicochem. Eng. Asp. 498 (2016) 66–73. https://doi.org/10.1016/j.colsurfa.2016.03.012.

[110] S. Al-Faraji, R.S. Al-Maamari, M. Aoudia, Sodium Alkyl Ether Sulfonates (SAES): Dual Anionic-Nonionic Behavior in Synthetic Brine Having High Salinity and Hardness, J. Surfactants Deterg. 18 (2015) 113–121. https://doi.org/10.1007/s11743-014-1593-2.

[111] G. Pinnawala, A. Davidson, I. Taylor, H. Yang, W. Slaughter, D.H. Kim, T. Malik, V. Dwarakanath, Characterization of carboxylate surfactant retention in high

temperature, hard brine sandstone reservoirs, Proc. - SPE Symp. Improv. Oil Recover. 2020-Augus (2020). https://doi.org/10.2118/200423-ms.

[112] Q. Zhang, Y. Li, Y. Song, J. Li, Z. Wang, Adsorption behavior of branched polyoxyethylene ether carboxylate surfactants, Colloids Surfaces A Physicochem. Eng. Asp. 538 (2018) 361–370. https://doi.org/10.1016/j.colsurfa.2017.09.050.

[113] Q. Zhang, Y. Li, Y. Song, H. Fu, J. Li, Z. Wang, Properties of vesicles formation of single-chain branched carboxylate anionic surfactant in aqueous solutions, J. Mol. Liq. 243 (2017) 431–438. https://doi.org/10.1016/j.molliq.2017.08.047.

[114] A.F. Belhaj, K.A. Elraies, M.S. Alnarabiji, F.A. Abdul Kareem, J.A. Shuhli, S.M. Mahmood, H. Belhaj, Experimental investigation, binary modelling and artificial neural network prediction of surfactant adsorption for enhanced oil recovery application, Chem. Eng. J. 406 (2021). https://doi.org/10.1016/j.cej.2020.127081.

[115] Tharwat F. Tadros, Applied Surfactants: Principles and Applications, 2005. https://doi.org/10.1002/3527604812.

[116] S. Adkins, G.P. Arachchilage, S. Solairaj, J. Lu, U. Weerasooriya, G. Pope, Development of thermally and chemically stable large-hydrophobe alkoxy carboxylate surfactants, in: SPE - DOE Improv. Oil Recover. Symp. Proc., 2012: pp. 1340–1349. https://doi.org/10.2118/154256-ms.

[117] Q. Zhang, Y. Li, Y. Song, J. Li, Z. Wang, Properties of branched alcohol polyoxyethylene ether carboxylates, J. Mol. Liq. 258 (2018) 34–39. https://doi.org/10.1016/j.molliq.2018.02.107.

[118] A. Scerbacova, I. Kopanichuk, A. Cheremisin, Effect of temperature and salinity on interfacial behavior of alkyl ether carboxylate surfactants, Pet. Sci. Technol. 0 (2022) 1–20. https://doi.org/10.1080/10916466.2022.2064872.

[119] X. Yue, X. Fan, Q. Li, X. Chen, C. Wang, Aggregation behaviors of alkyl ether carboxylate surfactants in water, J. Mol. Liq. 227 (2017) 161–167. https://doi.org/10.1016/j.molliq.2016.12.010.

[120] Q.L. Zhong, X.L. Cao, Y.W. Zhu, B.D. Ma, Z.C. Xu, L. Zhang, G.Y. Ma, L. Zhang, Studies on interfacial tensions of betaine and anionic-nonionic surfactant mixed solutions, J. Mol. Liq. 311 (2020). https://doi.org/10.1016/j.molliq.2020.113262.

[121] M. Souayeh, R.S. Al-Maamari, M. Karimi, M. Aoudia, Wettability alteration and oil recovery by surfactant assisted low salinity water in carbonate rock: The impact of nonionic/anionic surfactants, J. Pet. Sci. Eng. 197 (2021) 1–13. https://doi.org/10.1016/j.petrol.2020.108108.

[122] I. Herawati, P. Permadi, A. Rochliadi, T. Marhaendrajana, Adsorption of anionic surfactant on sandstone reservoir containing clay minerals and its effect on wettability alteration, Energy Reports. 8 (2022) 11554–11568. https://doi.org/10.1016/j.egyr.2022.08.268.

[123] A.F. Belhaj, K.A. Elraies, J.A. Shuhili, S.M. Mahmood, R.D. Tewari, Surfactant adsorption evaluation in the presence of crude oil at high reservoir temperature condition, Offshore Technol. Conf. Asia 2020, OTCA 2020. (2020). https://doi.org/10.4043/30141-ms.

[124] A.F. Belhaj, K.A. Elraies, J.A. Shuhili, S.M. Mahmood, U.T. Petronas, P. Carigali, S. Bhd, Static Adsorption Evaluation for Anionic- - Nonionic Surfactant Mixture on

Sandstone in the Presence of Crude Oil at High Reservoir Temperature Condition, SPE Reserv. Eval. Eng. (2022) 2–6.

[125] A. Al-badi, M. Souayeh, R.S. Al-maamari, M. Aoudia, Impact of the molecular structural variation of alkyl ether carboxylate surfactant on IFT reduction and wettability alteration capabilities in carbonates, Geoenergy Sci. Eng. 222 (2023) 211395. https://doi.org/10.1016/j.geoen.2022.211395.

[126] O. Massarweh, A.S. Abushaikha, The use of surfactants in enhanced oil recovery: A review of recent advances, Energy Reports. 6 (2020) 3150–3178. https://doi.org/10.1016/j.egyr.2020.11.009.

[127] Y. She, C. Zhang, M.A. Mahardika, A. Patmonoaji, Y. Hu, S. Matsushita, T. Suekane, Pore-scale study of in-situ surfactant flooding with strong oil emulsification in sandstone based on X-ray microtomography, J. Ind. Eng. Chem. 98 (2021) 247–261. https://doi.org/10.1016/j.jiec.2021.03.046.

[128] A.W. Cense, H.A. Van Der Linde, N. Brussee, J. Beljaars, A. Schwing, RELIABLE IS IN SITU MONITORING (ISSM) USING X-RAY ? SATURATION, in: Int. Symp. Soc. Core Anal., Avignon, France, 2014: pp. 1–12.

[129] J. Siavashi, A. Najafi, M. Sharifi, J. Fahimpour, M. Shabani, B. Liu, K. Liu, J. Yan, M. Ostadhassan, An insight into core flooding experiment via NMR imaging and numerical simulation, Fuel. 318 (2022) 123589. https://doi.org/10.1016/j.fuel.2022.123589.

[130] M. Fani, P. Pourafshary, P. Mostaghimi, N. Mosavat, Application of microfluidics in chemical enhanced oil recovery: A review, Fuel. 315 (2022) 123225. https://doi.org/10.1016/j.fuel.2022.123225.

[131] S. Gogoi, S. Borgohain, Review on microfluidic studies for EOR application Indian Institute of Technology, J. Pet. Explor. Prod. Technol. 9 (2019) 2263–2277. https://doi.org/10.1007/s13202-019-0610-4.

[132] Z. Qi, S. Pierobon, O. Serediak, J. Le, A. Pettigrew, A. Abedini, Effects of thief zones on displacement efficiency : Microfluidic pore-scale and conformance control analysis, Fuel. 316 (2022) 123371. https://doi.org/10.1016/j.fuel.2022.123371.

[133] A. Pereponov, D., Scerbacova, A., Kazaku, V., Hajiyev, M., Tarkhov, M. A., Shilov, E., Cheremisin, Application of microfluidics to optimize oil and gas field development technologies, Kazakhstan J. Oil Gas Ind. 5 (2023) 57–73.

[134] W. Zhou, L. Jiang, X. Liu, Y. Hu, Y. Yan, Molecular insights into the effect of anionic-nonionic and cationic surfactant mixtures on interfacial properties of oil-water interface, Colloids Surfaces A Physicochem. Eng. Asp. 637 (2022) 128259. https://doi.org/10.1016/j.colsurfa.2022.128259.

[135] A.M. Luz, T.J.P. do. Santos, G.D. Barbosa, C.L.M. Camargo, F.W. Tavares, A molecular study on the behavior of polyethoxylated alkyl ethers surfactants in a water/n-alkane interface, Colloids Surfaces A Physicochem. Eng. Asp. 651 (2022) 129627. https://doi.org/10.1016/j.colsurfa.2022.129627.

[136] C.D. Bruce, M.L. Berkowitz, L. Perera, M.D.E. Forbes, Molecular dynamics simulation of sodium dodecyl sulfate both in water: Micellar structural characteristics and counterion distribution, J. Phys. Chem. B. 106 (2002) 3788–3793. https://doi.org/10.1021/jp013616z.

[137] S. Liu, S. Yuan, H. Zhang, Molecular Dynamics Simulation for the Demulsification of O/W Emulsion under Pulsed Electric Field, Molecules. 27 (2022) 1–15. https://doi.org/10.3390/molecules27082559.

[138] H. Yan, X.L. Guo, S.L. Yuan, C.B. Liu, Molecular dynamics study of the effect of calcium ions on the monolayer of SDC and SDSn surfactants at the vapor/liquid interface, Langmuir. 27 (2011) 5762–5771. https://doi.org/10.1021/la1049869.

[139] S. Abdel-Azeim, S. Sakthivel, T.A. Kandiel, M.Y. Kanj, Specificity and Synergy at the Oil-Brine Interface: New Insights from Experiments and Molecular Dynamics Simulations, Energy and Fuels. 35 (2021) 14647–14657. https://doi.org/10.1021/acs.energyfuels.1c02133.

[140] Y. Chen, G. Xu, Improvement of Ca2+-tolerance by the introduction of EO groups for the anionic surfactants: Molecular dynamics simulation, Colloids Surfaces A Physicochem. Eng. Asp. 424 (2013) 26–32. https://doi.org/10.1016/j.colsurfa.2013.02.026.

[141] H. ze Gang, X. He, X. He, X. Bao, J. Liu, S. Yang, Y. Li, B.Z. Mu, Interfacial properties and salt tolerance of carboxylated nonylphenol ethoxylate surfactants, Colloids Surfaces A Physicochem. Eng. Asp. 616 (2021). https://doi.org/10.1016/j.colsurfa.2021.126222.

[142] N.N. Zulkifli, S.M. Mahmood, S. Akbari, A.A.A. Manap, N.I. Kechut, K.A. Elrais, Evaluation of new surfactants for enhanced oil recovery applications in high-temperature reservoirs, J. Pet. Explor. Prod. Technol. 10 (2020) 283–296. https://doi.org/10.1007/s13202-019-0713-y.

[143] Drelich J., Fang Ch., W. C.L., Measurement of Interfacial Tension in Fluid-Fluid Systems, Encycl. Surf. Colloid Sci. 3 (2002) 3152–3166. http://www.informaworld.com/10.1081/E-ESCS-120000636.

[144] D.D. Joseph, M.S. Arney, G. Gillberg, H. Hu, D. Hultman, C. Verdier, T.M. Vinagre, A spinning drop tensioextensometer, J. Rheol. (N. Y. N. Y). 36 (1992) 621–662. https://doi.org/10.1122/1.550311.

[145] T. Tichelkamp, Y. Vu, M. Nourani, G. Øye, Interfacial tension between low salinity solutions of sulfonate surfactants and crude and model oils, Energy and Fuels. 28 (2014) 2408–2414. https://doi.org/10.1021/ef4024959.

[146] N. Pal, N. Saxena, A. Mandal, Equilibrium and dynamic adsorption of gemini surfactants with di ff erent spacer lengths at oil / aqueous interfaces, Colloids Surfaces A. 533 (2017) 20–32. https://doi.org/10.1016/j.colsurfa.2017.08.020.

[147] M.K.J. Williams R. J., Phillips J. N., The critical micelle concentration of sodium lauryl sulphate at 25 C, Trans. Faraday Soc. 51 (1955) 728–737.

[148] R. Nagarajan, Self-Assembly : The Neglected Role of the Surfactant Tail †, Langmuir. 18 (2002) 31–38.

[149] Z. Wang, Z. Zhou, L. Han, X. Chen, H. He, Q. Zhang, Z. Xu, Q. Gong, L. Zhang, G. Ma, L. Zhang, The mechanism for lowering interfacial tension by extended surfactant containing ethylene oxide and propylene oxide groups, J. Mol. Liq. 359 (2022) 119364. https://doi.org/10.1016/j.molliq.2022.119364.

[150] I. Kopanichuk, A. Scerbacova, A. Ivanova, A. Cheremisin, A. Vishnyakov, The effect of the molecular structure of alkyl ether carboxylate surfactants on the oil –

water interfacial tension, J. Mol. Liq. 360 (2022). https://doi.org/10.1016/j.molliq.2022.119525.

[151] X.W. Song, L. Zhang, X.C. Wang, L. Zhang, S. Zhao, J.Y. Yu, Study on foaming properties of polyoxyethylene alkyl ether carboxylic salts with different structures, J. Dispers. Sci. Technol. 32 (2011) 247–253. https://doi.org/10.1080/01932691003657001.

[152] B. Gao, M.M. Sharma, A family of alkyl sulfate gemini surfactants. 2. Water – oil interfacial tension reduction, J. Colloid Interface Sci. 407 (2013) 375–381. https://doi.org/10.1016/j.jcis.2013.06.066.

[153] Chattoraj D., Adsorption and the Gibbs surface excess, Springer Science & Business Media, 2012.

[154] J.C. Berg, An introduction to interfaces & colloids: the bridge to nanoscience, World Scientific, 2010.

[155] N. Akhlaghi, S. Riahi, R. Parvaneh, Interfacial tension behavior of a nonionic surfactant in oil/water system; salinity, pH, temperature, and ionic strength effects, J. Pet. Sci. Eng. 198 (2021) 108177. https://doi.org/10.1016/j.petrol.2020.108177.

[156] P. Wei, J. Li, Y. Xie, X. Huang, L. Sun, Alkyl polyglucosides for potential application in oil recovery process: Adsorption behavior in sandstones under high temperature and salinity, J. Pet. Sci. Eng. 189 (2020). https://doi.org/10.1016/j.petrol.2020.107057.

[157] L. Guo, Y. Liu, S.S. Hu, Z.C. Xu, Q.T. Gong, L. Zhang, L. Zhang, Dynamic interfacial tensions of alkyl alcohol polyoxypropylene-oxyehtylene ether sulfonate solutions, J. Pet. Sci. Eng. 141 (2016) 9–15. https://doi.org/10.1016/j.petrol.2016.01.025.

[158] GROMACS Documentation. Release 2021.2, 2021.

[159] M. James, T. Murtola, R. Schulz, J.C. Smith, B. Hess, E. Lindahl, GROMACS : High performance molecular simulations through multi-level parallelism from laptops to supercomputers, SoftwareX. 2 (2015) 19–25. https://doi.org/10.1016/j.softx.2015.06.001.

[160] J.M. Stubbs, J.J. Potoff, J.I. Siepmann, Transferable potentials for phase equilibria. 6. United-atom description for ethers, glycols, ketones, and aldehydes, J. Phys. Chem. B. 108 (2004) 17596–17605. https://doi.org/10.1021/jp049459w.

[161] A. Vishnyakov, T. Weathers, A. Hosangadi, Y.C. Chiew, Molecular models for phase equilibria of alkanes with air components and combustion products I. Alkane mixtures with nitrogen, CO_2 and water, Fluid Phase Equilib. 514 (2020). https://doi.org/10.1016/j.fluid.2020.112553.

[162] M.G. Martin, J.I. Siepmann, Transferable potentials for phase equilibria. 1. United-atom description of n-alkanes, J. Phys. Chem. B. 102 (1998) 2569–2577. https://doi.org/10.1021/jp972543+.

[163] J. Fischer, D. Paschek, A. Geiger, G. Sadowski, Modeling of aqueous poly(oxyethylene) solutions: 1. Atomistic simulations, J. Phys. Chem. B. 112 (2008) 2388–2398. https://doi.org/10.1021/jp0765345.

[164] W.L. Jorgensen, D.S. Maxwell, J. Tirado-Rives, Development and testing of the OPLS all-atom force field on conformational energetics and properties of organic

liquids, J. Am. Chem. Soc. 118 (1996) 11225–11236. https://doi.org/10.1021/ja9621760.

[165] C. Abascal, J. L., & Vega, A general purpose model for the condensed phases of water: TIP4P/2005, J. Chem. Phys. 123 (2005).

[166] C. Zeron, I. M., Abascal, J. L. F., & Vega, A force field of Li+, Na+, K+, Mg2+, Ca2+, Cl−, and SO 4 2− in aqueous solution based on the TIP4P/2005 water model and scaled charges for the ions, J. Chem. Phys. 151 (2019).

[167] K. Humphrey, W., Dalke, A., & Schulten, VMD: Visual molecular dynamics, J. Mol. Graph. 14 (1996) 33–38.

[168] K. Giribabu, P. Ghosh, Adsorption of nonionic surfactants at fluid-fluid interfaces: Importance in the coalescence of bubbles and drops, Chem. Eng. Sci. 62 (2007) 3057–3067. https://doi.org/10.1016/j.ces.2007.03.002.

[169] E. Mayoral, J.A. Arcos-casarrubias, A.G. Goicochea, Self – assembly of model surfactants as reverse micelles in nonpolar solvents and their role as interfacial tension modifiers, Colloids Surfaces A Physicochem. Eng. Asp. 615 (2021) 126244. https://doi.org/10.1016/j.colsurfa.2021.126244.

[170] S. Kumar, P. Panigrahi, R.K. Saw, A. Mandal, Interfacial Interaction of Cationic Surfactants and Its Effect on Wettability Alteration of Oil-Wet Carbonate Rock, Energy and Fuels. 30 (2016) 2846–2857. https://doi.org/10.1021/acs.energyfuels.6b00152.

[171] S.S. Al-Jaroudi, A. Ul-Hamid, A.R.I. Mohammed, S. Saner, Use of X-ray powder diffraction for quantitative analysis of carbonate rock reservoir samples, Powder Technol. 175 (2007) 115–121. https://doi.org/10.1016/j.powtec.2007.01.013.

[172] A. Mukhametdinova, T. Karamov, N. Bogdanovich, S. Borisenko, S. Rudakovskaya, Wettability of organic-rich source rocks : case study on Bazhenov Formation (Abalak-Bazhenov group), Adv. Geosci. 54 (2020) 195–204. https://doi.org/https://doi.org/10.5194/adgeo-54-195-2020.

[173] A. Mukhametdinova, A. Kazak, T. Karamov, N. Bogdanovich, Reservoir Properties of Low-Permeable Carbonate Rocks: Experimental Features, Energies. 13 (2020) 1–25. https://doi.org/https://doi.org/10.3390/en13092233.

[174] T. Karamov; E. Leushina; E. Kozlova; M. Spasennykh, Broad Ion Beam–Scanning Electron Microscopy Characterization of Organic Porosity Evolution During Thermal Treatment of Bazhenov Shale Sample, SPE Reserv. Eval. Eng. (2022) 1–11. https://doi.org/https://doi.org/10.2118/210599-PA.

[175] K.E. Peters, Guidelines for Evaluating Petroleum Source Rock Using Programmed Pyrolysis, Am. Assoc. Pet. Geol. Bull. (1986). https://doi.org/10.1306/94885688-1704-11D7-8645000102C1865D.

[176] M.R. Kawelah, Interaction of Stabilized Alkylbenzene Sulfonate Surfactants on the Nanoscale with Water-Wet and Oil-Wet Carbonate Surfaces under High-Salinity and High-Temperature Conditions: A QCM-D Study, ACS Omega. 5 (2020) 10838–10846. https://doi.org/10.1021/acsomega.0c00478.

[177] M. Spasennykh, P. Maglevannaia, E. Kozlova, T. Bulatov, E. Leushina, Geochemical Trends Reflecting Hydrocarbon Generation , Migration and Accumulation in Unconventional Reservoirs Based on Pyrolysis Data (on the

Example of the Bazhenov Formation), Geosciences. 11 (2021) 307. https://doi.org/https://doi.org/10.3390/geosciences11080307.

[178] F. Behar, Rock-Eval 6 Technology : Performances and Developments, Oil Gas Sci. Technol. 56 (2001) 111–134. https://doi.org/10.2516/ogst:2001013.

[179] G. Jian, M. Puerto, A. Wehowsky, C. Miller, G.J. Hirasaki, S.L. Biswal, Characterizing adsorption of associating surfactants on carbonates surfaces, J. Colloid Interface Sci. 513 (2018) 684–692. https://doi.org/10.1016/j.jcis.2017.11.041.

[180] O. Massarweh, A.S. Abushaikha, Application of surfactants in enhancing oil recovery from tight carbonates: Physicochemical properties and core flooding experiments, Geoenergy Sci. Eng. 221 (2023) 211400. https://doi.org/10.1016/j.geoen.2022.211400.

[181] H. Ding, S.R. Rahman, Investigation of the Impact of Potential Determining Ions from Surface Complexation Modeling, Energy and Fuels. 32 (2018) 9314–9321. https://doi.org/10.1021/acs.energyfuels.8b02131.

[182] R.A. Lara Orozco, G.A. Abeykoon, R. Okuno, L.W. Lake, The impact of glycine on the zeta potential of calcite at different temperatures and brine compositions, Colloids Surfaces A Physicochem. Eng. Asp. 624 (2021). https://doi.org/10.1016/j.colsurfa.2021.126851.

[183] C.N. Lunardi, A.J. Gomes, F.S. Rocha, J. De Tommaso, G.S. Patience, Experimental methods in chemical engineering: Zeta potential, Can. J. Chem. Eng. 99 (2021) 627–639. https://doi.org/10.1002/cjce.23914.

[184] C. Walter, R.M. Rohner, Titration Applications Brochure 22 Surfactant Titration for METTLER TOLEDO, 1997.

[185] A. Bera, T. Kumar, K. Ojha, A. Mandal, Adsorption of surfactants on sand surface in enhanced oil recovery: Isotherms, kinetics and thermodynamic studies, Appl. Surf. Sci. 284 (2013) 87–99. https://doi.org/10.1016/j.apsusc.2013.07.029.

[186] K.Y. Foo, B.H. Hameed, Insights into the modeling of adsorption isotherm systems, Chem. Eng. J. 156 (2010) 2–10. https://doi.org/10.1016/j.cej.2009.09.013.

[187] A.F. Belhaj, K.A. Elraies, M.S. Alnarabiji, F.A. Abdul Kareem, J.A. Shuhli, S.M. Mahmood, H. Belhaj, Experimental investigation, binary modelling and artificial neural network prediction of surfactant adsorption for enhanced oil recovery application, Chem. Eng. J. 406 (2021) 127–081. https://doi.org/10.1016/j.cej.2020.127081.

[188] I. Langmuir, THE CONSTITUTION AND FUNDAMENTAL PROPERTIES OF SOLIDS AND LIQUIDS, J. Am. Chem. Soc. 38 (1916) 2221–2295. https://doi.org/10.1021/ja02268a002.

[189] H. Freundlich, Over the Adsorption in Solution, J. Phys. Chem. 57 (1906) 385–471.

[190] Temkin M.I., Kinetics of ammonia synthesis on promoted iron catalysts, Acta Physiochim. URSS. 12 (1940) 327–356.

[191] X. Deng, M. Shahzad, S. Patil, S. Muhammad, S. Hussain, X. Zhou, M. Mahmoud, Wettability alteration of locally synthesized cationic gemini surfactants on carbonate rock, J. Mol. Liq. 344 (2021) 117–817. https://doi.org/10.1016/j.molliq.2021.117817.

[192] I.W.R. Saputra, O. Adebisi, E.B. Ladan, A. Bagareddy, A. Sarmah, D.S. Schechter, The Influence of Oil Composition, Rock Mineralogy, Aging Time, and Brine Pre-soak on Shale Wettability, ACS Omega. 7 (2021) 85–100. https://doi.org/10.1021/acsomega.1c03940.

[193] R.J. Dunham, Classification of carbonate rocks according to Robert J. Dunhamdepositional textures, (1962) 108–121.

[194] S. Strand, E.J. Høgnesen, T. Austad, Wettability alteration of carbonates — Effects of potential determining ions (Ca2 + and SO42−) and temperature, Colloids Surfaces A Physicochem. Eng. Asp. 275 (2006) 1–10. https://doi.org/10.1016/j.colsurfa.2005.10.061.

[195] K.A.R. Gomari, A.A. Hamouda, R. Denoyel, Influence of sulfate ions on the interaction between fatty acids and calcite surface, Colloids Surfaces A Physicochem. Eng. Asp. Surfaces A. 287 (2006) 29–35. https://doi.org/10.1016/j.colsurfa.2006.03.018.

[196] K.A.R. Gomari, R. Denoyel, A.A. Hamouda, Wettability of calcite and mica modified by different long-chain fatty acids (C 18 acids), J. Colloid Interface Sci. 297 (2006) 470–479. https://doi.org/10.1016/j.jcis.2005.11.036.

[197] R. Gomari, Different Approaches to Understand Mechanism of Wettability Alteration of Carbonate Reservoirs, in: SPE Eur. Annu. Conf. Exhib., Amsterdam, The Netherlands, 2009. https://doi.org/https://doi.org/10.2118/121952-MS.

[198] M. Karimi, R.S. Al-Maamari, S. Ayatollahi, N. Mehranbod, Mechanistic study of wettability alteration of oil-wet calcite: The effect of magnesium ions in the presence and absence of cationic surfactant, Colloids Surfaces A Physicochem. Eng. Asp. 482 (2015) 403–415. https://doi.org/10.1016/j.colsurfa.2015.07.001.

[199] S. Das, A. Katiyar, N. Rohilla, Q. Nguyen, R.T. Bonnecaze, Universal scaling of adsorption of nonionic surfactants on carbonates using cloud point temperatures, J. Colloid Interface Sci. 577 (2020) 431–440. https://doi.org/10.1016/j.jcis.2020.05.063.

[200] P.S. Hammond, E. Unsal, Forced and Spontaneous Imbibition of Surfactant Solution into an Oil-Wet Capillary : The Effects of Surfactant Diffusion Ahead of the Advancing Meniscus, Langmuir. 119 (2010) 6206–6221. https://doi.org/10.1021/la903924m.

[201] P.S. Hammond, E. Unsal, Spontaneous Imbibition of Surfactant Solution into an Oil-Wet Capillary: Wettability Restoration by Surfactant À Contaminant Complexation, Langmuir. 27 (2011) 4412–4429. https://doi.org/https://doi.org/10.1021/la1048503.

[202] M. Salehi, S.J. Johnson, J. Liang, Mechanistic Study of Wettability Alteration Using Surfactants with Applications in Naturally Fractured Reservoirs, Langmuir. 24 (2008) 14099–14107. https://doi.org/https://doi.org/10.1021/la802464u.

[203] S. Kalam, S.A. Abu-khamsin, M.S. Kamal, S.M.S. Hussain, K. Norrman, M. Mahmoud, S. Patil, Adsorption Mechanisms of a Novel Cationic Gemini Surfactant onto Different Rocks, Energy & Fuels. 36 (2022) 5737–5748. https://doi.org/10.1021/acs.energyfuels.2c00684.

[204] A. Kasha, H. Al-hashim, W. Abdallah, R. Taherian, B. Sauerer, Effect of Ca2+ ,

Mg2+ and SO42 − ions on the zeta potential of calcite and dolomite particles aged with stearic acid, Colloids Surfaces A Physicochem. Eng. Asp. 482 (2015) 290–299. https://doi.org/10.1016/j.colsurfa.2015.05.043.

[205] N. Hemmati, A. Tabzar, M.H. Ghazanfari, Adsorption of sodium dodecyl benzene sulfonate onto carbonate rock : Kinetics , equilibrium and mechanistic study, J. Dispers. Sci. Technol. 39 (2018) 687–699. https://doi.org/10.1080/01932691.2017.1382373.

[206] J. Brinck, F. Tiberg, Adsorption Behavior of Two Binary Nonionic Surfactant Systems at the Silica - Water Interface, Langmuir. 7463 (1996) 5042–5047.

[207] G. Jian, M.C. Puerto, A. Wehowsky, P. Dong, K.P. Johnston, G.J. Hirasaki, S.L. Biswal, Static Adsorption of an Ethoxylated Nonionic Surfactant on Carbonate Minerals, Langmuir. 32 (2016) 10244–10252. https://doi.org/10.1021/acs.langmuir.6b01975.

[208] G.L. Aranovich, New polymolecular adsorption isotherm, J. Colloid Interface Sci. 141 (1991) 30–43. https://doi.org/10.1016/0021-9797(91)90299-N.

[209] J. Søndergaard, C.J. Jørgensen, Field Portable X-Ray Fluorescence (pXRF) Spectrometry for Chemical Dust Source Characterization: Investigations of Natural and Mining-Related Dust Sources in Greenland (Kangerlussuaq Area), Water. Air. Soil Pollut. 232 (2021). https://doi.org/10.1007/s11270-021-05095-2.

[210] Sikandar Kumar, A. Burukhin;, A. Cheremisin, P. Grishin, Wettability of Carbonate Reservoirs: Effects of Fluid and Aging, in: SPE Russ. Pet. Technol. Conf., OnePetro, Virtual, n.d. https://doi.org/https://doi.org/10.2118/201834-MS.

[211] S. Of, R. Characterization, NEW X RAY SCANNING SYSTEM FOR SPECIAL CORE ANALYSES IN, (n.d.).

[212] V.M. Dobrynin, A.G.. Kovalev, A.M.. Kuznetsov, V.N. Chernoglazov, Phase permeability of oil and gas reservoirs, VNIIOENG, Moscow, URSS, 1988.

[213] M. Shahzad, K. Mohamed, M. Mohammed, H. Salaheldin, I. Hussein, Clay minerals damage quantification in sandstone rocks using core flooding and NMR, J. Pet. Explor. Prod. Technol. 9 (2019) 593–603. https://doi.org/10.1007/s13202-018-0507-7.

[214] S. Jafari, D. So, M. Shari, A.H. Sarapardeh, Toward mechanistic understanding of natural surfactant fl ooding in enhanced oil recovery processes: The role of salinity , surfactant concentration and rock type, J. Mol. Liq. 222 (2016) 632–639. https://doi.org/10.1016/j.molliq.2016.07.086.

[215] A. Kornilov, A. Zhirov, A. Petrakov, T. Rogova, Y. Kurelenkova, I. Afanasiev, G. Sansiev, G. Fedorchenko, G. Fursov, M. Kubrak, T. Altmann, N. Lichterfeld-Weber, C. Bittner, G. Oetter, E. Helwig, Selection of effective surfactant composition to improve oil displacement efficiency in carbonate reservoirs with high salinity formation water, Soc. Pet. Eng. - SPE Russ. Pet. Technol. Conf. 2019, RPTC 2019. (2020). https://doi.org/10.2118/196772-ru.

[216] A. Cense, J. Reed, P. Egermann, SCAL FOR GAS RESERVOIRS: A CONTRIBUTION FOR BETTER EXPERIMENTS, in: Int. Symp. Soc. Core Anal., Snowmass, Colorado, USA, 2016.

[217] A.K. Flaaten, Q.P. Nguyen, G.A. Pope, J. Zhang, A Systematic Laboratory

Approach to Low-Cost, High-Performance Chemical Flooding, in: SPE/DOE Improv. Oil Recover. Symp., Tulsa, Oklahoma, USA, 2008.

[218] A.F. Belhaj, K.A. Elraies, H.K. Sarma, J.A. Shuhili, S.M. Mahmood, M.S. Alnarabiji, Surfactant partitioning and adsorption in chemical EOR: The neglected phenomenon in porous media, Soc. Pet. Eng. - SPE/IATMI Asia Pacific Oil Gas Conf. Exhib. 2021, APOG 2021. (2021). https://doi.org/10.2118/205676-MS.

[219] A.F. Belhaj, K.A. Elraies, M.S. Alnarabiji, J.A.B.M. Shuhli, S.M. Mahmood, L.W. Ern, Experimental Investigation of Surfactant Partitioning, Energies. (2019).

[220] A.K. Flaaten, P. Quoc, J. Zhang, H. Mohammadi, Alkaline / Surfactant / Polymer Chemical Flooding Without the Need for Soft Water, SPE J. (2010).

[221] K. He, Z. Yue, C. Fan, L. Xu, M.A.H. Service, Agent : A Way to Optimize Surfactant Performance in Unconventional, in: SPE Int. Symp. Oilf. Chem., Woodlands, texas, USA, 2015.

[222] H. Mahani, A.L. Keya, S. Berg, R. Nasralla, Electrokinetics of carbonate/brine interface in low-salinity waterflooding: Effect of brine salinity, composition, rock type, and pH on ζ-potential and a surface-complexation model, SPE J. 22 (2017) 53–68. https://doi.org/10.2118/181745-pa.

[223] N. Saxena, A. Kumar, A. Mandal, Adsorption analysis of natural anionic surfactant for enhanced oil recovery : The role of mineralogy , salinity , alkalinity and nanoparticles, J. Pet. Sci. Eng. 173 (2019) 1264–1283. https://doi.org/10.1016/j.petrol.2018.11.002.

[224] N. Saxena, S. Kumar, A. Mandal, Adsorption characteristics and kinetics of synthesized anionic surfactant and polymeric surfactant on sand surface for application in enhanced oil recovery, Asia-Pacific J. Chem. Eng. 13 (2018). https://doi.org/10.1002/apj.2211.

[225] G.J. Hirasaki, C. a Miller, M. Puerto, Recent Advances in Surfactant EOR, 115386 (2008) 3–5.

[226] C.D. Yuan, W.F. Pu, X.C. Wang, L. Sun, Y.C. Zhang, S. Cheng, Effects of Interfacial Tension, Emulsification, and Surfactant Concentration on Oil Recovery in Surfactant Flooding Process for High Temperature and High Salinity Reservoirs, Energy and Fuels. 29 (2015) 6165–6176. https://doi.org/10.1021/acs.energyfuels.5b01393.

[227] A. Rezaei, M. Riazi, M. Escrochi, R. Elhaei, Integrating surfactant, alkali and nano-fluid flooding for enhanced oil recovery: A mechanistic experimental study of novel chemical combinations, J. Mol. Liq. 308 (2020) 113106. https://doi.org/10.1016/j.molliq.2020.113106.

[228] R. Saha, R.V.S. Uppaluri, P. Tiwari, Effects of interfacial tension, oil layer break time, emulsification and wettability alteration on oil recovery for carbonate reservoirs, Colloids Surfaces A Physicochem. Eng. Asp. 559 (2018) 92–103. https://doi.org/10.1016/j.colsurfa.2018.09.045.

[229] C.H. Giles, D. Smith, A. Huitson, A General Treatment and Classification of the Solute Adsorption Isotherm, J. Colloid Interface Sci. 47 (1974) 755–765.

[230] K. Vijayaraghavan, T.V.N. Padmesh, K. Palanivelu, M. Velan, Biosorption of nickel(II) ions onto Sargassum wightii: Application of two-parameter and three-

parameter isotherm models, J. Hazard. Mater. 133 (2006) 304–308. https://doi.org/10.1016/j.jhazmat.2005.10.016.

[231] A.P. Terzyk, P.A. Gauden, P. Kowalczyk, Giles ' classification of solute adsorption isotherms for binary non-electrolyte solutions via lattice DFT supported by experimental sorption data from aqueous solutions on carbonac ..., in: Carbon Mater. Theory Pract., Research Signpost, Kerala, India, 2008.
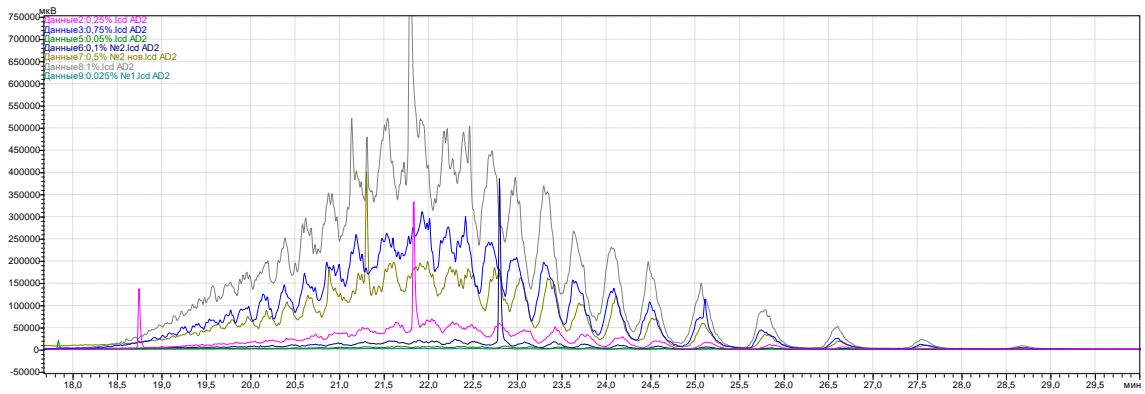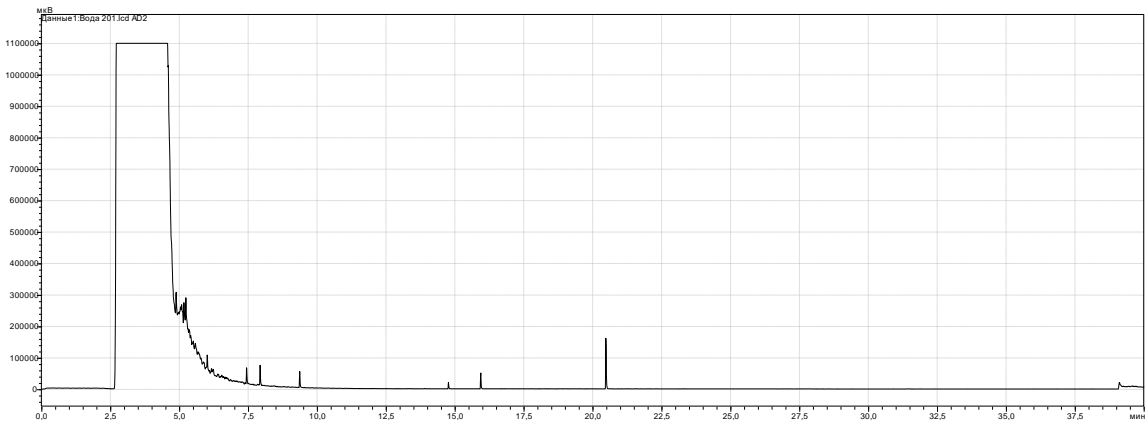
Appendix

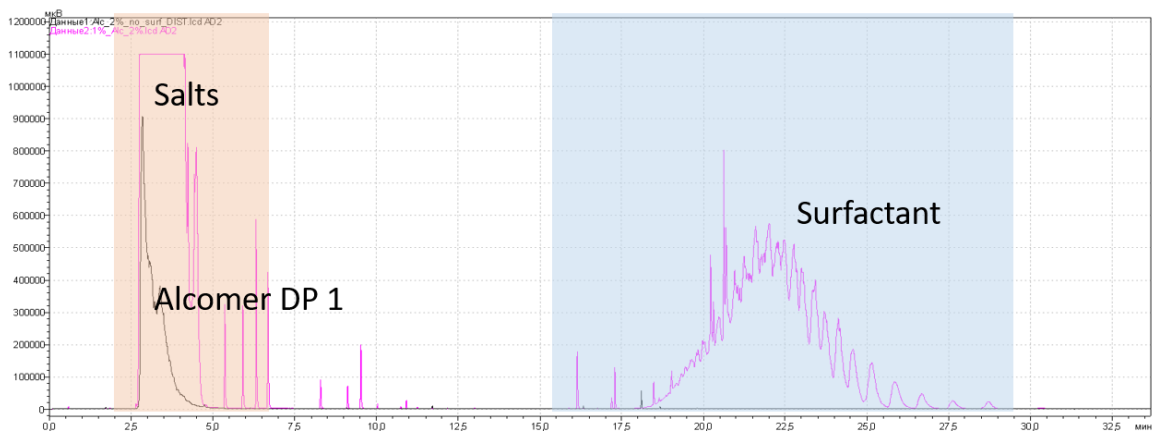Co-Ka1 (1.789010 A)
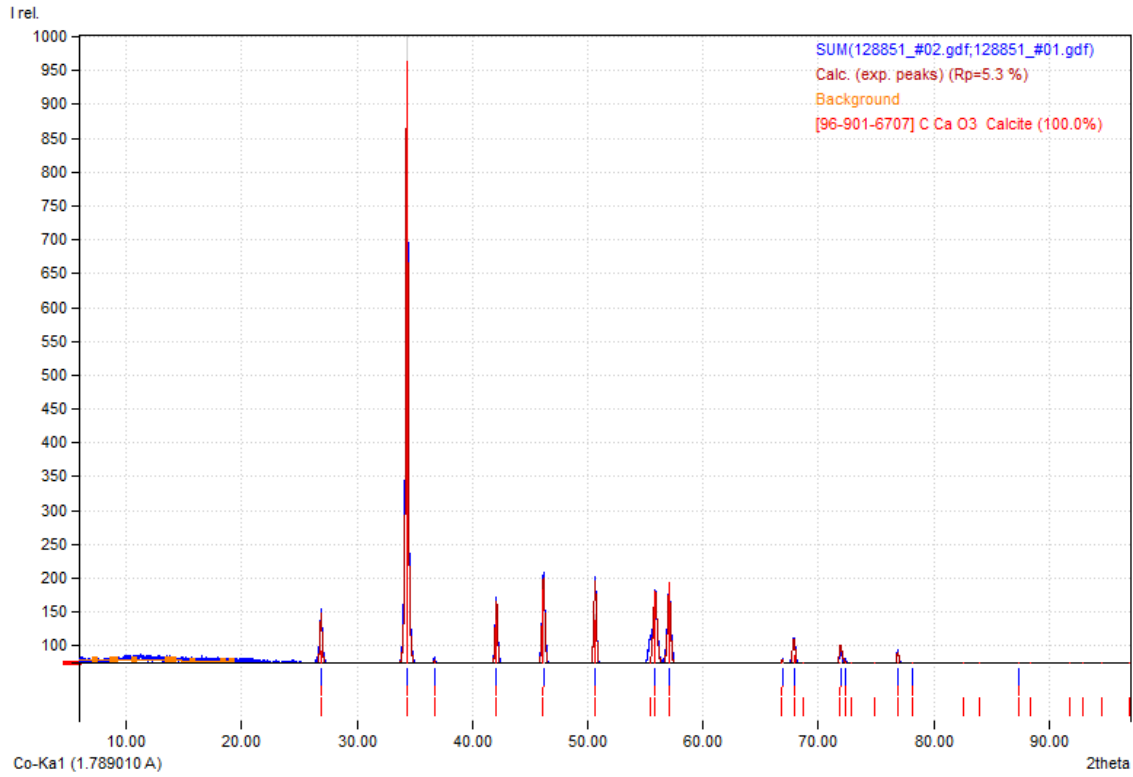
XRD of carbonate rock
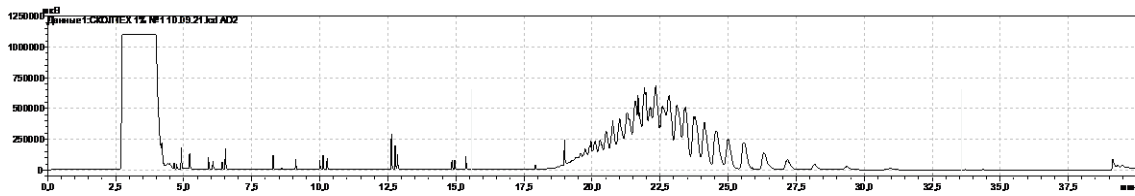
Peak shape of surfactant 1 wt% solution (operating concentration)

Dataset for calibration curve (chromatograms of surfactant solutions with different concentrations)
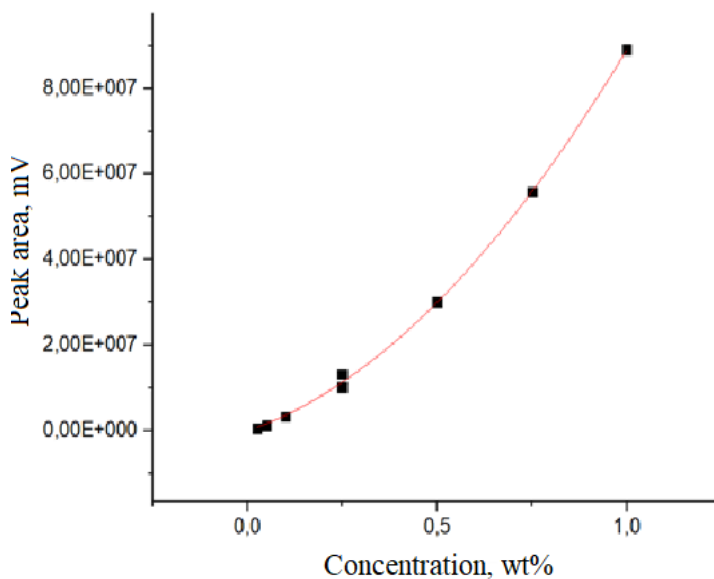

Chromatogram of artificial brine (201 g/L)

Comparison of chromatograms of Alcomer DP 1 solution on distilled water (black) with 1 wt% surfactant solution in artificial brine with Alcomer DP 1 (pink)
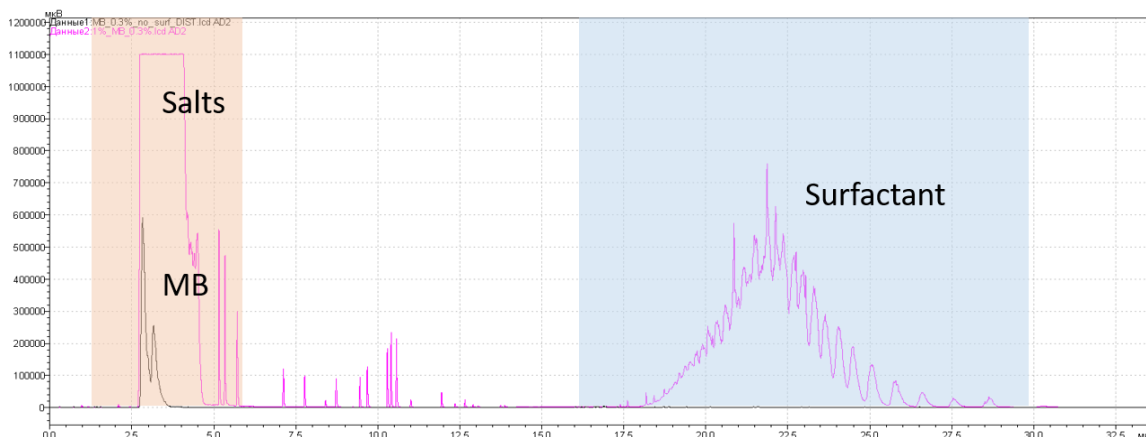
Comparison of chromatograms of sodium metaborate tetrahydrate solution on distilled water (black) with 1 wt% surfactant solution in artificial brine with MB (pink)

Calibration curve with $R^2 = 0.9997$ described with Eq. (S1)

$$y = 3{,}10486 \cdot 10^7 \cdot x^2 + 5{,}79824 \cdot 10^7 \cdot x$$

Compatibility of adsorption inhibitors with 1 wt% surfactant solution in brine at 70°C, day 14

Chemical	Concentration, wt%							
	0.05	*0.1*	*0.2*	*0.3*	*0.5*	*1*	*-*	*-*
Sodium metaborate tetrahydrate	C*	C	O	O	O	P	-	-

182

Sodium tetraborate decahydrate	T	P	P	P	P	P	-	-
	0.05	*0.1*	*0.25*	*0.5*	*0.75*	*1*	*1.5*	*2*
Ammonium hydroxide	P	P	P	P	P	P	P	P
Sodium silicate	P	P	P	P	P	P	P	P
Ethanolamine	T	T	P	P	P	P	P	P
Sodium polystyrene sulfonate	O	O	O	O	O	O	O	O
Sodium polyacrylate (Flosperse 1000)	C	C	P	P	P	P	P	P
Sodium polyacrylate (Flosperse 3000)	C	C	P	P	P	P	P	P
Sodium polyacrylate Alcomer DP 1	C	C	C	C	C	C	C	C

*C – clear, O – opalescence, T – turbid, P – precipitation

Appearance of surfactant solutions with the addition of sodium metaborate tetrahydrate after 14 days of heating at 70°C

Appearance of surfactant solutions with the addition of Alcomer DP 1 after 14 days of heating at 70°C